A MODELING STUDY OF $PM_{2.5}$ AIR POLLUTION IN CHINA:

PRIMARY AND SECONDARY INORGANIC AEROSOLS

A Thesis

by

LI WU

Submitted to the Office of Graduate and Professional Studies of
Texas A&M University
in partial fulfillment of the requirements for the degree of

MASTER OF SCIENCE

Chair of Committee,	Qi Ying
Committee Members,	Bill Batchelor
	Renyi Zhang
Head of Department,	Robin Autenrieth

May 2015

Major Subject: Civil Engineering

ABSTRACT

Quantitative information on sources and source region contributions to particulate matter (PM) concentration in China is currently poorly understood but is urgently needed to make emission control strategies. In this study, source-oriented Community Multi-scale Air Quality (CMAQ) models are used to study the formation of and source contributions to primary and secondary PM in China.

The results show that inter-regional transport of sulfate, nitrate and ammonium ion (SNA) occurs frequently, especially in the winter. The emissions from non-local regional can contribute 30-70% of the total SNA in different regions and seasons. It is also found that surface heterogeneous reactions of NO_2 and SO_2 and higher emissions of NH_3 are needed to better reproduce the observed high concentrations of SNA in Beijing, and potentially in other areas. Residential sources account for significant fractions (19%-68% in Beijing and 6%-30% in Shanghai) of primary $PM_{2.5}$, with higher contributions occur in winter. Industrial emissions are important throughout the year (15%-45% in Beijing and 39%-60% in Shanghai). Dust contributions can be as much as 20-30% in spring and fall seasons. Contributions to primary $PM_{2.5}$ from other sources are relatively small. In Shanghai, local emissions account for 70-90 % of primary $PM_{2.5}$. However, local emissions only contribute to 45%-55% of primary $PM_{2.5}$ in Beijing. These suggest that inter-regional emission control strategies are necessary to reduce PM pollution in China. Source and source region contributions to primary $PM_{2.5}$ components are determined using a novel

multi-linear regression technique that combines the observation data and the source-oriented model predictions of primary $PM_{2.5}$ mass concentrations.

DEDICATION

I would like to delicate this work to my dear parents. Their encouragement and support are always helping me overcome difficulties in life and study.

ACKNOWLEDGEMENTS

I would like to thank my advisor, Dr. Qi Ying, who provided me an opportunity to be a research group member and let me involved into a very interesting research topic for my thesis. He is always offering patient and helpful guidance on research and studies, without which I could not achieve my progress on thesis. I also would like to express my gratitude to my committee member, Dr. Bill Batchelor and Dr. Renyi Zhang for the support throughout my research and studies. I feel honored to have them in my thesis committee.

In addition, I would like to thank the faculty and staff at Texas A&M University for making studying at TAMU to be a pleasant experience.

Last, but not the least, I would like to thank the group members, Dr. Jingyi Li, Dr. Hongliang Zhang, Peng Wang and Gang Chen for support and help during studies and research.

TABLE OF CONTENTS

Page

LIST OF FIGURES

Page

LIST OF TABLES

Page

1. INTRODUCTION

Fine particulate matter ($PM_{2.5}$) - those particles with an aerodynamic diameter of less than 2.5 μm is now receiving worldwide attention in terms of its adverse human health effects and visibility degradation (Li et al., 2013b). Particulate Matter (PM) is classified into primary and secondary PM in terms of the sources of formation. Primary aerosol is released to the atmosphere directly from various sources including vehicle emission, stationary coal burning, soil dust, marine aerosol, etc. Secondary aerosol, on the other hand, is formed within the atmosphere from precursor gases such as sulfur dioxide (SO_2), nitrogen dioxide (NO_2) and nitrogen monoxide (CO) through series of reactions (Seinfeld and Pandis, 2006). Particulate Matter pollutant emission comes from both natural and anthropogenic sources. The former one includes wind-blown dust, sea salt, volcanic ash, pollens and biogenic emission. Man-made sources include fossil fuel combustion, industrial production process, construction and residential activities (Kelly and Fussell, 2012).

$PM_{2.5}$ is a complex mixture of sulfate (SO_4^{2-}), nitrate (NO_3^-), ammonium (NH_4^+), water (H_2O), organic and element carbon (OC and EC), soil dust, trace metal elements including Al, SI, TI, Fe, Mn, Cr, Mg, etc. Among them, nitrate, sulfate and ammonium ions are the predominant inorganic species of $PM_{2.5}$, making up approximately half of total $PM_{2.5}$ mass (Chan and Yao, 2008; Querol et al., 2004; Tsimpidi et al., 2007; Yang et al., 2011). Nitrate, ammonium and majority of sulfate, are secondary in nature and thus are expected to have significant regional impact beyond the areas where the emissions are emitted (Wu

et al., 2009). Emission of precursors gases such as SO_2, NO_x in one region can transport for a long distance and have impact on secondary aerosol in areas hundreds or thousands kilometers away (Ying et al., 2014b). For example, in a previous study, long range transport of SO_2 from power plant emissions in the northwest US is found to have significant impact on sulfate concentration in east Texas (Zhang and Ying, 2010) and Wu et al. (2009) reported that Hebei, Shandong and Tianjin provinces are the major source areas of SO_4^{2-} in Beijing, China during summer time.

PM pollution poses adverse effect both for human health and the environment. Previous epidemiological studies indicated relationship between mortality and morbidity and ambient PM concentration. Particularly, fine particle is believed to pose greater health risks than coarse particles since they are more likely to penetrate into the lungs, resulting in respiratory and cardiovascular disease (Wu et al., 2014). Also particle with diameter between 0.4 to 1.0 μm, which is within the range of $PM_{2.5}$, have the highest extinction potential in the atmosphere (the wavelength of visible light is between 0.4 to 0.7) (Zhuang et al., 2014). The adverse impact of $PM_{2.5}$ pollution is not only regional, but also global. By using hierarchical modeling approach and observation analysis, modulated mid-latitude cyclone is found to be affected by Asian aerosol pollution (Wang et al., 2014b).

China, presently the second largest economy in the world in terms of the GDP, has undergone rapid economic growth since the end of twentieth century. Associated with economy growth are its growing energy consumptions, reliance on coal, and rapidly increasing vehicle population, which have placed a heavy burden on air quality (Zhuang et al., 2014). As a consequence, emission of SO_2 and NO_x in China increased dramatically

by more than 60% and 80% from 2006 to 2010, eventually accounting for 32 and 31% of global emission respectively in 2010 (Zhao et al., 2014).

As a consequence of the high level of precursor gas emissions, airborne PM pollution in China has become a significant environmental concern because of its increased frequency of occurrence in recent years. The number of haze days has shown an increasing trend since the end of 1990s and visibility during haze days can be decreased rapidly (Zhao et al., 2011). According to air quality measurement data released by Ministry of Environmental Protection in China in 2013, 69 cities in China failed to reach to national standard of $PM_{2.5}$ (35 μg/m3). The most severe $PM_{2.5}$ pollution occurs in Xingtai, Hebei Province with an annual average of 155.2 $\mu g/m^3$. Seven of the top 10 worst polluted cities are in Hebei Province, which shadow quit significant impact on the $PM_{2.5}$ condition in Beijing, the Capital city of China. In haze days, aerosol loadings can be extremely high with maximum hourly concentrations of 200-1000 $\mu g/m^3$ (Wang et al., 2014a; Wang et al., 2006b; Zhao et al., 2013).

High emission level, formation of substantial amount of secondary aerosols and adverse meteorological conditions are generally regarded as the principal factors causing the severe haze events in China (Zheng et al., 2013). The release from coal-fired power plants, cement production, iron and steel production, chemical production, transportation and residential combustion provide sufficient precursors for haze formation. Adverse meteorological conditions with weak surface winds, low mixing layers, thick temperature inversion layer and lower troposphere that transport large amount of water vapor facilitate

the formation and accumulation of airborne aerosol and increasing the $PM_{2.5}$ concentration (Wang et al., 2014c; Zhang et al., 2014).

Many studies on aerosol have revealed that SNA are the most abundant component of $PM_{2.5}$ during haze pollution events in China (Sun et al., 2006; Zhao et al., 2013). Sometimes the formation mechanisms are difficult to be explained by traditional formation pathway of SNA, which are gas phase or aqueous phase chemistry, given the adverse atmospheric conditions. For example, low O_3 concentration in the atmosphere, dim days with low solar-radiations are unfavorable to gas-phase oxidation by hydroxyl radical (OH), in-cloud oxidation by dissolved ozone (O_3) and peroxide (H_2O_2) (Zhao et al., 2013). Besides the gas-phase and aqueous-phase chemistry, heterogeneous chemistry is considered as an alternative pathway for nitrate and sulfate aerosol formation in the atmosphere. The ambient measurement has verified the existence of heterogeneous reactions with SO_2, N_2O_5 and HNO_3 (Lammel and Leip, 2005; McNaughton et al., 2009; Usher et al., 2003).

As secondary PM is formed in regional scales, contributions to secondary SNA from local sources and sources from other regions need to be quantified to design effective collaborative emission control measures. Several previous studies have been documented (Chen et al., 2007; Wang et al., 2013) to quantify contribution of different source regions to $PM_{2.5}$ nitrate and sulfate in China using chemical transport models. But almost all of them were focused on one single city (Jia et al., 2008; Wang et al., 2008) or limited area such as the Pearl River Delta (PRD) (Liu et al., 2013).

The Community Multi-scale Air Quality (CMAQ) Model, a three-dimensional mechanistic chemical model (CTM), has been applied extensively to study the emission, chemical formation, transformation and removal of gaseous and particulate air pollutants (Buzcu et al., 2006; Li et al., 2013a; Zhang et al., 2012). Evaluation of the CMAQ modeling system against observation data has shown the model has considerable skill in simulating PM (Eder and Yu, 2006; Foley et al., 2010). A generic scheme of CMAQ is shown in figure 1.

Meteorological condition, emission inventory, initial and boundary condition compose the main parts of the input to the model system. After the processing of the CMAQ Chemistry –Transport Model (CCTM), the concentrations of more than 100 species in gas and aerosol state are generated in the simulation output. The latest version of CMAQ is v5.0.2, which was released in April, 2014. Details of the model improvement will be discussed in later model description.

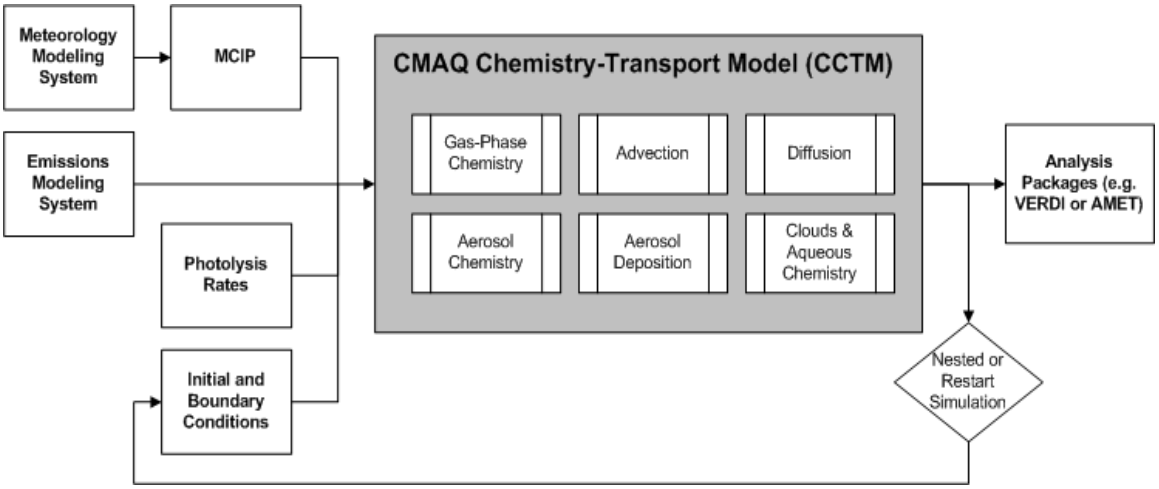

Figure 1 General process scheme of CMAQ model *

* Source is from CMAQ wiki website (http://www.airqualitymodeling.org/cmaqwiki/index.php?title=CMAQ_version_5.0_%28February_2010_release%29_OGD)

However, despite the general good simulation performance of CMAQ, many studies reveal that there has been a tendency to underestimate SO_4^{2-} especially in summertime when using CMAQ to simulate ambient PM condition (Luo et al., 2011; Sarwar et al., 2013). This under-prediction of secondary PM impairs the model simulation performance and hampers the validity of further utilization of the simulation results in post-analysis. The missing pathway for SO_4^{2-} could be the heterogeneous chemistry, which is mentioned above and also be the gas phase chemistry, for example the additional OH oxidation reactions (Lu et al., 2013).

This study is aimed to improve the understanding of PM air pollution in China. The objectives of this study are to (1) determine inter-regional transport secondary inorganic $PM_{2.5}$ components (SO_4^{2-}, NO_3^{2-} and NH_4^+) (Chapter 2); investigate several approaches to

improve predicted SO_4^{2-} NO_3^-, and ammonium (NH_4^+) concentration (Chapter 3); and (3) determine source contribution to primary particulate matter and its chemical components (Chapter 4).

2. LOCAL AND INTER-REGIONAL CONTRIBUTION TO $PM_{2.5}$ NITRATE AND SULFATE IN CHINA*

2.1 Mechanism description

A source-oriented version of the CMAQ model (based on CMAQ version 4.7.1), which was previously applied to determine the contribution of different source sectors to secondary $PM_{2.5}$ is used to quantify the contributions of different source regions to sulfate and nitrate concentration in China. The details of this source apportionment approach to predict secondary PM have been documented by Ying and Kleeman (2006) and its implementation in study in the domain of China has been reported in a previous publication (Zhang et al., 2012). The first application of the source-oriented method for determining the source regional contribution has been documented by Ying and Kleeman (2009) for a case study in California. In summary, the SAPRC-99 photochemical mechanism was modified to include additional reactions so that NO_x and SO_2 and their gas phase reaction products from different sources or source regions are separately tracked. For example, for NO_2 emissions from region A and B, the following reactions with hydroxyl radical (OH) are included:

* Part of this chapter is reprinted with permission from "Local and Inter-regional Contributions to $PM_{2.5}$ Nitrate and Sulfate in China" by Qi Ying, Li Wu, et al., 2014, *Atmospheric Environment*, 94, 582-592, Copyright [2014] by Elsevier

$$NO_2^A + HO \rightarrow HNO_3^A \quad (1a)$$

$$NO_2^B + HO \rightarrow HNO_3^B \quad (1b)$$

The current version of the modified SAPRC-99 mechanism with 304 gas phase species and 2000 gas phase reactions in the source-oriented CMAQ model can track up to 9 sources or source-regions simultaneously in a single simulation. Although almost all particulate nitrate is secondary, combustion of high sulfate fuel can lead to significant amount of primary sulfate particles (Zhang, 2004). In this part of study, the source-oriented CMAQ model for secondary aerosol was further updated to allow source region apportionment of primary nitrate and sulfate particles. Essentially, emissions of primary nitrate and sulfate from different regions are tagged as different nitrate and sulfate species. The secondary PM nitrate and sulfate source apportionment capability can be turned off by using non-source oriented gas phase emissions so that only primary PM source regional apportionment is given.

2.2 Model application

January and August of 2009 were simulated to investigate the variation of source region contributions to nitrate and sulfate under different meteorological and emission condition. These two months were chosen because they are typical representative of summer and winter time, which have different climatology conditions that affect regional emissions, formation and transport secondary PM. Fig. 2 shows the modeling domain and the eight source regions designated in this study: (1) North China. (2) Northeast China. (3) East

China, (4) Central China, (5) South China, (6) Southwest China, (7) Northwest China, and (8) other regions in the domain outside China. The designation of regions is based on a typical administrative division of the country. The contribution from boundary conditions (i.e. transport of primary and secondary PM from upwind sources outside the computation domain) is also separately resolved. The domain consists of 197 × 129 grid cells, covering most part of East Asia with a horizontal resolution of 36 km. The overall vertical range of model is approximately 20 km above the ground level and is divided into 18 vertical layers with the first layer's thickness of 35m.

The meteorological inputs were generated by the Weather Research Forecast (WRF) model v3.3. The initial and boundary conditions for simulations were generated using the default CMAQ profiles. Emission inputs were generated based on the 2006 Asia Emission Inventory for the Intercontinental Chemical Transport Experiment (INTEX-B) study, which is described in detail by Zhang et al. (2009). The anthropogenic NH_3 emissions were based on the NH_3 emission inventory for the year 2000 as described by Streets et al. (2003). Biogenic emissions were generated using the MEGAN biogenic emission processor (v2.04, http://acd.ucar.edu/~guenther/MEGAN/MEGAN/.htm). Windblown dust emissions from soil erosion were also included based on the dust emission profiles described by (Choi and Fernando, 2008) . Emissions of NO_x, SO_2 and primary NO_3^- , SO_4^{2-} of a typical weekday in January and August is referred as Table 1 by Ying et al. (2014b).

Two sets of simulations were conducted to investigate regional contribution for both primary and secondary nitrate and sulfate. In the first set of simulation, primary nitrate and sulfate were not separately tracked and source regional apportionment is only

applicable to secondary PM. In the second run, primary nitrate and sulfate were marked by different source regions and incorporated into the apportionment model so that both primary and secondary regional contribution can be determined. The contributions to primary nitrate and sulfate were determined by the difference of the two sets of simulations.

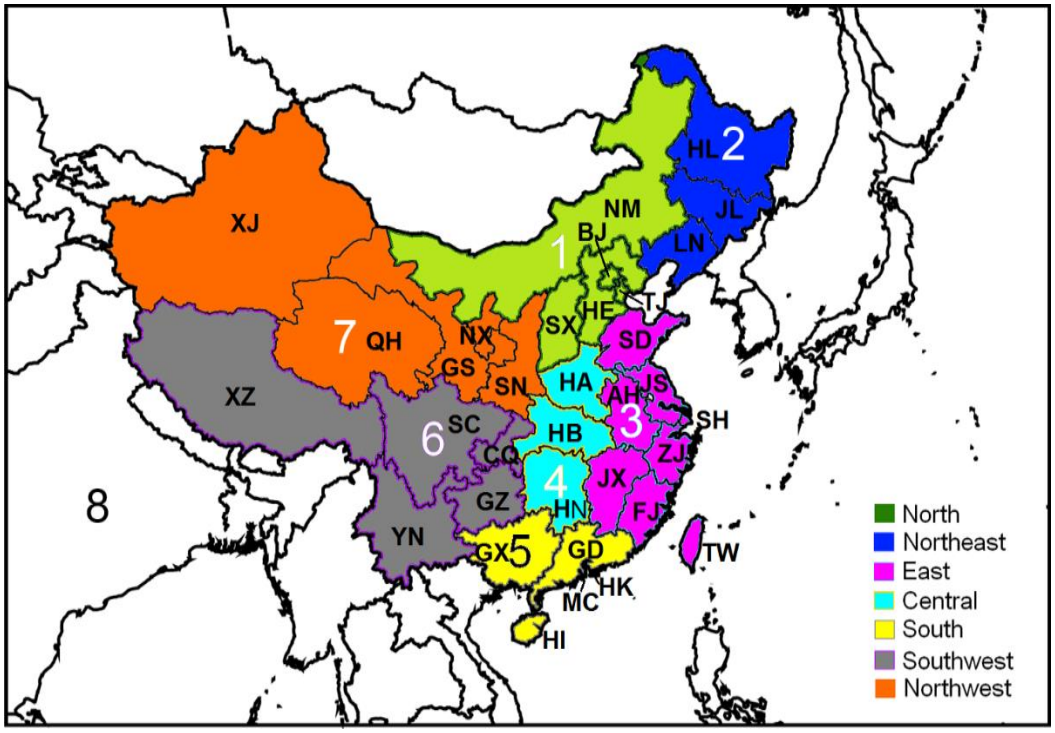

Figure 2 Emission source region designation and abbreviation of 34 provincial level divisions. (Qi Ying, Li Wu et al., 2014b)

2.3 Results and discussion

Performance of the WRF model for the same modeling period and domain has been shown in Table 1 of Zhang et al. (2012). The predicted near-surface wind speed, wind direction, temperature and relative humidity all reasonably agree with observation within the typical WRF model performance range. As shown in Fig. 3 of Zhang et al. (2012), CMAQ model

predictions generally capture the concentration and day-to-day variation of the secondary nitrate and sulfate at 6 stations in China (5 at Peal River District, 1 at Tsinghua University, Beijing). Model performance statistics (Mean Fractional Bias, or MFB; Mean Fractional Error, or MFE) shown in Tab. 1 suggest that the model generally agree well with observation, but nitrate and sulfate are under-predicted. The under-prediction is most likely due to the underestimation of the INTEX-B emission and missing pathway for inorganic aerosol formation such as heterogeneous reactions (Buzcu et al., 2006). Synoptic circulation patterns and WRF simulation uncertainty can also effect the CMAQ model simulation results. Despite the above factors of uncertainty, the model generally represents the formation and regional transport of secondary inorganic aerosols in typical summer and winter.

	# points	Mean pred. ($\mu g/m^3$)	Mean obs ($\mu g/m^3$)	MFB	MFE
January					
$PM_{2.5}$ (all sites)	3271	35	41.4	-0.22	0.57
Nitrate(Tsinghua)	15	3.3	8.1	-0.41	0.79
Nitrate(PRD)	24	6.5	10.4	-0.48	0.81
Sulfate(Tsinghua)	15	3.5	9.2	-0.78	0.88
Sulfate(PRD)	24	8.4	11.2	-0.57	0.61
August					
$PM_{2.5}$ (all sites)	3251	33	27.2	-0.07	0.72
Nitrate(Tsinghua)	-	-	-	-	-
Nitrate(PRD)	23	0.9	2.7	-1.15	1.32
Sulfate(Tsinghua)	-	-	-	-	-
Sulfate(PRD)	23	6.7	7.5	-0.06	0.32

Table 1 Summary of model performance of $PM_{2.5}$ mass, nitrate and sulfate for Jan. and Aug. 2009 (Qi Ying, Li Wu et al., 2014b)

2.3.1 Wintertime regional distribution

Fig. 3 shows the regional distribution of January monthly average total, primary, secondary nitrate and sulfate. Fig 3(a) shows that $PM_{2.5}$ nitrate has a wide regional distribution with a maximum concentration of ~30$\mu g/m^3$. The most polluted areas by

nitrate are located at North Central Plain and Sichuan Basin. (b) and (c) results indicate that nitrate is dominantly secondary aerosol with a very low concentration of primary aerosol less than 0.2μg/m^3. Fig. 3(d) suggests that the maximum concentration of sulfate total as ~18 μg/m^3 occurs in Sichuan Basin, Southwest part of China. For the rest high-populated area including Central, East and south China, the concentrations are approximately 4-8 μg/m^3. Lower temperature and solar radiation in winter reduces the rate of the photochemical reactions that convert SO_2 into H_2SO_4. In addition, higher wind speed in winter leads to faster dilution of SO_2 emission. Those two factors together may explain the relatively lower concentration of sulfate. Primary sulfate concentration can be as high as 2μg/m^3 in parts of the Central and East of China, indicating that primary sulfate, mostly generated from power plant, could be a big concern to the total sulfate concentration.

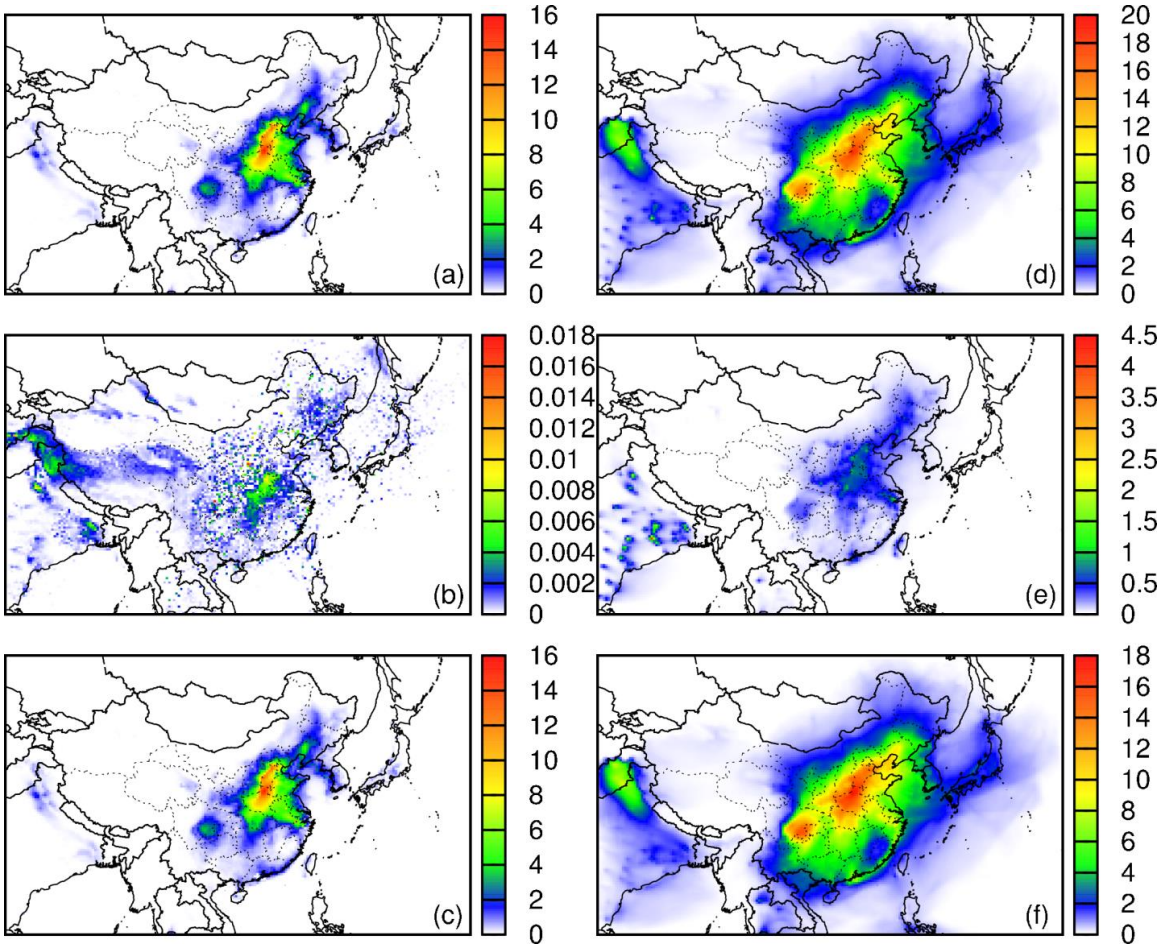

Figure 3 Regional distributions of August 2009 average $PM_{2.5}$ (a) total nitrate, (b) primary nitrate, (c) secondary nitrate, (d) total sulfate, (e) primary sulfate and (f) secondary sulfate concentrations. (Qi Ying, Li Wu et al., 2014b).

Fig. 4 illustrates contribution of emissions from each source regions to overall regional primary and secondary nitrate and sulfate in January 2009. Significant regional transport occurs at the emission from NCP and Lower Middle Yangtze Plain (LMYP, Eastern part

of China). In winter time of China, the north wind originated from Siberia Plain is dominant throughout the whole country. So the emission from North part of China (Region 1) can transport over large distance and has significant impact on the aerosol formation in South China. On the other hand, because of the geographical separation by mountain ranges or plateau, emissions from Sichuan Basin in Southwest China (S6), South China (S5) and Northeast (S3) are limited in their respective regions. The last column shows that the secondary sulfate in January has even boarder spatial distribution than nitrate. This phenomenon is due to longer life time of SO_2 in winter. Also SO_2 is emitted from large point sources with power generation industry, which is usually distributed into atmosphere up to a few hundred meters. Those two factors allow SO_2 to transport a longer distance than NO_x (Ying et al., 2014b).

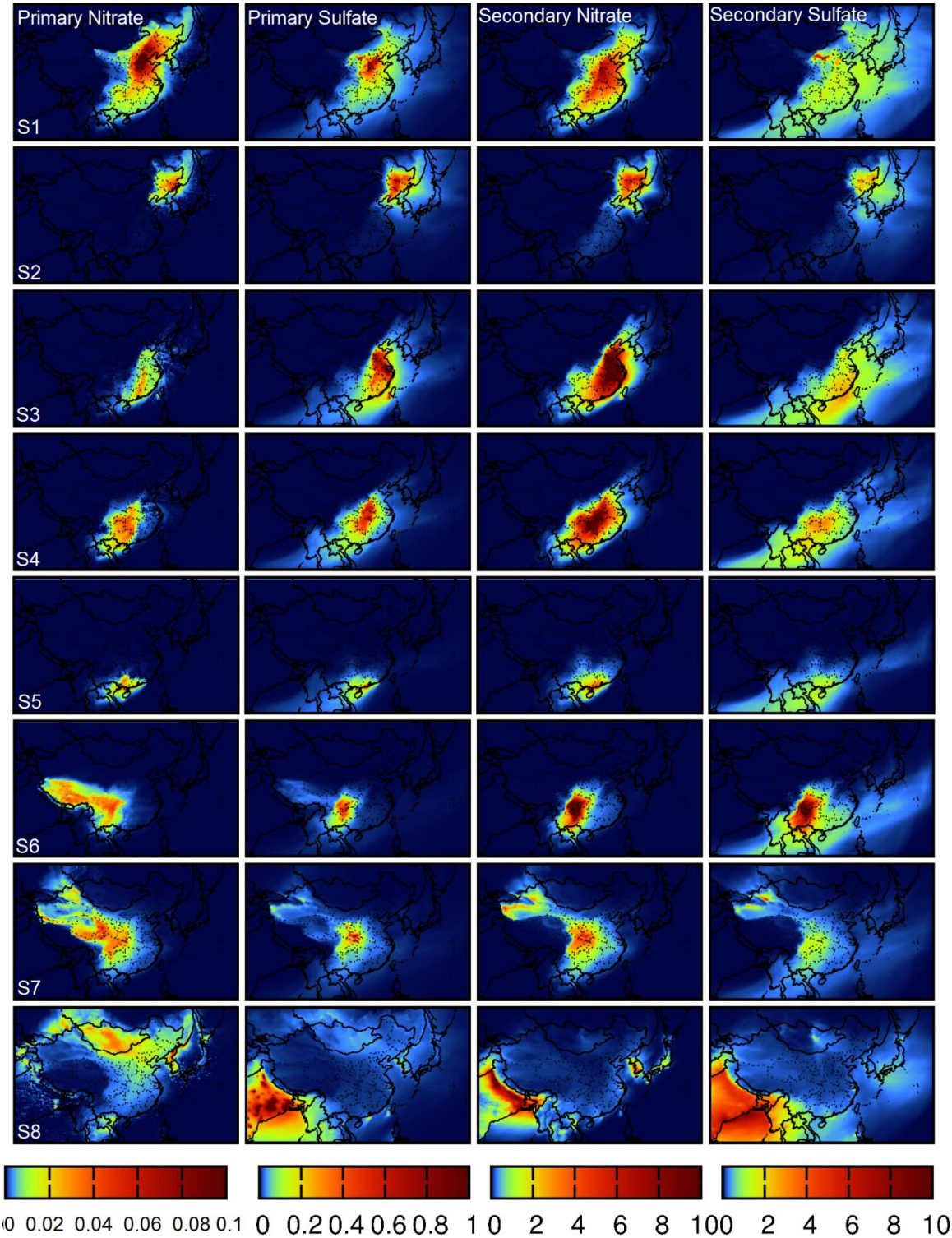

Figure 4 Regional contributions to average primary and secondary $PM_{2.5}$ nitrate and sulfate in January, 2009. Units are $\mu g/m^3$. The scales of the panels are different to better illustrate spatial distribution (Qi Ying, Li Wu et al., 2014b).

2.3.2 Summer time regional distribution

Fig. 5 shows the regional distribution of August average primary and secondary sulfate and nitrate from all source region combined. Summer time nitrate has a relatively lower concentration compared to January results because higher temperature tends to drive the partitioning of semi-volatile ammonium nitrate off the particle phase (Aw and Kleeman, 2003). Highest concentration reaches only up to 16 $\mu g/m^3$ at south NCP. (Beijing & Hebei Province). Primary nitrate is negligible with a concentration less than 0.02$\mu g/m^3$. Sulfate suggest more significant regional distribution than nitrate in summer time and the highest concentration occurs at Sichuan Basin and North China as ~ 18$\mu g/m^3$. Primary sulfate still accounts for a non-negligible fraction of the total sulfate with a maximum concentration of 2 $\mu g/m^3$.

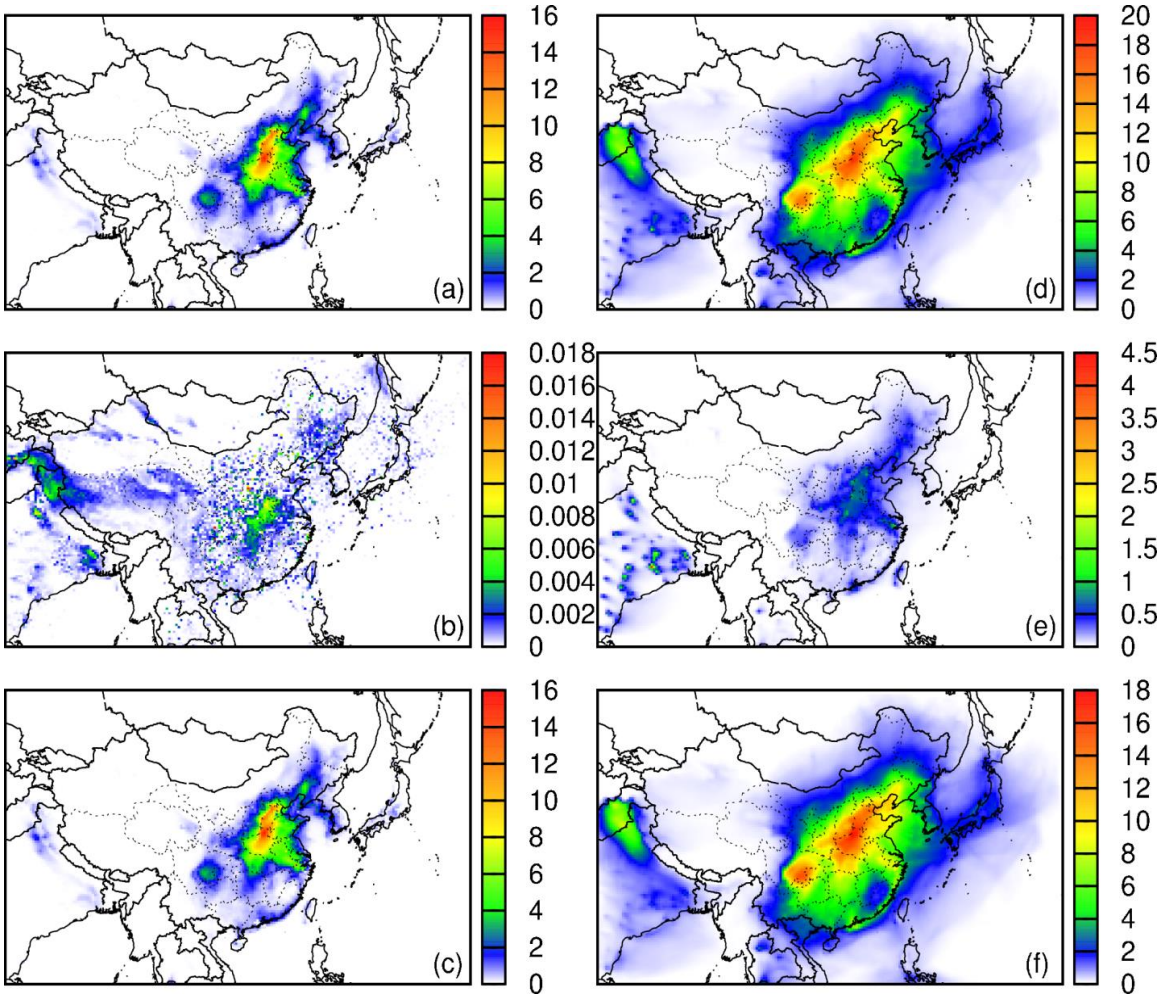

Figure 5 Regional distribution of August 2009 average $PM_{2.5}$ (a) total nitrate, (b) primary nitrate, (c) secondary nitrate, (d) total sulfate, (e) primary sulfate and (f) secondary sulfate concentrations (Qi Ying, Li Wu et al., 2014b).

Fig. 6 illustrates the contribution of emissions from each source region to the regional primary and secondary nitrate and sulfate in August, 2009. Unlike the wide regional distribution of nitrate and sulfate in winter, summertime aerosol suggest less inter-regional transport event. This is firstly because of the subtropical high that leads to lower wind speed in summer, and also more precipitation that removes aerosol through both in-cloud

and below-cloud scavenging during regional transport. Emissions from North (S1), East (S3), Central (S4) and Southwest (S6) contribute higher nitrate and sulfate concentration than other source regions' emissions. NO_x emissions from North, East and Central China lead to nitrate concentration of 10.3, 9.8 and 5.5 μg/m^3. Emissions of SO_2 from North and Southwest China lead to highest sulfate concentration of 10.2 and 11.4 μg/m^3.

2.3.3 Regional contribution to secondary nitrate and sulfate at provincial level

Table 2 shows a ranked list of monthly population-averaged concentrations of combined nitrate and sulfate for all provincial level division of China. The relative contributions of emissions from each region are also calculated. Population-averaged concentration is used because in many provinces of China, there is strong variation of population density and higher pollutant concentration occurs at higher population area. The simple average can't correctly represent the overall pollutant concentration and corresponding health risk in a province or region. Equation 2 shows the way that population-averaged concentration is determined.

$$C^j = \frac{\sum_{i=1}^{N} Pi C_i^j}{\sum_{i=1}^{N} Pi} \quad (2)$$

Where N is the total number of grid cells in a given province; i is the grid cell index. Pi is the population density in the ith grid cell in a province. C_{ij} is the predicted concentration in ith grid cell from j source region. Gridded population density needed for Equation 2 is included in the Supplementary material.

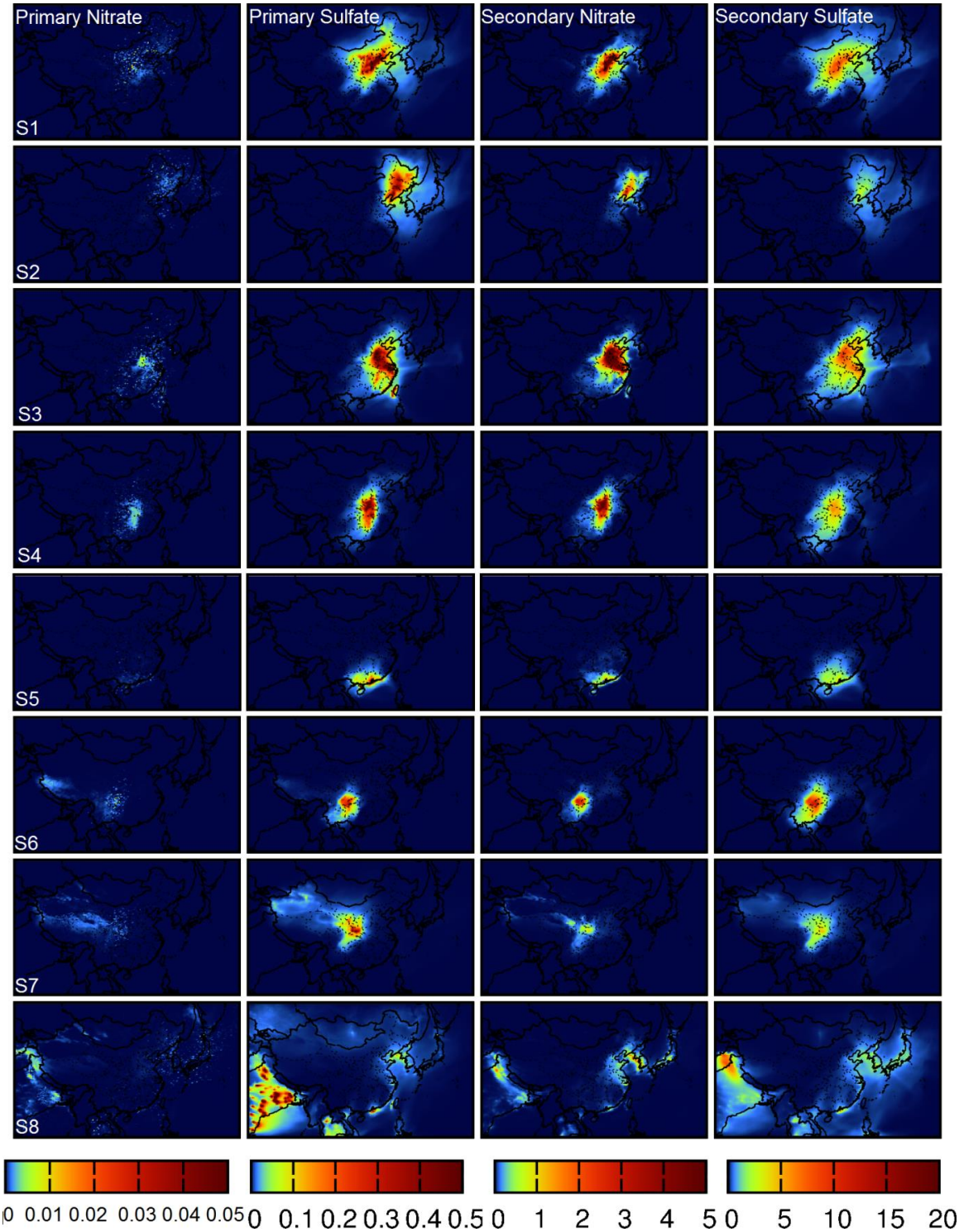

Figure 6 Regional contributions to average primary and secondary $PM_{2.5}$ nitrate and sulfate in August, 2009. Units are $\mu g/m^3$. The scales of the panels are different to better illustrate spatial distribution (Qi Ying, Li Wu et al., 2014b).

2.3.3.1 Wintertime source region contributions

Table 2. shows January 2009 population weighted average concentrations of $PM_{2.5}$ nitrate + sulfate for each provincial level division in China and contributions of each source region to the total concentrations. The highest three provincial concentration around 30μg/m^3 occurs in Chongqing (CQ), Sichuan (SC) and Guizhou (GZ), which are all located in the Southwest part of China (Table 2). About half (from 44.7% to 62%) concentration are contributed from the local emission and other main source regions include Central (S4) and Northwest (S7) China. The pollutants in this area are dominantly coming from local emissions because this highly populated area is surrounded by mount ranges that limit the precursor gas transport. The next ten provinces have an average S + N concentration over 18μg/m^3. Nine out of ten provinces are in East and Central China, where the local emission amount is relatively higher than other regions. In addition to dominant local emission contribution, ranging from 31.5% to 60.7%, emission from North China (S1) can be also an important source contribution. For example, Henan province which is located in Region 4, has a regional contribution from North China (S1) as 37.6%. This indicates that most of the secondary PM due to emissions from North China gets transported out of the region to significantly affect air quality in the downwind provinces in the south.

2.3.3.2 Summertime source region contributions

Table 3 shows the ranked list of monthly provincial population weighted average S + N concentration and source region contribution for August 2009. Peak N + S concentration

is relatively lower than January. Highly polluted area shifted from Southwest and East China to North China. Two municipalities, Beijing and Tianjin and surrounding HeBei province are among the top four of the list. More than 60% contribution is from local emission and the emission from East China is the most important regional contributor. In summertime, the wind from the ocean contiguous to the Southeast China brings precursor gas to North China and form secondary aerosols. Henan province ranks the second place in the list with a S + N concentration of 22.4 $\mu g/m^3$, which is resulted from comparable contribution from East, North China and local emissions because its location in the Central China. Concentrations in the Southwest China provinces are significantly lower in summer and mostly due to local source.

	S0	S1	S2	S3	S4	S5	S6	S7	S8	Total
Chongqing (CQ,6)	2.1%	9.8%	0.1%	4.7%	24.9%	1.3%	46.4%	10.0%	0.8%	33.3
Sichuan (SC, 6)	2.3%	6.1%	0.0%	3.3%	12.7%	0.6%	62.0%	12.2%	0.8%	32.1
Guizhou (GZ,6)	2.0%	10.3%	0.2%	6.9%	24.5%	2.7%	44.7%	7.2%	1.5%	29.0
Anhui (AH,3)	2.5%	24.4%	0.6%	44.5%	22.1%	0.2%	1.1%	3.7%	1.0%	27.0
Hunan (HN, 4)	2.5%	17.3%	0.6%	20.5%	45.3%	2.6%	4.8%	5.2%	1.1%	27.0
Hubei (HB, 4)	2.7%	20.7%	0.5%	19.3%	43.0%	0.4%	5.0%	7.7%	0.7%	26.7
Jiangxi (JX, 3)	2.4%	16.5%	0.6%	48.2%	21.8%	2.5%	3.5%	3.0%	1.4%	24.0
Jiangsu (JS, 3)	2.7%	21.8%	0.9%	57.0%	12.6%	0.2%	0.8%	2.2%	1.7%	23.5
Shandong (SD, 3)	3.1%	30.6%	1.5%	47.1%	14.1%	0.0%	0.3%	2.2%	1.1%	21.6
Zhejiang (ZJ, 3)	2.7%	16.3%	0.8%	60.7%	11.8%	0.8%	1.8%	2.4%	2.8%	20.8
Henan (HA, 4)	3.6%	37.6%	0.4%	13.9%	31.5%	0.0%	3.1%	9.1%	0.8%	20.1
Guangxi (GX, 5)	2.7%	13.9%	0.7%	19.1%	29.4%	15.7%	10.9%	4.6%	3.1%	19.1
Shanghai (SH, 3)	3.1%	18.9%	1.3%	59.8%	9.4%	0.3%	0.9%	1.8%	4.5%	18.3
Guangdong (GD, 5)	2.6%	11.0%	0.6%	36.5%	13.7%	23.5%	5.0%	2.1%	5.1%	16.3
Yunnan (YN, 6)	3.0%	7.5%	0.1%	5.2%	16.5%	3.2%	49.8%	6.1%	8.6%	15.1
Fujian (FJ, 3)	3.0%	13.5%	0.6%	60.0%	9.9%	2.7%	4.5%	2.4%	3.4%	14.9
Shaanxi (SN, 7)	6.8%	14.1%	0.0%	0.6%	7.6%	0.5%	17.9%	51.0%	1.4%	11.5
Tianjin (TJ, 1)	6.0%	66.9%	4.6%	11.5%	6.8%	0.0%	0.1%	1.9%	2.2%	11.4
Hebei (HE, 1)	6.0%	66.7%	2.4%	8.1%	9.9%	0.0%	0.8%	4.6%	1.6%	11.3
Jilin (JL, 2)	6.8%	24.0%	55.7%	8.3%	1.8%	0.1%	0.4%	0.6%	2.4%	10.6
Hainan (HI, 5)	2.9%	8.8%	0.6%	27.6%	14.4%	29.0%	7.9%	2.4%	6.4%	9.8
Heilongjiang (HL, 2)	8.1%	19.3%	67.6%	2.8%	0.4%	0.0%	0.0%	0.2%	1.5%	9.7
Beijing (HJ, 1)	8.6%	79.3%	2.8%	2.6%	1.4%	0.0%	0.0%	2.7%	2.5%	7.8
Ningxia (NX, 7)	10.1%	41.4%	0.0%	0.0%	0.7%	0.1%	6.3%	39.3%	2.1%	7.7
Shanxi (SX, 1)	9.2%	53.7%	0.0%	0.3%	5.8%	0.0%	4.9%	24.2%	1.8%	7.3
Liaoning (LN, 2)	9.8%	13.5%	32.4%	33.0%	5.6%	0.0%	0.1%	1.3%	4.3%	7.2
Taiwan (TW, 3)	4.0%	11.5%	0.7%	60.2%	6.0%	2.4%	6.8%	2.5%	5.8%	6.3
Gansu (GS, 7)	12.4%	3.7%	0.0%	0.5%	3.1%	0.4%	23.5%	53.6%	2.8%	6.2
Neimeng (NM, 1)	13.6%	69.0%	6.9%	0.9%	0.1%	0.0%	0.1%	5.5%	3.9%	4.6
Xinjiang (XJ, 7)	21.4%	0.1%	0.0%	0.0%	0.0%	0.0%	0.0%	71.9%	6.6%	4.4
Qinghai (QH, 7)	31.8%	0.7%	0.0%	0.0%	0.2%	0.0%	2.1%	57.0%	8.2%	2.2
Xizang (XZ, 6)	66.7%	0.0%	0.0%	0.0%	0.0%	0.0%	6.9%	0.4%	25.9%	0.7

Table 2 January 2009 population weighted average concentrations of $PM_{2.5}$ nitrate + sulfate for each provincial level division in China and contributions of each source region to the total concentration. (Qi Ying, Li Wu et al., 2014b)

* See Figure 2 for the locations of these provincial level divisions. Although the Special Administrative Regions of Hong Kong (HK) and Macao (MC) are provincial level divisions, they are not included in this table because of their small areas. S0 represents contributions from boundary conditions.

	S0	S1	S2	S3	S4	S5	S6	S7	S8	Total
Tianjin (TJ, 1)	1.1%	59.0%	0.9%	31.5%	3.4%	0.0%	0.3%	0.6%	3.3%	23.4
Henan (HN, 4)	0.5%	23.9%	0.3%	35.9%	36.2%	0.2%	0.8%	1.2%	1.0%	22.4
Hebei (HE, 1)	1.0%	61.0%	0.8%	24.3%	9.6%	0.0%	0.4%	0.9%	2.0%	20.9
Beijing (BJ, 1)	1.2%	71.3%	0.6%	20.6%	3.3%	0.0%	0.2%	0.8%	1.9%	19.8
Shandong (SD, 3)	1.1%	16.7%	1.7%	69.7%	5.4%	0.1%	0.5%	0.6%	4.2%	17.7
Shanxi (SX, 1)	0.9%	59.5%	0.1%	12.2%	20.3%	0.1%	1.1%	5.4%	0.3%	14.0
Sichuan (SC, 6)	0.4%	6.5%	0.0%	4.0%	6.9%	0.5%	70.3%	11.1%	0.3%	13.4
Jiangsu (JS, 3)	0.8%	8.1%	1.8%	78.0%	3.1%	0.7%	0.6%	0.5%	6.4%	13.1
Chongqing (CQ, 6)	0.3%	6.7%	0.0%	5.8%	12.6%	1.5%	67.9%	4.7%	0.5%	12.6
Anhui (AH, 3)	0.5%	8.0%	0.8%	73.6%	10.9%	1.3%	0.8%	0.6%	3.4%	12.4
Liaoning (LN, 2)	2.3%	28.7%	29.5%	27.1%	2.2%	0.0%	0.2%	0.4%	9.7%	12.3
Hubei (HB, 4)	0.4%	13.6%	0.1%	26.0%	51.0%	3.7%	2.8%	1.0%	1.4%	11.9
Shaanxi (SN, 7)	0.8%	26.8%	0.0%	9.4%	17.8%	0.3%	10.6%	33.9%	0.4%	11.1
Shanghai (SH, 3)	0.7%	4.9%	1.8%	74.8%	1.7%	0.7%	0.4%	0.3%	14.6%	10.4
Zhejiang (ZJ, 3)	0.4%	3.4%	1.0%	81.9%	1.3%	1.1%	0.3%	0.3%	10.5%	8.0
Hunan (HN, 4)	0.5%	6.9%	0.0%	28.4%	44.5%	15.5%	1.6%	0.3%	2.1%	7.3
Jilin (JL, 2)	4.1%	22.0%	46.1%	16.8%	1.9%	0.0%	0.2%	0.4%	8.5%	6.6
Guizhou (GZ, 6)	0.4%	1.5%	0.0%	7.3%	13.5%	5.8%	68.1%	1.8%	1.7%	6.4
Guangdong (GD, 5)	1.0%	0.1%	0.0%	11.0%	3.8%	63.0%	0.0%	0.0%	21.0%	5.5
Jiangxi (JX, 3)	0.6%	2.4%	0.0%	61.7%	13.1%	16.9%	0.1%	0.2%	4.8%	4.6
Fujian (FJ, 3)	0.7%	0.4%	0.1%	73.9%	0.7%	13.6%	0.1%	0.1%	10.3%	4.6
Ningxia (NX, 7)	2.7%	21.3%	0.0%	2.0%	3.5%	0.1%	12.9%	57.3%	0.3%	4.4
Gansu (GS, 7)	2.5%	14.9%	0.0%	2.4%	5.2%	0.2%	21.6%	52.9%	0.3%	4.3
Guangxi (GX, 5)	1.1%	0.6%	0.0%	16.8%	26.1%	47.9%	2.2%	0.1%	5.3%	4.1
Neimeng (NM, 1)	5.6%	58.3%	10.6%	11.7%	3.6%	0.0%	0.7%	7.3%	2.2%	4.1
Heilongjiang (HL, 2)	8.7%	17.7%	57.8%	8.7%	0.8%	0.0%	0.1%	0.5%	5.7%	3.1
Taiwan (TW, 3)	2.0%	16.8%	0.6%	67.3%	1.4%	2.2%	0.6%	0.4%	8.8%	2.9
Yunnan (YN, 6)	0.6%	0.8%	0.0%	4.2%	8.8%	1.1%	80.2%	2.5%	1.7%	2.7
Qinghai (QH, 7)	6.4%	7.5%	0.0%	0.4%	0.9%	0.0%	7.5%	76.5%	0.8%	1.9
Hainan (HI, 5)	7.5%	0.2%	0.0%	11.3%	0.5%	68.8%	0.1%	0.1%	11.6%	1.3
Xinjiang (XJ, 7)	54.5%	0.0%	0.0%	0.0%	0.0%	0.0%	0.0%	43.1%	2.4%	0.6
Xizang (XZ, 6)	28.7%	0.9%	0.0%	1.7%	1.7%	0.4%	18.0%	9.9%	38.6%	0.1

Table 3 August 2009 population weighted average concentrations of $PM_{2.5}$ nitrate+sulfate for each provincial level division in China and contributions of each source region to the total concentration. (Qi Ying, Li Wu et al., 2014b)

* See Figure 2 for the locations of these provincial level divisions. Although the Special Administrative Regions of Hong Kong (HK) and Macao (MC) are provincial level divisions, they are not included in this table because of their small areas. S0 represents contributions from boundary conditions.

2.3.4 Time series of regional source contribution at selected megacities

Temporal variations of the extent of regional transport of secondary PM species are evaluated in three megacities and one city cluster: Beijing, Shanghai, Chongqing and Peal River District (PRD). These four megacities and city cluster have approximately 1.4% of the total area of China, while accounting for about 14% of the total population.

Fig. 7 presents the nitrate and sulfate daily variation and relative contribution from source regions of the four cities/regions in January. For Beijing, local emission is the dominant contributor to the total concentration, accounting more than 90% on most days. Boundary contribution is another important source for sulfate on particular days (Jan. 21-25). In shanghai, local emission is also dominant for sulfate and nitrate formation, while the emission from North China could also be an important factor. On relatively cleaner days (Jan. 19-21), influence from North China and boundary increase, leading to rapid cleanup of the accumulated concentrations. Chongqing and PRD concentration are resulted from relatively more complex contributors. Besides the local contribution, emission from North, Central and East China are also significant on most days. For sulfate concentration in PRD, local contribution can be as low as about 20 %, suggesting long range transport of emission from northern area.

As discussed before, in summer time, the inter-regional transport is not as strong as winter due to the influence of the subtropical high. In Beijing, concentration of nitrate and sulfate increase when the emission from southern area reaches (Aug. 15-17) partially because Beijing is surrounded by mountains to the north, northwest and west. Concentration in

Shanghai stays lower before Aug. 11 because of the Typhoon Morakot. After that, nitrate concentration remain relatively low while sulfate concentration increase to a higher level and the peak occurs on Aug. 25 when emissions from North China joins. Nitrate concentration in Chongqing ranges from 5 to 8 $\mu g/m^3$ from August 7 to August 14 with more than 90% contribution from local emission. Increase of sulfate concentration during this period is correlated with increasing in inter-regional transport of emissions from North China. For PRD, emission from ocean which is contiguous to the southern boundary of China and local emission play important play roles on most days. The emission from Northern and Central China are no longer a significant contributor.

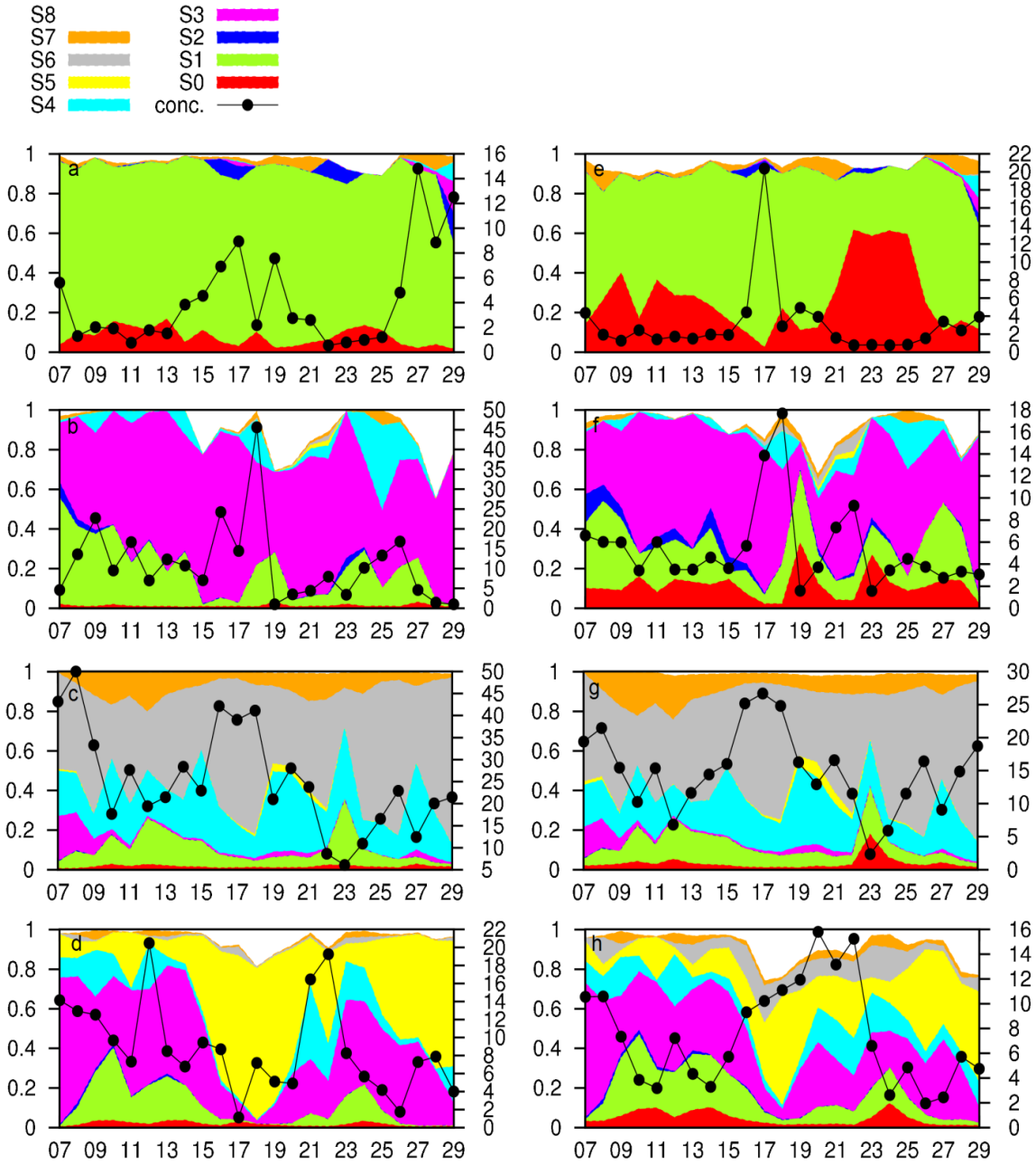

Figure 7 Time series of relative regional contributions to $PM_{2.5}$ nitrate (a-d) and sulfate (e-h) for Beijing (a,e), shanghai (b,f), Chongqing (c,g) and the Pearl River Delta (PRD) region (d,h) in January, 2009. The black dots are predicted concentrations of $PM_{2.5}$ nitrate and sulfate in units of $\mu g/m^3$ (second y-axis). (Qi Ying, Li Wu et al., 2014b)

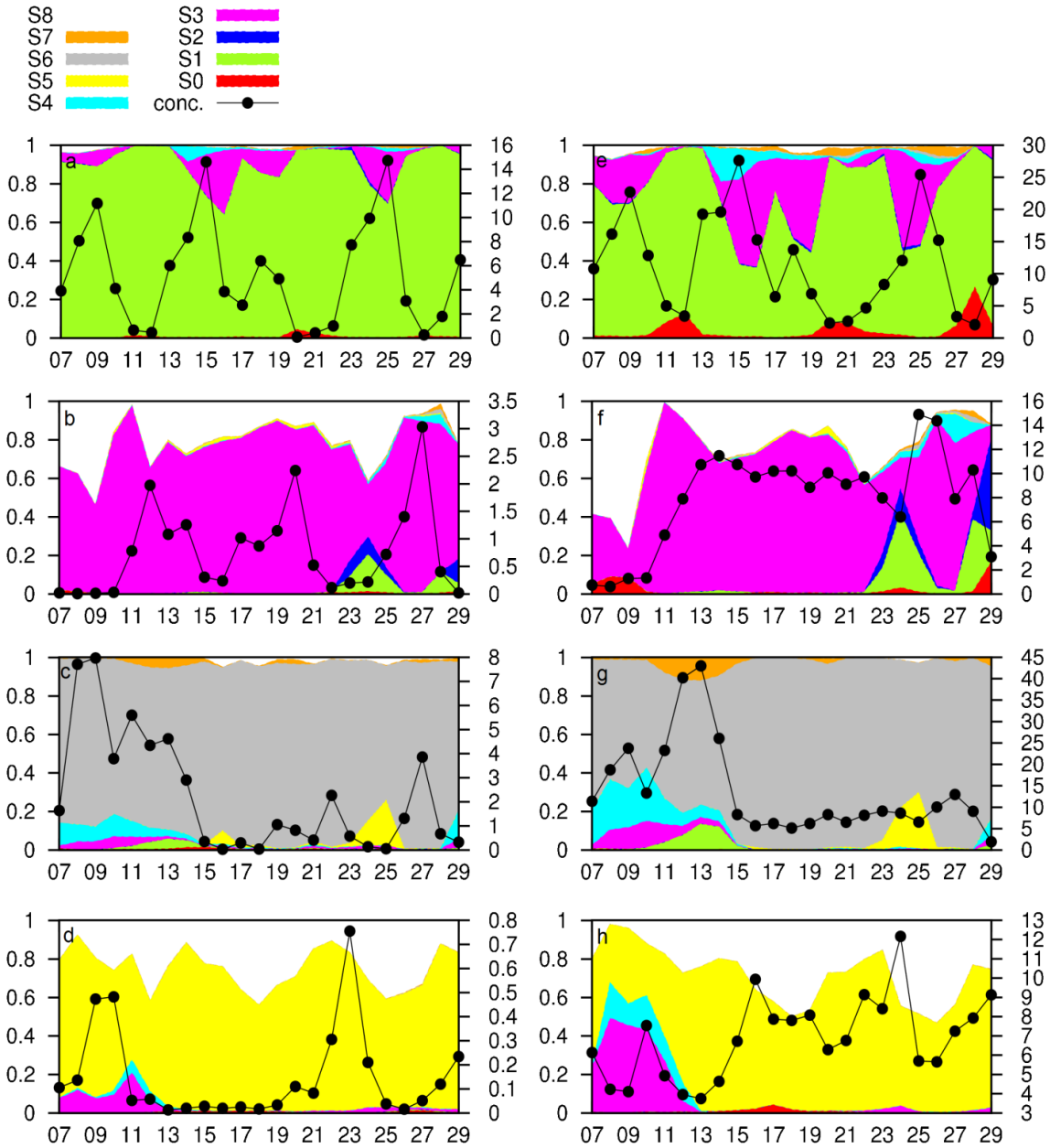

Figure 8 Time series of relative regional contributions to $PM_{2.5}$ nitrate (a-d) and sulfate (e-h) for Beijing (a,e), Shanghai (b,f), Chongqing (c,g) and the PRD region (d,h) in August, 2009. The black dots are predicted concentrations of $PM_{2.5}$ nitrate and sulfate in units of $\mu g/m^3$ (second y-axis). (Qi Ying, Li Wu et al., 2014b)

2.4 Conclusions

The model simulation results reveals distinct spatial and temporal distributions and inter-regional transport patterns of $PM_{2.5}$ nitrate and sulfate in China during winter (January) and summer (August) episodes. In winter, widespread high concentration of nitrate occurs in the NCP and MLYP. The emission of NOx from the North China can transport for a long distance to the Southern China and increase the formation of secondary nitrate. Sulfate shows even more significant regional distribution throughout the most area of China than nitrate. The top five provinces with highest nitrate plus sulfate population-weighted concentration are Chongqing, Sichuan, Guizhou, Anhui and Hunan, which are influenced by emissions from North, Central and East China. In summer, due to the subtropical high, the inter-regional transport of precursor gas is less significant than winter. Three of the top five provinces (Tianjin, Hebei and Beijing) are located in North China and have more than 55% of local region contributions. In addition to emissions from North China, approximately 30% of the S + N concentrations in four of the top five high concentration provinces (Tianjin, Henan, Hebei and Shandong) are due to emissions from East China. Daily analysis of four megacities also indicates stronger and more frequent inter-regional transport in winter than summer. Although local emission is a dominant contributor, long range transport from other regions can be important for some regions in particular time period.

3. HETEROGENEOUS REACTIONS AND OTHER FACTORS THAT AFFECT SECONDARY INORGANIC AEROSOL FORMATION

Previous simulation results on $PM_{2.5}$ concentration in China have shown that secondary inorganic components in $PM_{2.5}$ including sulfate, nitrate and ammonium during severe haze episode are under-predicted (Zheng et al., 2014a; Zheng et al., 2014b). The high concentrations of $PM_{2.5}$ SNA need additional explanation. Although heterogeneous chemistry is thought to play an important role in the production of sulfate and nitrate during haze days, they are not sufficiently implemented in the CMAQ model. Also Fe(III) and Mn(II) concentrations are important in aqueous chemistry for sulfate formation. This part of study is aimed to (1) test the applicability and sensitivity of adding heterogeneous reactions of NO_2 and SO_2 on SNA formation; (2) test the possibility to better predict Fe(III) and Mn(II) concentration from their relationship with EC concentration, and thus improve the simulation performance on sulfate.

3.1 Mechanism description

As the most updated version of CMAQ model, CMAQ v5.0.2 has made some new features and improvements over the previous popular version 4.7.1. Some of important changes that lead to the aerosol model performance include: newly incorporated aerosol module AERO6 adds 9 new $PM_{2.5}$ species such as iron (AFEJ), aluminum (AALJ),titanium (ATIJ), etc, so that trace metal concentrations can be simulated directly; Gas phase chemistry module of SAPRC-07 (Carter, 2010) is implemented as a upgraded mechanism

to replace the old SAPRC-99; Reaction rate coefficient are upgraded based on more recent experimental data (Alexander et al., 2009; Jacobson, 1997; Martin and Good, 1991); CMAQ5.0.2 also includes a diagnostic feature of sulfate tracking so that predicted sulfate concentration from different formation pathways can be determined.

Particulate SO_4^{2-} can be formed through gas phase oxidation of SO_2 to sulfuric acid following gas-to-particle partitioning or by aqueous oxidation of dissolved SO_2 (S(IV)). Several aqueous phase chemical pathways have been identified for the conversion of S(IV) to $S(VI)^-$. (Seinfeld and Pandis, 2006). These aqueous-phase oxidation pathways include the reactions of S(IV) by hydrogen peroxide(H_2O_2), dissolved ozone (O_3), dissolved oxygen catalyzed by iron (Fe(III)) and manganese (Mn(II)),methylhydroperoxide (MHP), peroxyacetic acid (PAA). These gas and aqueous pathways are implemented in CMAQ models.

Numerous experimental and modeling studies have demonstrated the significance of heterogeneous reactions on the particle surface, which lead formation of secondary PM. For example, the laboratory study of Li et al. (2006) has shown that the amount of SO_2 loss via the heterogeneous reactions on dust particle is comparable to loss via the gas-phase oxidation under high dust concentration condition. Using a global model, Dentener et al. (1996) found that the interactions of N_2O_5, O_3 and HO_2 radical with particles in high dust atmosphere affect the photochemical oxidants cycle and cause O_3 decrease by up to 10%. Buzcu et al. (2006) have found that heterogeneous reactions of SO_2 is necessary to explain the observed sulfate enhancements during the wood smoke episode in Southwest Texas.

In this study, heterogeneous reactions on particle surface are modeled as a surface uptake process. The formation rate of secondary PM components are determined by the impinging rate of precursor gas molecules with particle surface the uptake coefficient. Equation (3) shows the rate of change of particulate sulfate due to heterogeneous reaction of gas phase SO_2.

$$d\left[SO_4^{2-}\right]/\,dt = \gamma * \frac{1}{4} A\left[SO_2\right] * v_{SO_s} \quad (3)$$

where γ is the uptake coefficient of SO_2 and v is the mean molecular velocity of SO_2, calculated as $\sqrt{8RT/\pi M}$ (M is the molecular weight of SO_2; T is temperature in K; and R is the universal gas constant) and A is the effective particle surface area.

Wang et al. (2012) summarized some important heterogeneous reactions and corresponding uptake coefficients. Two of the most important reactions that affect nitrate and sulfate concentration in polluted urban areas are heterogeneous reactions of NO_2 and SO_2 on particle surface. The NO_2 heterogeneous reaction is already implemented in CMAQ but with a lower uptake coefficient. In the study, the uptake coefficient is updated to 1.5 x 10^{-4}. Reactions of SO_2 is added to CMAQ5.0.2 using the same approach as in Ying et al. (2014a) with γ of 2.0 x 10^{-5}.

$$NO_2 + Particle \rightarrow NO_3^- \qquad \text{R1,} \quad \gamma = 1.5 \times 10^{-4}$$

$$SO_2 + Particle \rightarrow SO_4^{2-} \qquad \text{R2,} \quad \gamma = 2.0 \times 10^{-5}$$

Another update of S (VI) formation simulation in the current study is to the Fe (III) and Mn (II) catalyzed oxidation by O_2 (R3), which is an important pathway for S (IV) transformation to S (VI) (Seinfeld and Pandis, 2006).

$$S\ (IV)\ +\ \frac{1}{2}O_2 \xrightarrow{Fe^{3+},Mn^{2+}} S\ (VI) \qquad \text{R3}$$

The reactions catalyzed by Fe^{3+} and Mn^{2+} are PH dependent and the reactions rate in the old CMAQ model (version 4.x) are based on Martin and Hill (1987) Concentration of Fe^{3+} and Mn^{2+} in the CMAQ v4.x are set to prescribed low "background" values of 0.01 μg/m^3 and 0.005 μg/m^3, respectively, without considering the spatial and seasonal variation (Appel et al., 2013). This might be appropriate for relatively clean conditions in the United States but is obviously inappropriate for more polluted regions such as China where concentrations of Fe and Mn can be as high as 1.3 and 0.09 μg/m^3 (Yang et al., 2011) under some conditions. In this study, two approaches will be used to determine Fe(III) and Mn(III) concentrations. One approach is to use a statistically derived relationship between Fe and Mn concentration and EC. Based on an extensive literature review of existing China-based measurements (Cao et al., 2012; Gu et al., 2011; Kebin He, 2001; Louie et al., 2005; Sun et al., 2004; Wang et al., 2006a; Yang et al., 2011; Ye, 2002), the following relationships are derived (Fig.9). Linear regression is used to derive the correlation, considering the measurement uncertainty (York et al., 2004).

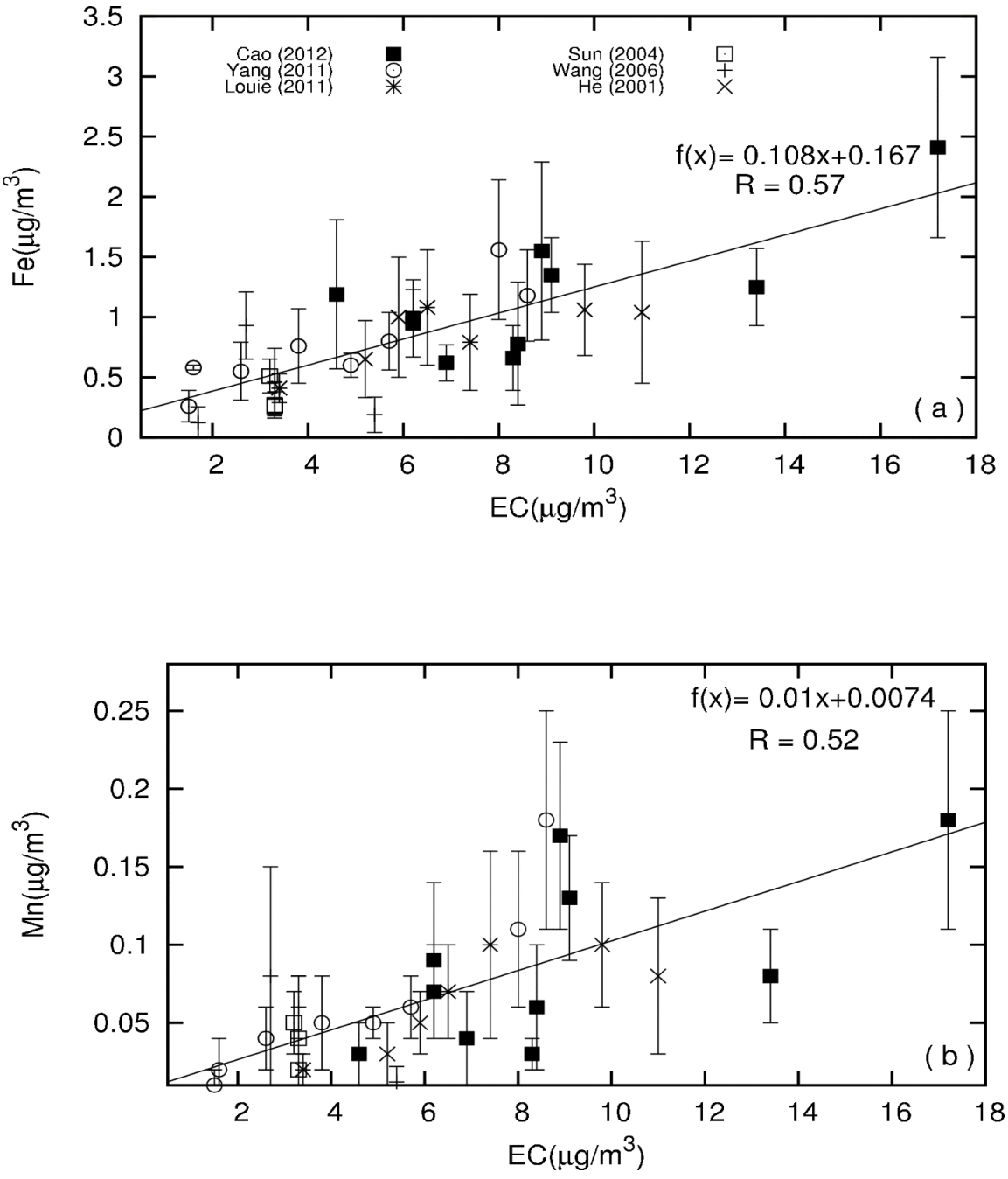

Figure 9 Fe and Mn correlation with EC derived from observation data. Error bar represents reported uncertainty. Symbols vary from different related references.

The second approach is to predict concentration of Fe^{3+} and Mn^{2+} directly based on the estimated emission rates of these two species. For this purpose, representative PM speciation profiles with trace elements based on the SPECIATE data base from US EPA (http://cfpub.epa.gov/si/speciate/) are adopted to generate emissions of trace elements for the primary $PM_{2.5}$ emissions of various sectors. The predicted elemental concentrations of Fe and Mn are used to estimate the soluble Fe^{3+} and Mn^{2+} assuming that 50% of the Fe and Mn are soluble, and 10% of the soluble Fe is Fe^{3+} during day time and 50% of the soluble Fe is Fe^{3+} at night.

3.2 Model application

Four one-month simulation periods are used in this part of study, which are January and March in 2013, and August and October in 2012 representing winter, spring, summer and autumn conditions respectively. The time periods are chosen also because there are available observation data to evaluate model performance. The model domain is the same as that used in the first part of this study (Fig. 1), with a resolution of 36 km in horizontal directions. WRF simulation also has a resolution of 36 km. Input data for WRF simulation comes from National Center for Environmental Prediction (NCEP) Final Analysis (FNL) data sets. The major physics options include the Thompson micro physics scheme, Goddard shortwave scheme, Grell 3D ensemble cumulus scheme, Unified Noah land surface model, and YSU planetary boundary layer scheme.

Emissions are extremely important to the accuracy of air quality modeling results. In this part of study, the Multi-resolution Emission Inventory for China (MEIC) developed by

Tsinghua University, China (He, 2012) is used. The MEIC is under active development and is continuously updated and improved. Compared with previous inventories (such as TRACE-P (Jacob et al., 2003) or INTEX-B (Zhang et al., 2009)), the major improvements of MEIC include unit-based emission inventory for power plants and cement plants (Wang et al., 2014a).

The CMAQ version 5.0.2 is used in this study. Aerosol module and gas chemistry are AERO6 and SPRAC07tb_st, respectively. Observation data is obtained from Beijing University of Aeronautics and Astronautics (BUAA). Measurement data are collected on BUAA campus, which is located near the north forth ring in Beijing and about 12 km northwest of the city center. Daily 23-hr integrated $PM_{2.5}$ samples were collected using a five-channel Spiral Ambient Speciation Sampler (SASS, Met One Inc.). Two 47 mm Teflon filters were used to collect $PM_{2.5}$ mass, and elemental and water soluble ion for analysis respectively. A quartz fiber filter was used to collect $PM_{2.5}$ for EC and OC from 2012-2013.

3.3 Results and discussion

3.3.1 Evaluation of meteorological predictions

The predicted temperature (T2) and relative humidity (RH) at 2m above surface, and wind speed (WS) and wind direction (WD) at 10m above surface are compare with observation data from the National Climatic Data Center (NCDC). There are 6 stations surrounding Beijing with hourly or every-third-hour observations, with a total of ~1600 data samples. The observations from the stations are compared with the WRF predictions at the grid

cells where the stations are located. Model performance statistics including mean observation (OBS), mean prediction (PRE), mean bias (MB) and gross error (GE) are calculated and the results are shown in Table 5. For wind speed and temperature, the bias between observation and prediction are mostly less than 1 m/s and 1.5 T respectively in all four seasons. For wind direction and relative humidity, because of complexity of influence, the bias are relatively higher especially in some seasons such as fall and winter, but they are still in a not large range. Generally WRF model has good performance on the meteorological condition simulation and the performance statistics are comparable to other studies using WRF (Fast et al., 2006; Misenis and Zhang, 2010; Zhang and Dubey, 2009).

Variable	Statistics	Jan. 2013	March 2013	Aug. 2012	Oct. 2012
T2 (K)	OBS	267.3	278.0	297.4	285.7
	PRE	266.1	278.7	298.4	287.0
	MB	1.2	0.7	1.0	1.3
	GE	3.7	2.6	2.8	2.9
WS (m/s)	OBS	3.0	3.4	2.8	3.2
	PRE	3.2	4.1	3.3	3.7
	MB	0.2	0.7	0.5	0.5
	GE	1.3	1.6	1.2	1.5
WD (degree)	OBS	187.5	173.4	160.3	198.7
	PRE	209.9	180.0	154.0	219.2
	MB	10.5	-8.01	-6.4	15.5
	GE	46.3	40.1	62.5	49.5
RH (%)	OBS	64.9	47.7	69.9	55.5
	PRE	63.6	39.7	55.3	39.3
	MB	-1.4	-8.0	-14.6	-16.2
	GE	19.2	16.0	20.0	20.5

Table 4 Performance statistics of WRF meteorology predictions for January, March 2013 and August, October 2012.

* OBS: mean observation. PRE: mean prediction. MB: mean bias. GE: gross error

3.3.2 Regional distribution of SNA

Five simulations are conducted for the purpose of this study. The base case simulation S1 uses the default CMAQv5.0.2 configuration. Enhanced nitrate formation due to faster NO_2 surface uptake reaction is tested in the second set of simulation S2. Previous studies have explored the response of SNA to precursor emission changes (Wang et al., 2013). They found that composite SNA levels did not respond linearly to SO_2 or NO_x emission changes, while NH_3 plays an important role in determining total SNA concentrations. Thus, in the third set of simulation (S3), NH_3 emissions are scaled to determine the sensitivity of NH_3 emission on SNA concentration. Modifications made in S2 are also adapted in S3. SO_2 heterogeneous reactions are added in the fourth simulation S4, in addition to all the changes made in S3. In the last simulation S5, updated Fe and Mn concentrations obtained from EC/Fe and EC/Mn relationships (see Fig. 9) are incorporated, in addition to all the changes in S3 adopted. SO_2 heterogeneous reaction is not included in this set of simulation.

Figure 10 shows the regional distributions of January average $PM_{2.5}$ nitrate, sulfate, ammonium and mass concentrations. The first row presents the concentrations of these species from the base case simulation S1. Wide spatial distributions are found for nitrate, sulfate and ammonium. In East and Southwest China, nitrate concentration is more than 10 $\mu g/m^3$, and high concentration of ~30 $\mu g/m^3$ occurs in Central China. The most polluted areas caused by sulfate are located at North China Plain (NCP) and Northeast China, which also are the regions of most intensive industrial activities in China. Generally, by looking at the $PM_{2.5}$ mass concentration in S1, most $PM_{2.5}$ pollution in China occurs at the middle,

east and southwest part of China. The increase of concentration due to higher value of NO_2 uptake coefficient (from $7x10^{-7}$ to $1.5x10^{-4}$) relative to base case simulation is shown in the secondary row of Fig. 10. Nitrate concentration gets increased significantly especially in the NCP and Northeast China, while the maximum increase reach up to ~ 20μg/m^3. Sulfate and ammonium concentrations increase slightly by less than 5 μg/m^3. Increasing the NH_3 emissions by a factor of 3 (S3) leads to significant increase of the nitrate concentration throughout the domain, as shown in the third row of the figure. The maximum nitrate increase, compared to the base case, can reach up to 50 μg/m^3 in Central and NCP of China. NH_4^+ concentration increases by 5-10 μg/m^3 and has a very similar regional distribution with nitrate. However, SO_4^{2-} concentration doesn't change significantly. This is because gas phase sulfuric acid condenses onto particles quickly and completely even without NH_3 due to very low surface vapor pressure of sulfuric acid. The additional NH_3 reacts with nitrate acid to form less volatile NH_4NO_3 aerosol. In S4, the heterogeneous reaction of SO_2 leads to increased sulfate concentration up to 30-40 μg/m^3 in Central China and in Sichuan Basin, where emission rates are high. NH_4^+ also increases more than that in S3 in Central China, as additional NH_3 is partitioned into the particle phase to form ammonium sulfate. Spatial distribution patterns and concentrations predicted in S5 are similar to those predicted in S4 for all the four species. For the total $PM_{2.5}$ mass concentration, the change is mostly due to the combined variation of SNA, and can be as high as 100 μg/m3 comparing to base case (S1).

The results for other seasons are shown in the Appendix. Fig. S-2 shows that SNA concentrations are relatively lower in March than those in January and are not as broadly

distributed. Higher nitrate formation from the NO_2 heterogeneous reaction only leads to an increase of NO_3^- concentration by up to 10 μg/m^3 (S2). When NH_3 emission is increased by 3 times, NO_3^- concentration increases more significantly but sulfate and ammonium concentrations only increase slightly. Lower $PM_{2.5}$ concentration leads to less aerosol surface area, and more vertical mixing is available in March than in January. Both lead to lower nitrate concentration. The differences between S4 and S5 and the base case are also small, based on the regional distribution plot. In August (Fig. S-3), SNA concentrations are even lower and show less broad regional distribution. The decrease of secondary inorganic PM components is due to enhanced mixing and more frequent rainfall during summertime, as discussed in the first part of the study. Compared with the base case simulation results, only slight changes of NO_3^- and NH_4^+ concentrations can be noticed in the NCP area, indicating that heterogeneous reactions may not be an important pathway for secondary aerosol formation in summer time due to lower available particle surface area and NO_2 concentrations (S3). Gas-phase and aqueous-phase chemistry play more important roles in the formation of SNA in summertime. Fig. S-4 shows the result of the October, 2012 simulation, and the regional distribution patterns of SNA are similar to that of March for the base case simulation. The highest nitrate concentration occurs in NCP and Sichuan Basin, while sulfate and ammonium ion have relative consistent concentrations throughout the most East, Central and South China with an average concentration of approximately 15 μg/m^3 and 5 μg/m^3, respectively. SO_2 heterogeneous reaction (S4) and using Fe (III) and Mn (II) from EC correlations (S5) lead to largest increase of SNA and $PM_{2.5}$ mass concentrations from the base case simulation.

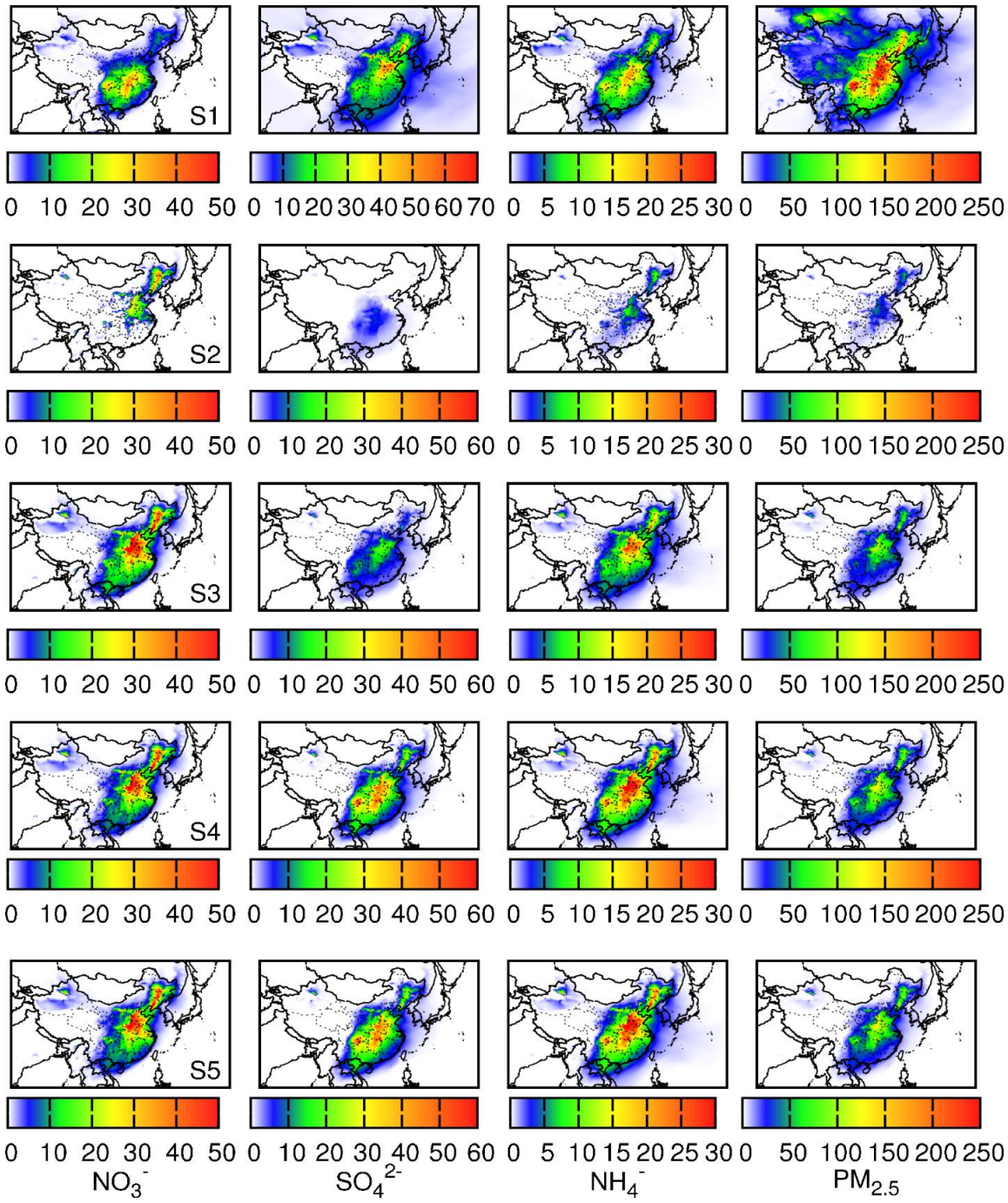

Figure 10 Regional distribution of nitrate, sulfate, ammonium and $PM_{2.5}$ mass concentration in Jan. The first row (S1) shows the concentration in base case simulation and from 2nd to 5th row (S2-S5), the plots represent the differences (Sx-S1) between each simulation and the base case simulation. Units are $\mu g/m^3$.

3.3.3 Model performance analysis

In this section, predicted January $PM_{2.5}$ nitrate, sulfate, ammonium and mass concentrations in Beijing are compared with observations made at BUAA.

The base case simulation (S1) underestimates NO_3^- and NH_4^+ concentration significantly on most days. For sulfate and $PM_{2.5}$ mass concentration, the model prediction agrees better with observations and the day-to-day variation is also captured on most days. With increased NO_2 heterogeneous reaction rate in S2, nitrate concentration gets significantly increased by 10-50 $\mu g/m^3$ and shows better agreement with observations. It should be noticed that the spatial variation of NO_3^- is more distinct than other species, which is likely caused by the large variations of NO_2 emission within the surrounding areas of Beijing. NH_4^+ concentrations also get increased but still are lower than observations, indicating that most NH_3 in the gas phase has been used in the base case simulation to form NH_4NO_3 aerosol. Additional NO_3^- from heterogeneous reaction cannot lead to more NH_4^+ formation from gas-to-particle portioning of NH_3. It is likely that NH_3 emission is underestimated near Beijing. In S3, NH_3 emission is increased by a factor of 3, and the NH_4^+ prediction gets significantly better in terms of both daily average concentration and day-to-day variations. NO_3^- , SO_4^{2-} and $PM_{2.5}$ mass concentrations are also increased. In S4, including the SO_2 heterogeneous reaction in addition to NO_2 heterogeneous reaction and three times NH_3 emission increase lead to higher concentrations of SO_4^{2-} in some periods (January 10-13; January 17-20). On the rest of the days, sulfate concentrations are comparable with those in S3. This change does not significantly increase the NO_3^-, NH_4^+ and $PM_{2.5}$ mass concentrations. Applying the concentration of Fe(III)/Mn(II) derived from their

relationships with EC over-predicts SO_4^{2-} concentration on most days although the model captures the trend of daily variation correctly. The results imply that while this is an important pathway of sulfate formation, more data sets on EC-Fe(III) and EC-Mn(II) are needed to improve the predictability of Fe and Mn concentrations from EC, which might be location or season specific. Sulfur tracking analysis indicates that in January, O_2 oxidation pathway catalyzed by Fe^{3+}/Mn^{2+} is the most important pathway to form sulfate, accounting for more 90% contribution (see section 3.3.5).

In March (Fig. S-5), all four species (SNA and $PM_{2.5}$ mass) show relatively uniform spatial distribution in Beijing and surrounding areas. The base case simulation under-predicts SNA concentration significantly, approximately by 10-50 $\mu g/m^3$. Increasing NH_3 emission by three times and increasing the NO_2 uptake coefficient (S3) lead to better simulation performance on NO_3^- concentrations, while NH_4^+ and SO_4^{2-} concentrations are still get underestimated. In S4, including SO_2 heterogeneous reaction further increases sulfate and ammonium concentration simultaneously especially on peak days, although the peak SO_4^{2-} concentrations are still over-predicted (S4). In S5, the Fe/Mn-EC correlation approach leads to much better prediction of SO_4^{2-} concentrations, indicating the potential feasibility to applying this approach to improve SO_4^{2-} model performance when accurate emissions of Fe and Mn are available.

In August (Fig. S-6), the results are evaluated between August, 10^{th} and August, 20^{th}, during which the observations are available. The base case CMAQ simulation still underestimates SNA and $PM_{2.5}$ mass concentration (S1). Faster NO_2 heterogeneous reaction and higher NH_3 emissions increase NO_3^- and NH_4^+ concentration (S3). However,

the differences between S3, S4 and S5 are not significant and the additional changes applied cannot explain the high SO_4^{2-} concentration observed on August 17-19. In summer, precursor concentration of SO_2 and NO_2 are relatively lower compared to January since there are less emission from residential sources. Sulfur tracking analysis (Fig 12), which will be shown in the following discussion, indicate that O_2 Fe/Mn oxidation pathway makes insignificant contribution to the total SO_4^{2-} in summer concentration so the modification this approach has limited impact on the predicted SO_4^{2-} (see section 3.5.5).

Large spatial gradient of NO_3^- concentration in fall (9/15-10/21) can be seen in Fig. S-7. The model is able to capture the day-to-day variations of SNA and $PM_{2.5}$ mass concentrations in all simulations. Predictions in S3 agree with observations quite well, with a slight overestimation of NO_3^-. Including SO_2 heterogeneous reaction (S4) increases SO_4^{2-} on some of the peak days. It should be noted that the result difference between S3 and S5 is very small, which suggests the predicted Fe(III) and Mn(II) concentrations in S3 are very similar to those derived values based on statistical relationships with EC during this episode.

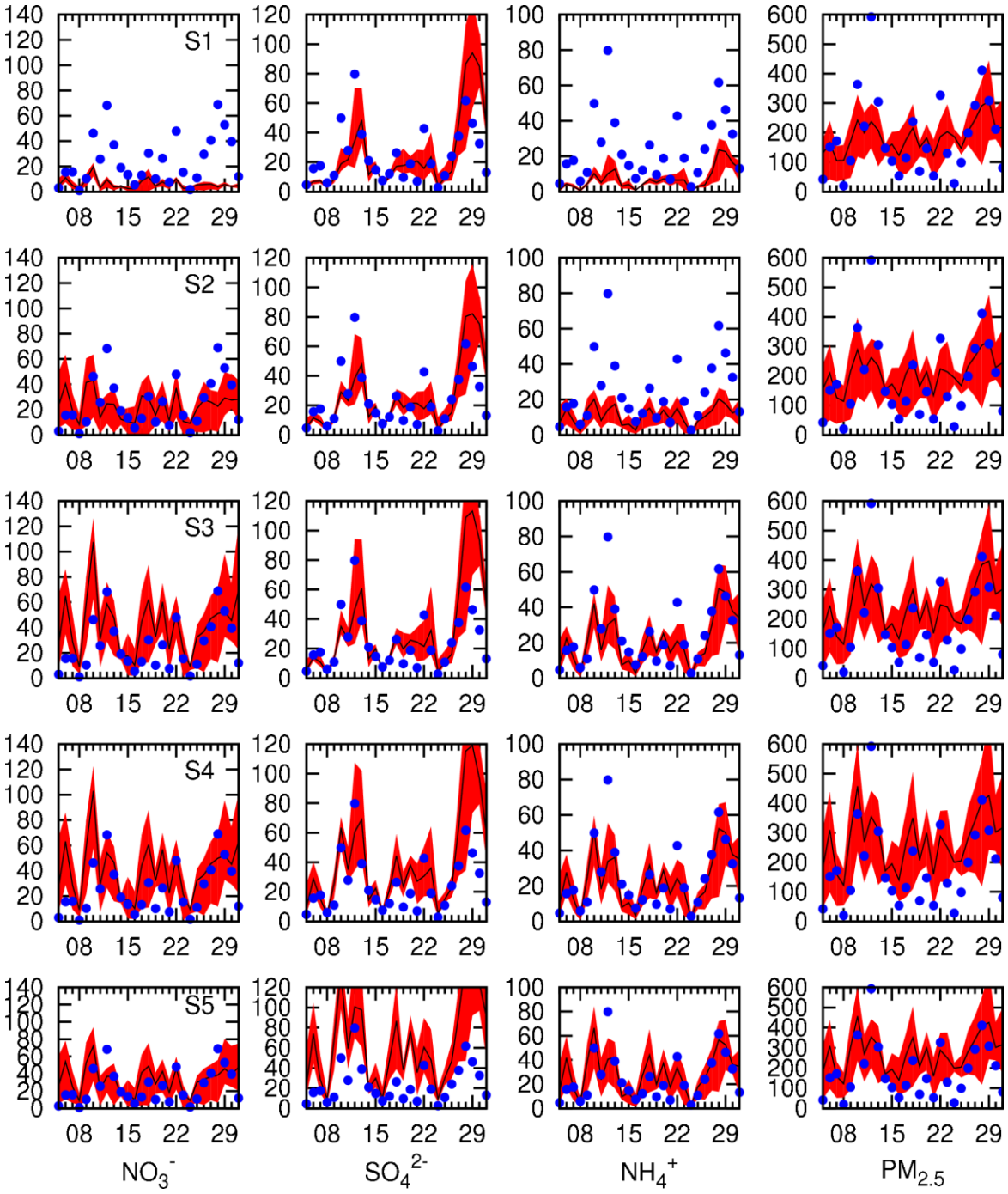

Figure 11 Time series of predicted and observed concentration of January, 2013 nitrate, sulfate, ammonium ions and $PM_{2.5}$ mass concentration of 5 sets of simulations in Beijing. Blue dots are observation data and red shaded area is the range of concentrations in the 3x3 model grid cells centered on the observation site in Beijing. Solid black line is the average of concentrations of the 9 grid cells. From top to bottom are simulations 1 to 5, respectively. Units are $\mu g/m^3$.

3.3.4 Statistical model performance evaluation

Performance statistics are shown in Table 6, Mean Fractional Bias(MFB), as calculated in equation 4, is used to evaluate the model performance on SNA and $PM_{2.5}$ in all simulations, which is recommended as one of the key statistical performance measures by (EPA, 2007). In this guidance, a satisfactory performance is indicated by an MFB within ± 60% base on Boylan and Russell (2006).

$$MFB = \frac{1}{N}\sum_{i=1}^{N}\frac{(C_m - C_o)}{\left(\frac{C_o + C_m}{2}\right)} \quad (4)$$

MFB for predicted $PM_{2.5}$ mass concentrations are less than 50% for almost all sets of simulations. For all seasons, base case concentrations of SNA are under-predicted, except for NO_3^- and SO_4^2 in fall. NO_3^- is mostly overestimated especially after introducing the heterogeneous reaction of SO_2 and increasing the NH_3 emission. Generally the second set of simulation (S2) gives the best performance except for fall results. In fall, base case simulation already has a good simulation performance with a MFB of 4.1%. Sulfate in January and fall season are mostly over-predicted in base case and the introduction of NO_2, SO_2 heterogeneous reactions further lead to higher over-estimation. In March and August, when sulfate concentrations are under-predicted in base case, the heterogeneous reaction together with the increase of NH_3 emission can bring better agreement with

observations. The influence of Fe/Mn modification is also seasonal dependent. In January it bring the largest over-prediction, but for the rest of the season, it leads to better performance compared with other simulations. NH_4^+ is mostly underestimated in most simulations of different episodes and the worst case is in March with a MFB of -161.9%. All the modifications (S2-S5) increase the NH_4^+ concentration and the trend of growth implies strong corresponding effect with sulfate increment.

Season	Simulation	NO_3^-	SO_4^-	NH_4^+	$PM_{2.5}$
Jan	S1	-90.9%	-7.8%	-108.9%	22.7%
	S2	17.1%	2.8%	-61.5%	33.3%
	S3	64.0%	16.4%	-12.9%	45.5%
	S4	62.1%	42.4%	-2.45%	48.23%
	S5	48.3%	88.21%	21.05%	54.62%
March	S1	-63.9%	-109.9%	-161.9%	24.3%
	S2	-24.9%	-86.7%	-106.2%	31.7%
	S3	13.5%	-82.3%	-74.6%	40.3%
	S4	12.8%	-42.0%	-58.9%	43.4%
	S5	10.8%	-6.9%	-42.1%	46.7%
August	S1	-35.4%	-16.9%	-36.0%	-12.1%
	S2	0.1%	-23.5%	-23.5	-9.6%
	S3	43.2%	-21.87%	-0.2%	2.7%
	S4	42.9%	-8.7%	5.4%	5.2%
	S5	43.1%	-19%	1.2%	3.32%
Fall	S1	4.1%	9.2%	-34.0%	27.1%
	S2	68.7%	26.0%	13.0%	41.7%
	S3	99.4%	30.9%	35.3%	51.3%
	S4	98%	55.4%	43.7%	54.0%
	S5	99.4%	34.0%	36.2%	52.0%

Table 5 Mean fractional bias (MFB) of $PM_{2.5}$ mass, nitrate, sulfate and ammonium for January in Beijing.

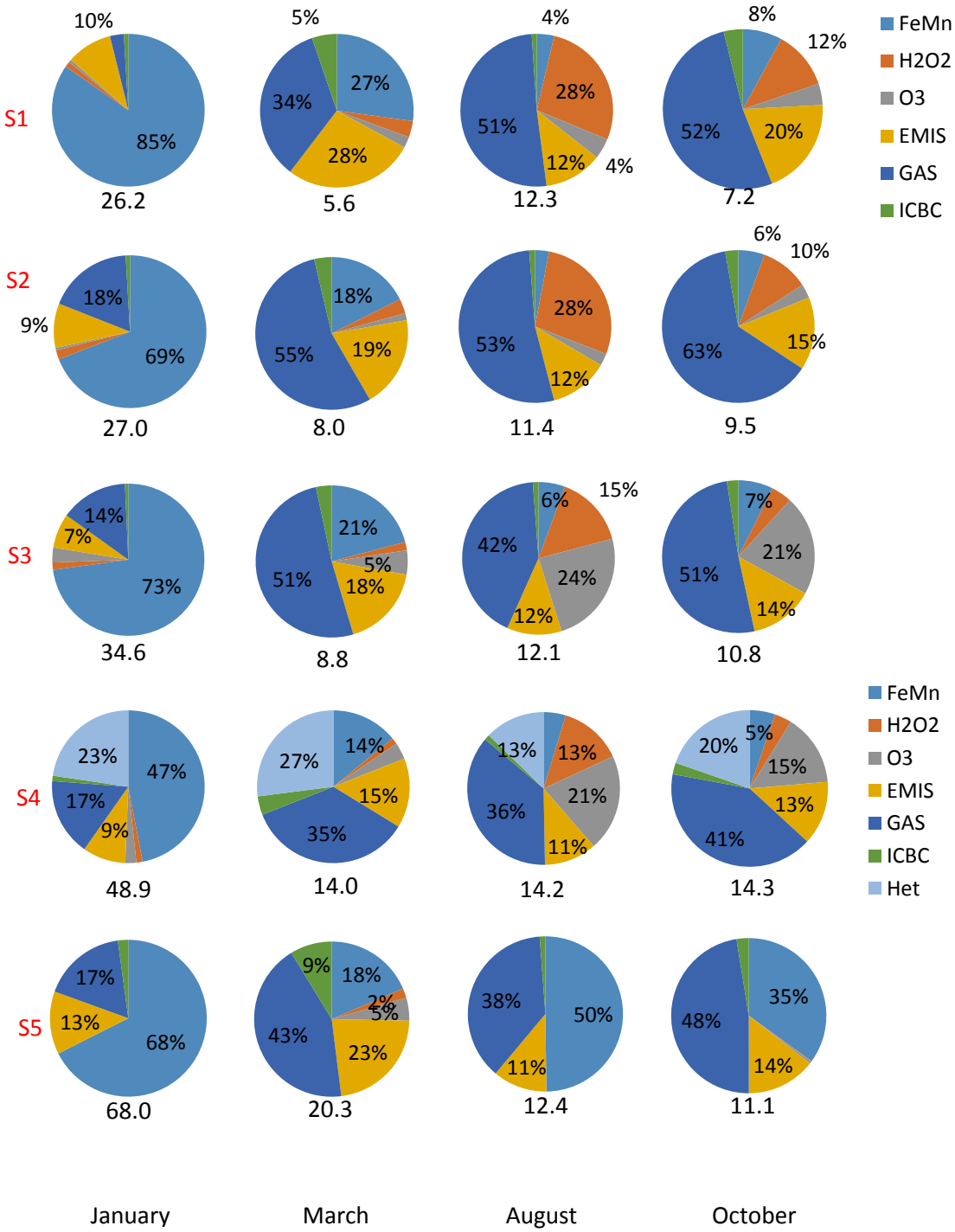

Figure 12 Monthly average SO42- concentration in Beijing and relative contributions from each pathway for simulations sets S1 to S5. Predicted SO_4^{2-} concentration is under each pie plot. Units are $\mu g/m^3$. The percentage contributions of main pathways are marked.

3.3.5 Sulfur tracking

Sulfate formation from different pathways are separately tracked in the simulations to determine the importance of these different pathways, as shown in Fig. 12. In January, Fe/Mn catalyzed oxidation is the dominant formation pathway, accounting for approximately 70% or more total sulfate formation in all simulations except for S4 which includes the SO_2 heterogeneous reaction.

The importance of gas phase pathway increases from negligible to approximately 15-20% when NO_2 heterogeneous reaction is included because the additional NO_2 lost on aerosol surface reduces OH loss via NO_2+OH reactions, and higher OH concentrations lead to higher sulfate formation from the gas phase oxidation pathway. Approximately 10% of the sulfate is due to primary emissions.

In other seasons, gas phase chemistry is the most important contributor since higher temperature atmosphere and stronger solar radiation are favorable for the gas phase oxidation pathway. The total sulfate concentrations are significantly lower than those in January and primary sulfate emission becomes another important source with a fraction of contribution ranging from ~10% to ~25%. Aqueous oxidation by H_2O_2 and dissolved O_3 oxidation can also generate a large amount of fractional contribution in summer and fall while O_2 oxidation by Fe/Mn is more important in spring. The analysis on simulation 4 indicates the amount of sulfate generated through heterogeneous reaction is significant, contributing to approximately 25% of the total sulfate as a result of competing with gas phase and Fe/Mn oxidation pathways for SO_2 emission. In simulation 5, adopted Fe/Mn

concentration from EC relationship increase this pathway's impact on the total sulfate formation. For example, summer sulfate in other simulations has little fraction of Fe/Mn catalyzed oxidation contribution (less than 5%), but in S5, the contribution is increased to about 50%.

3.4 Conclusions

CMAQ 5.0.2, a most recently updated version, is applied to simulate PM2.5 nitrate, sulfate, ammonium and mass concentration in China in four seasonal episodes. Four sets of sensitivity sets of simulations, along with sulfur tracking analysis, are conducted to study the NO_2 and SO_2 heterogeneous reactions' impact on aerosol concentration prediction and the potential to improve SO_4^{2-} simulation performance by using statistically derived Fe/Mn-EC correlations. The results have shown that, all base case simulations, without heterogeneous reactions of SO_2 and NO_2, under-predict SNA concentration in all four seasons. Increasing NO_2 heterogeneous reaction coefficient leads to increasing NO_3^- and NH_4^+ concentration significantly. Heterogeneous reaction of NO_2 alone cannot explain the under-prediction of ammonium ion and increasing NH_3 emission by 3 times lead to better predictions. Increasing of NH_3 emissions also leads to increase in predicted NO_3^- and NH_4^+ concentrations, indicating the original emission of NH_3 is not correctly represented and NH_4^+ is a limiting factor in forming NO_3^- and SO_4^{2-} aerosols. SO_2 heterogeneous reactions can significantly increase predicted SO_4^{2-} concentration. The difficulty in applying the SO_2 heterogeneous reaction is the uptake coefficient, which is not well understood. In this study, all uptake coefficients are set as a constant number regardless of the seasonal and topographical variation, and the aerosol composition.

Modifying Fe/Mn concentration obtains good simulation performance in March simulations by significantly increasing the predicted total sulfate concentrations, but in August and October, it does not change the total sulfate concentration significantly. Although the importance of this pathway is increased in those two months, total sulfate concentration does not change and the importance of other aqueous pathways is significantly reduces, suggesting the aqueous pathways are limited by the solubility of SO_2 in these months. In summary, in highly polluted areas and episodes such as those experienced in China recently, heterogeneous chemistry is an important pathway to explain the inorganic aerosol formation. The reaction rate and applicable condition in heterogeneous chemistry need further study.

4. THE REGIONAL DISTRIBUTION AND SOURCE CONTRIBUTION TO PRIMARY $PM_{2.5}$ IN CHINA

Primary PM accounts for a significant fraction of $PM_{2.5}$ mass concentration in China, especially during wintertime when secondary PM formation is relatively low due to slower photochemical reactions. Carbonaceous components, such as elemental carbon (EC) and organic matter (OM) account for a significant fraction of primary PM. Even though the contributions of trace elements to primary PM mass are not significant, they can have significant adverse public health effects (e.g. cadmium and lead) and actively participate in aerosol chemistry (e.g. iron and manganese) that leads to formation of secondary PM. While previous researches using receptor models provide useful information on the sources of primary PM in locations where the measurements are taken, spatial distribution, source contribution and regional transport of primary PM cannot be determined. In this part of the study, the contributions of sources and source regions to primary PM pollution are quantitatively determined by applying a source-oriented CMAQ model.

4.1 Mechanism description

A source-oriented CMAQ model for primary PM (CMAQ-p) is applied to determine the source apportionment of primary PM. The general concept behind the source-oriented CMAQ is to track the emissions, transport, chemical and physical transformation and dry/wet deposition processes of gaseous and particulate air pollutants from multiple emission sources independently. In the CMAQ-p model, the total primary $PM_{2.5}$ mass

concentration from a number of PM emissions sources are tracked using source-specific tracers for their advection, diffusion, and dry/wet deposition of primary PM in the atmosphere. The concentrations of chemical components in primary PM are not explicitly simulated by the model. Instead, once the concentration of the primary $PM_{2.5}$ mass from each source are determined, the concentration of primary PM components can be determined during the post-process stage, using source specific emissions profiles as shown in Equation 5

$$C_{i,j} = A_{i,j} T_i \tag{5}$$

where $C_{i,j}$ represents the concentration of the j^{th} chemical component from the i^{th} particle emission category. A is the source profile matrix so that $A_{i,j}$ represents the mass of the j^{th} chemical species per unit mass of PM emitted from the i^{th} emission source. T_i is the model predicted particle mass concentration for the i^{th} source.

This technique is further expanded to track primary PM emissions from different source regions, similar to the technique described in Section 3.1. In this case, total number of $PM_{2.5}$ tracers will be N*M where N is the total number of sources and M is the total number of source regions.

4.2 Model application

The model domain, emission and meteorological inputs are identical to the previous study. Since the purpose of this part is to study the source apportionment of primary PM, the

default secondary aerosol formation chemistry in the CMAQ model is used, and the changes discussed in the previous chapter are not applied. Emission is generated based on the MEIC inventory, and primary $PM_{2.5}$ emission from 5 sources (1: Residential; 2: Transportation; 3: Power; 4: Industries; 5: Open burning) and eight regions or cities of China (1: Beijing; 2: Hebei; 3: Northeast; 4: Northwest; 5: Central; 6: Southeast; 7: Southwest; 8: Shanghai) are individually tracked in the model simulation. Fig. 13 shows the designation of each source region in the model domain.

Primary PM emissions from windblown dust and sea salt are calculated online and are tracked separately from other sources. However, their emissions are not region-specific.

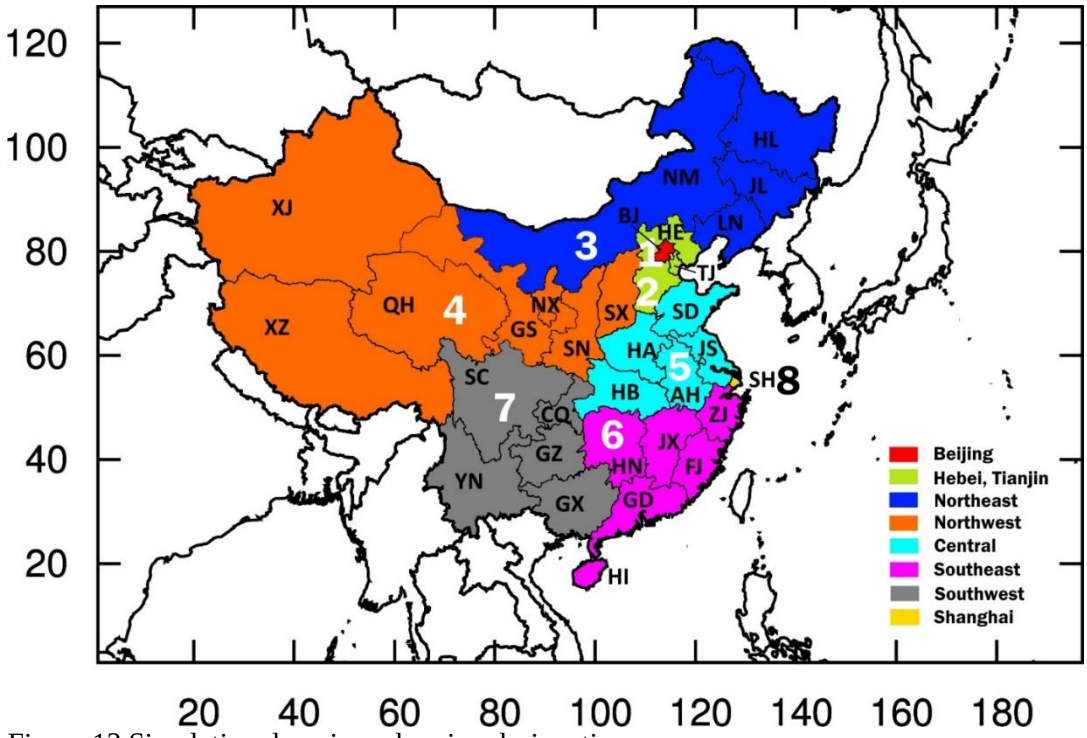

Figure 13 Simulation domain and region designation.

4.3 Results and discussion

4.3.1 Primary PM by source

Fig. 14 shows the spatial distribution of primary $PM_{2.5}$ in January from each source. Residential sector is the most important source of primary PM pollution in East, Central and South China. High concentration occurs in the NCP, Northeast and Central China and in Sichuan Basin with a monthly average of 70 $\mu g/m^3$. Another important source of emission is industrial activities, which can result in up to ~20 $\mu g/m^3$ in Central China and NCP. Primary $PM_{2.5}$ from vehicle exhaust and power plants are relatively low, with concentrations less than 5 $\mu g/m^3$ in the whole domain. The peak contribution of windblown dust to primary $PM_{2.5}$ occurs in Northwest China, where windblown dust from the Gobi desert and other dust source regions contribute to a maximum $PM_{2.5}$ concentration of ~15 $\mu g/m^3$. Open burning (include forest fire and agriculture burning) only contributes to the primary a small fraction of primary $PM_{2.5}$ in Southwest China.

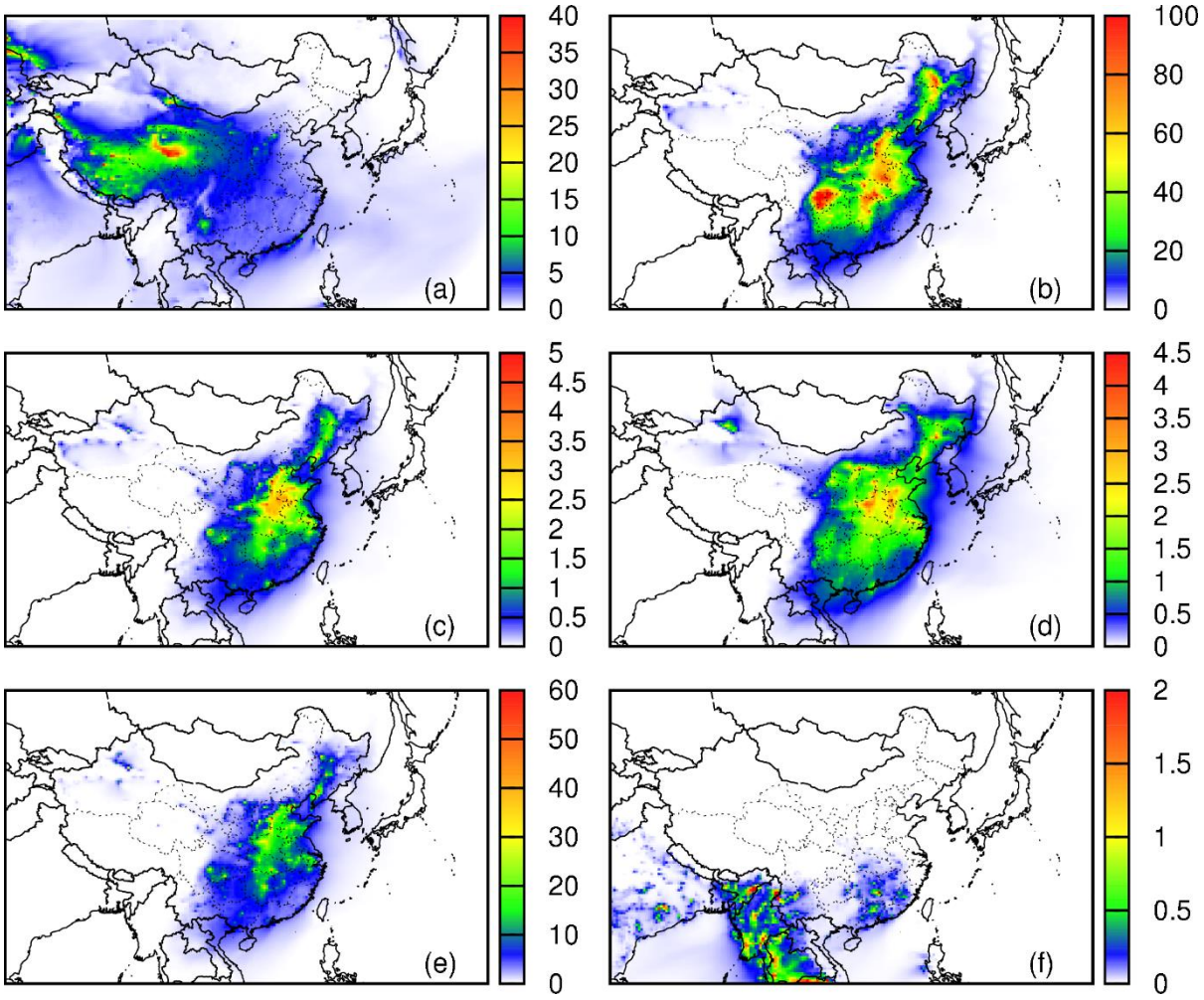

Figure 14 Regional distribution of source contributions to primary $PM_{2.5}$. Panel (a) - (f) represent primary $PM_{2.5}$ concentrations due to (a)dust, (b)residential, (c)transportation, (d)power plant, (e)industry and (f)open burning emissions, respectively. Units are $\mu g/m^3$.

Fig. 15 illustrates the spatial distribution of primary PM in January originated from each region. Contributions of different sectors in the same region are combined. Compared to secondary PM pollutants, primary aerosol shows less inter-regional transport and the concentration in a region is more likely influenced by local emissions within the region.

In contrast, precursors of secondary PM take longer time to be converted to secondary PM and thus secondary PM can be transferred over longer distance (Ying and Kleeman, 2009). All Northern regions of China (region1, 2 and 3) suffer high pollution of primary PM in winter due to residential heating and industrial activities. Southwest (region 7) also shows high concentrations mostly due to population density and geographical conditions that limit the dispersion of air pollutants. Fig. 15 shows that the total primary PM in Central, East and NCP of China has a monthly average of ~50 $\mu g/m^3$, which exceeds the Chinese Ambient Air Quality Standard (CAAQS), Grade II (35 $\mu g/m^3$) for $PM_{2.5}$ annual concentration.

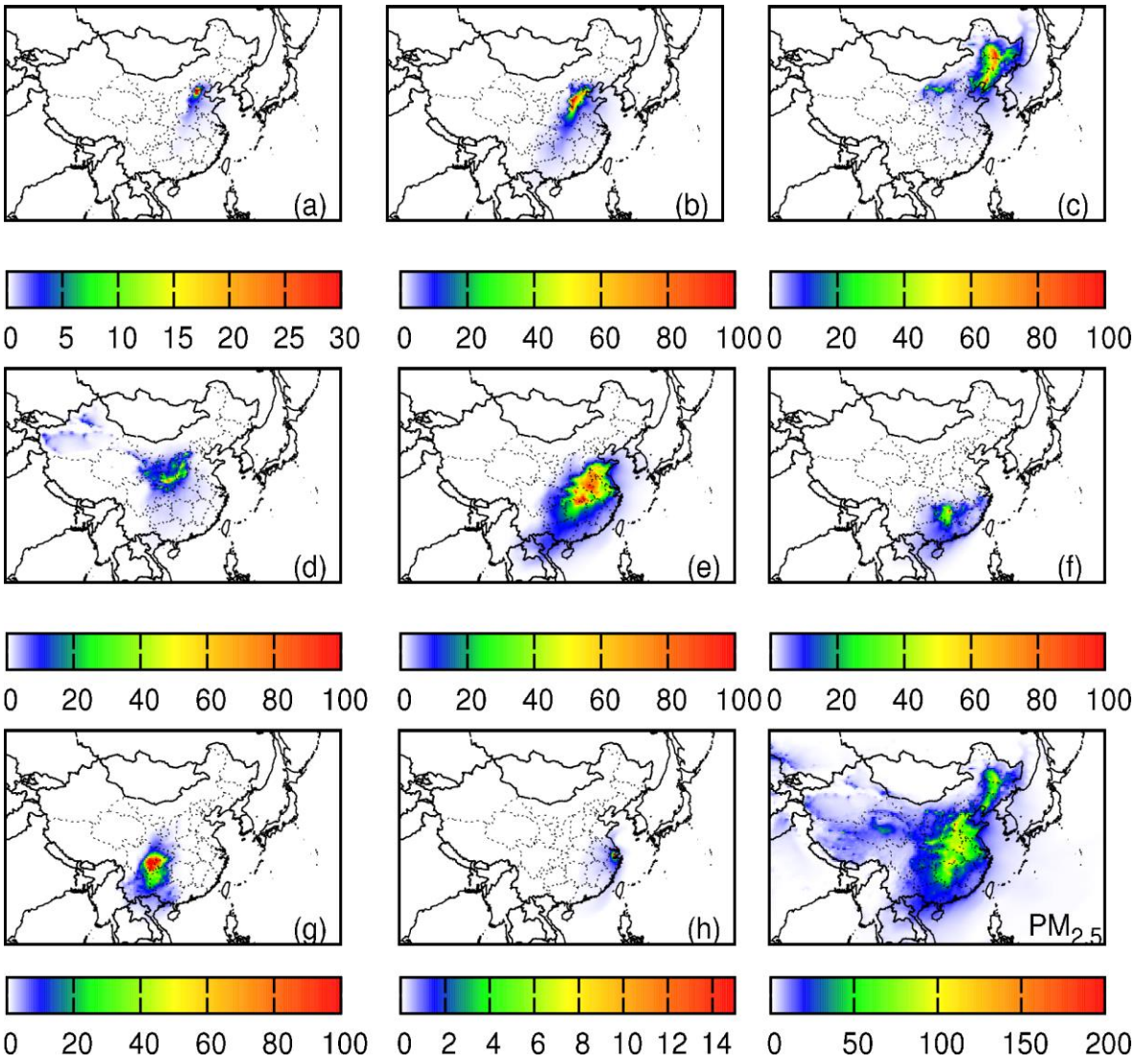

Figure 15 Regional distribution contributions to primary $PM_{2.5}$ concentration from different source regions. Panels (a) - (h) represent contributions due to regions 1 to 8 respectively. The bottom right panel shows the total primary $PM_{2.5}$ concentration. Units are $\mu g/m^3$.

In summer, less primary PM is emitted from residential sources resulting in monthly average concentrations less than 15 μg/m^3. Transportation and power plant contributions are still lower than other sources. The most significant emission source is industrial activities, which leads to as much as 20 μg/m^3 in the NCP area. Dust emissions from the Gobi desert regions in West China lead to high PM concentration but its influence is limited in the North and West China. Open burning impact is higher in summer-time in Southeast China with a maximum concentration of ~4 μg/m^3.

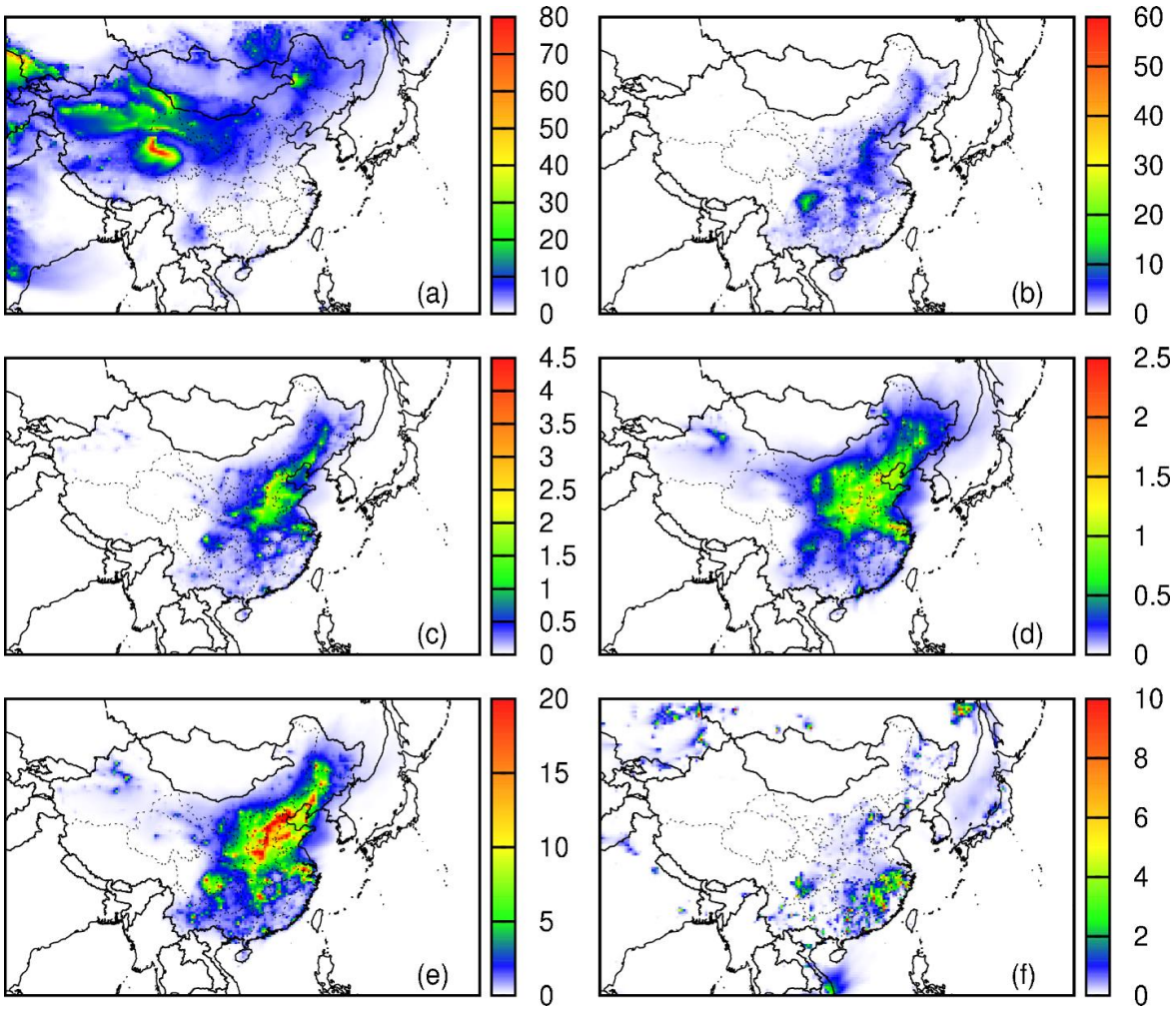

Figure 16 Similar result as Fig. 13, but for August. Units are μg/m^3.

Fig. 17 shows the spatial distribution of primary $PM_{2.5}$ in August from each region. Lower concentrations from all source regions and less inter-regional transport are found throughout the domain. This can be explained by the western Pacific subtropical high that reduces air motion and removal of particulate matter due to more frequent wet deposition in summer. The highest concentration occurs in Southwest China with a maximum concentration of 20 $\mu g/m^3$. Other regions such as Northern and Central also have high concentration of Primary PM with an average concentration of ~15 $\mu g/m^3$ and ~10 $\mu g/m^3$. Total primary $PM_{2.5}$ is generally under 50 $\mu g/m^3$. Results for other season can be found in Appendix and are not fully discussed here.

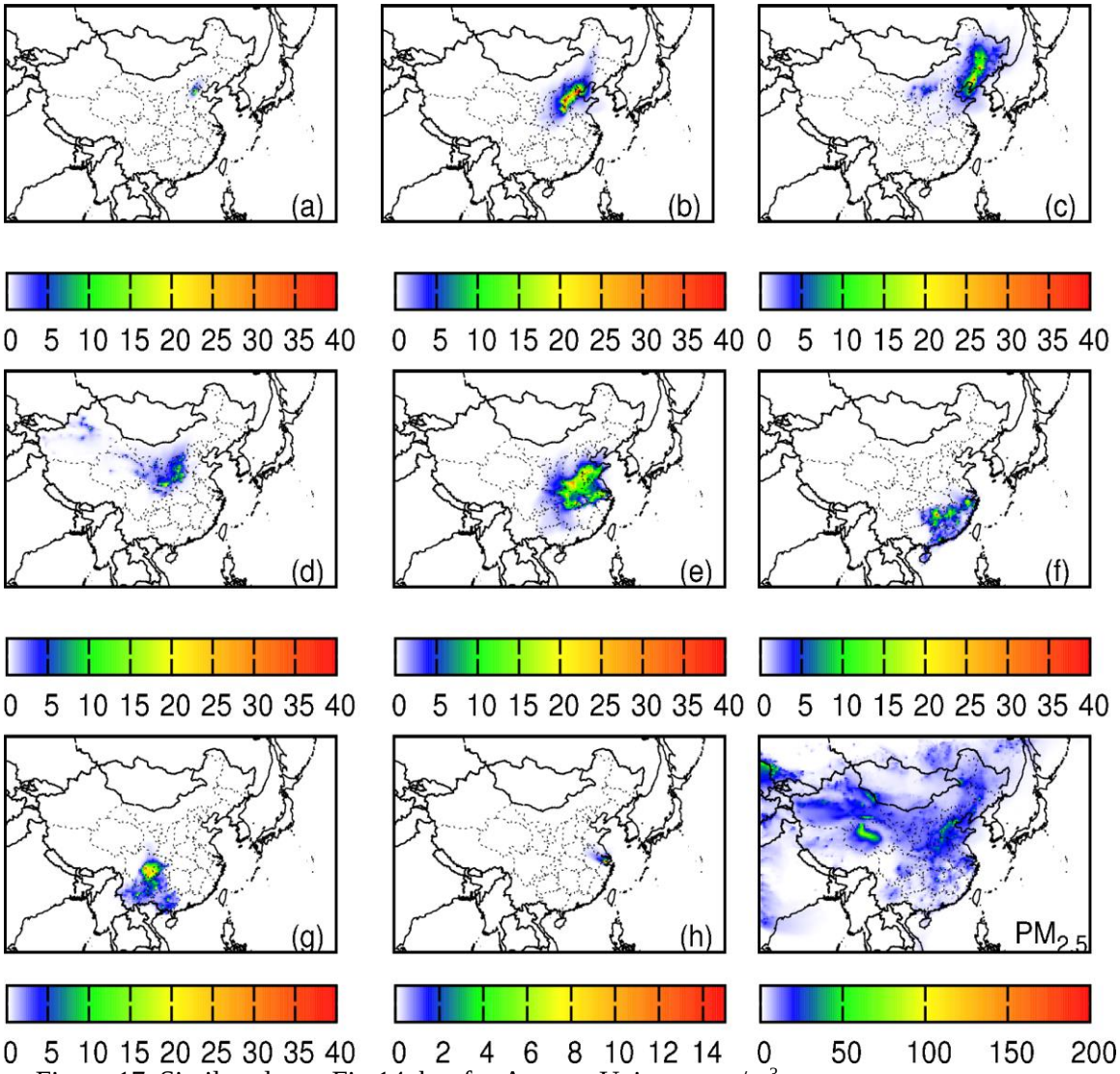

Figure 17 Similar plot as Fig 14, but for August. Units are μg/m^3.

4.3.2 Relative contribution to Primary $PM_{2.5}$ concentration in Beijing and Shanghai

Fig. 18 shows the relative contribution to primary PM in Beijing and Shanghai from individual sources and regions. Since there are six source sectors and eight regions, 6 x 8 contributors can have an impact on primary PM in every single grid cell to a different

extent. For Beijing, the 9 most important contributors are listed and the rest is summed in the "others" category. In winter (January), more than 40% of the primary PM is from local residential emission Residential emission from local and the Hebei Province combined contribute to more than 65 % of the total primary PM. In spring (March) and fall (October) seasons, frequent sand storm events originated from the desert regions in West China result in the increase of the contribution of windblown dust to primary $PM_{2.5}$. Residential emissions in spring, summer and fall are much lower than those in winter. Industrial activities in Hebei have significant impacts in all months, with contribution to primary $PM_{2.5}$ ranges from 30% to 45%. In order to improve the air quality of Beijing, a lot of industries have been moved to Hebei Province. However, the above analysis suggests that this approach is not sufficiently effective since emissions from Hebei's industries eventually can affect Beijing air quality at a great degree especially when the meteorological condition is favorable to inter-regional transport.

Eleven major source contributors are listed for primary $PM_{2.5}$ in Shanghai and the rest contributors are grouped into the "others" category. Unlike Beijing, local industry is the most important contributor in all seasons, with contributions ranging from 35% to 60%. The second largest contribution of primary PM is dust emission especially in spring and fall. Contributions from residential emission (5%-20%) are significantly lower than these in Beijing in most seasons.

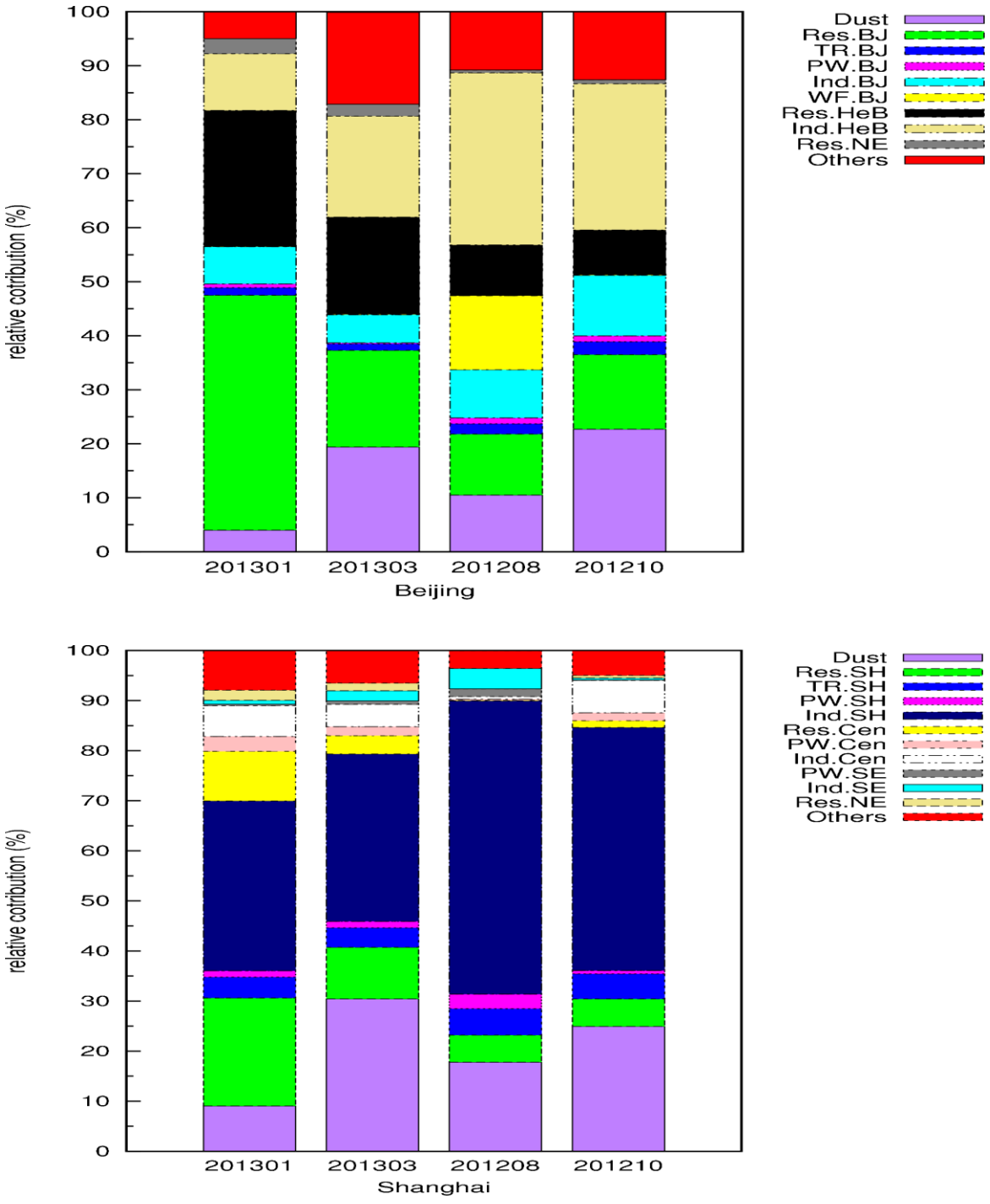

Figure 18 Relative contributions to primary $PM_{2.5}$ from major source/source regions in Beijing and Shanghai in four seasons. (Res=Residential; TR= Transportation; PW= Power Plants; Ind. = Industry; WF= Open burning; SH=Shanghai; BJ= Beijing; Cen.=Central China; SE= Southeast China; NE=Northeast China)

4.3.3 Primary $PM_{2.5}$ components

Concentrations of chemical components of primary $PM_{2.5}$ can be determined using Equation 5. The model performance is strongly dependent on the accuracy of the source-specific $PM_{2.5}$ speciation profiles. In this part of the study, two different sets of $PM_{2.5}$ speciation profiles are used to predict primary $PM_{2.5}$ components. The first approach is to adopt the profiles provided by EPA SPECIATE data base. SPECIATE is the EPA repository of volatile organic and particulate matter speciation profiles of air pollution sources. It is widely used to create speciated emissions inventories for air quality modeling, and also to provide inputs for the chemical mass balance based receptor models. However, studies have shown that fractions of the PM components in primary $PM_{2.5}$ from Chinese sources may be different from those used in the US, thus lead to poor agreement between estimated and observed concentrations.

In the second approach, a multi-linear regression technique was used to determine the fraction of the $PM_{2.5}$ components in primary $PM_{2.5}$ emissions based on minimizing the following objective equations:

$$Q = \sum_{m=1}^{Nd}\left\{W_m\left[\sum_{j=1}^{Ns}\left(A_j S_{j,m}\right) - C_m\right]\right\}^2 \quad (6)$$

For a given primary $PM_{2.5}$ component, C_m is the observed concentration of that component in the m^{th} aerosol sample. $S_{j,m}$ is the model predicted contributions of the j^{th} source to primary $PM_{2.5}$ in the m^{th} sample (see section 4.3.1). A_j is the fraction of the PM component in primary $PM_{2.5}$ from the j^{th} emission source; W_m is the sample-specific weighting factor based on the relative difference

between the observed and predicted primary $PM_{2.5}$ mass concentrations. N_S is the number of emission sources and N_d is the number of samples used in the analysis. The minimization procedure is to find the appropriate A_j values so that Q is minimized, under the constrain that A_j is positive and less or equal to 1. By applying this method, the source-specific fractions for primary $PM_{2.5}$ components available in the BUAA data set are shown in Table 7. For power plant emissions, the fractions of some elements, such as K and Cl^-, in primary $PM_{2.5}$ are very close to one and the sum of all the factors is greater than 1. This is mainly because the contribution of power plant emissions to primary $PM_{2.5}$ mass is very small (see Fig. 12, 16 and 18) and thus could have large uncertainties. Under-prediction of the primary $PM_{2.5}$ mass (which does not significantly affect the total primary $PM_{2.5}$ because it is dominated by residential and industrial sources) could lead to over-estimation of the factors in the profiles from linear-regression that does not impose a constraint on the sum of the fractions for a single source. A total of 84 samples (from all four months) were included in the analysis. Five hundred bootstrap runs using random sampling with replacement were conducted to estimate the uncertainty to the profiles.

Species	Dust	Residential	Transportation	Power Plants	Industries	Open-fire
K	0.023(0.023)	0.019(0.008)	0.006(0.046)	0.988(0.087)	0.092(0.025)	0.003(0.008)
Na	0.011(0.012)	0.012(0.003)	0.008(0.034)	0.274(0.165)	0.016(0.008)	0.002(0.009)
OC	0.079(0.12)	0.717(0.086)	0.321(0.454)	0.176(0.357)	0.264(0.167)	0.295(0.386)
EC	0.025(0.042)	0.159(0.014)	0.073(0.233)	0.009(0.073)	0.255(0.045)	0.122(0.149)
Al	0.030(0.011)	0.001(0.001)	0.017(0.032)	0.167(0.071)	0.001(0.003)	0.003(0.016)
Si	0.084(0.019)	0.001(0.001)	0.017(0.038)	0.224(0.108)	0.004(0.006)	0.005(0.025)
Ca	0.082(0.017)	0.001(0.002)	0.091(0.092)	0.101(0.111)	0.002(0.005)	0.002(0.016)
Ti	0.003(0.001)	0.000(0.000)	0.001(0.003)	0.016(0.008)	0.000(0.000)	0.001(0.004)
Fe	0.015(0.019)	0.001(0.002)	0.005(0.032)	0.685(0.221)	0.023(0.014)	0.003(0.020)
Mn	0.002(0.002)	0.000(0.034)	0.002(0.005)	0.046(0.024)	0.002(0.001)	0.000(0.000)
Cr	0.003(0.035)	0.002(0.000)	0.000(0.000)	0.005(0.002)	0.003(0.036)	0.003(0.035)
Cu	0.001(0.001)	0.001(0.002)	0.001(0.004)	0.012(0.010)	0.002(0.001)	0.000(0.000)
Zn	0.013(0.013)	0.004(0.001)	0.002(0.012)	0.387(0.145)	0.012(0.008)	0.005(0.007)
As	0.001(0.001)	0.001(0.001)	0.000(0.001)	0.010(0.013)	0.000(0.001)	0.001(0.003)
Ba	0.000(0.003)	0.000(0.000)	0.005(0.006)	0.001(0.002)	0.001(0.001)	0.002(0.005)
Pb	0.001(0.003)	0.005(0.002)	0.000(0.003)	0.209(0.079)	0.004(0.005)	0.000(0.000)
Cl^-	0.451(0.117)	0.116(0.027)	0.055(0.195)	0.985(0.114)	0.075(0.072)	0.000(0.000)

Table 6 Speciation profile of primary $PM_{2.5}$ based on multi-linear regression. Numbers in brackets are the standard deviations estimated using bootstrap.

Fig. 19 shows the daily variation of observed primary $PM_{2.5}$ component concentrations and predicted concentrations using the two approaches. Simulation with SPECIATE emission profile has good performance for some of the species such as Ti, EC and Ca. But for the rest species, model is either under-predicting (K, Na, Fe) or over-predicting (Al,Si) to a large scale. Large biases are also found in terms of day-to-day variation. The predictions using the profiles shown in Table 7 have similar model performance for Ti, Ec and Ca but much better performance for all other elements except Mn. In terms of six other trace metals (Cr, Cu, Zn, Pb, Ba, As), which are not included in the SPECIATE profile provided by EPA, their predictions are compared with observations in Fig. 20. The results show that the model that uses the multi-linear regression derived profiles can capture the day-to-day variations for those metals, except for Cr, which is with very low concentration and thus of high measurement uncertainty.

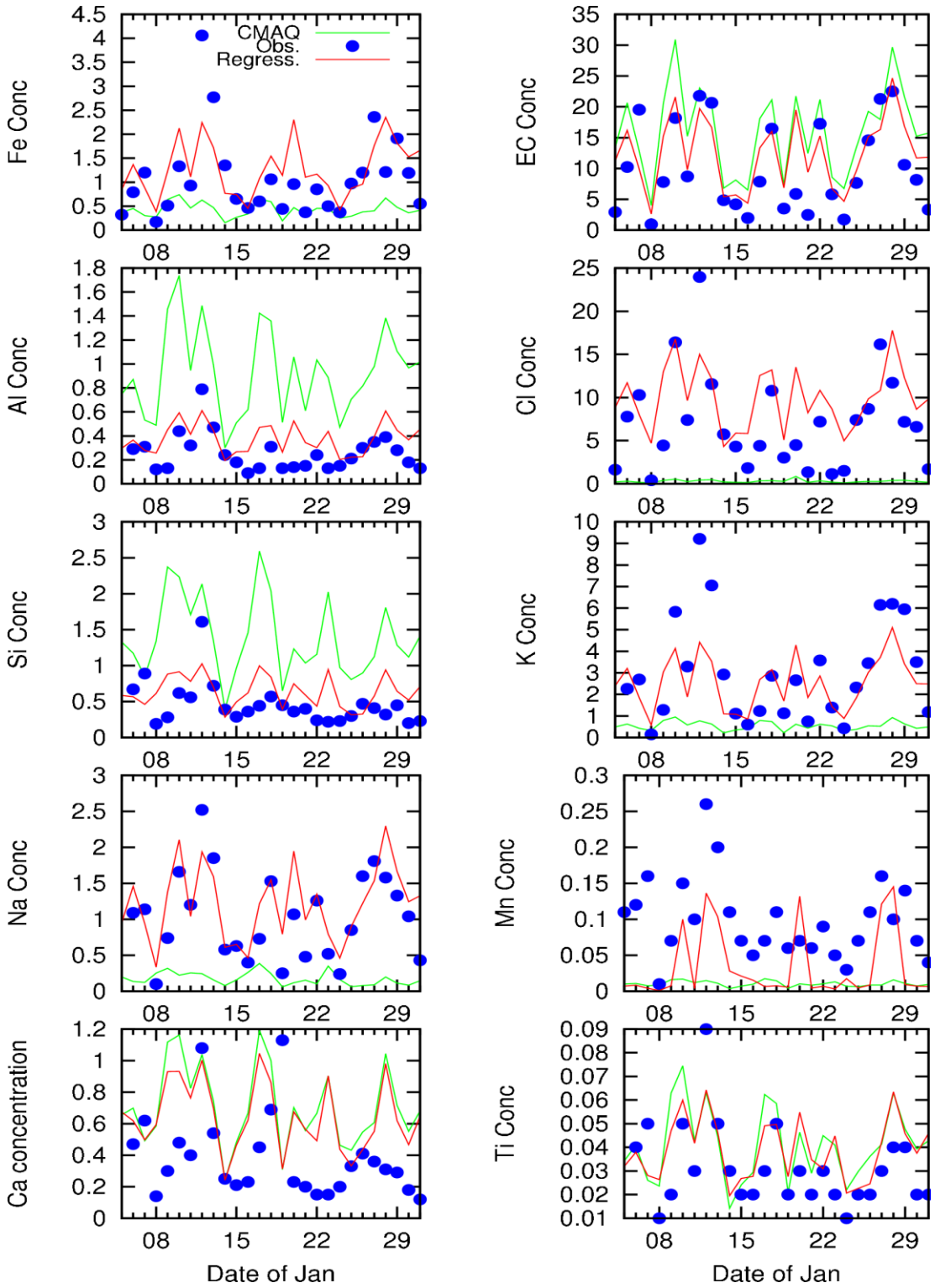

Figure 19 Time series of observed and predicted trace metal concentrations in January 2013. Blue dot represents observation, red solid line shows the prediction using SPECIATE profile and the blue dash line shows the prediction with calculated profile. Units are $\mu g/m^3$.

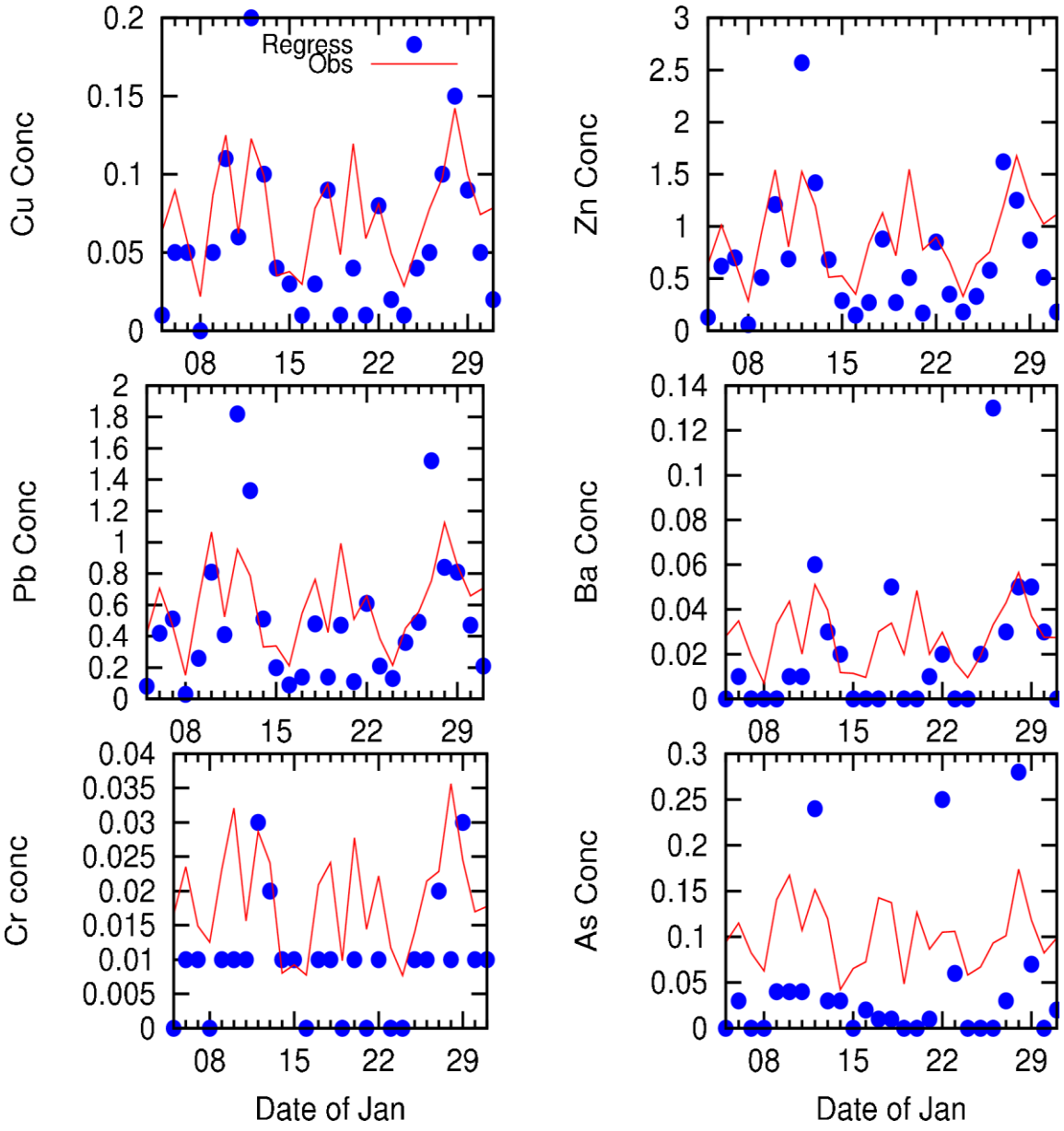

Figure 20 Time series of observed and predicted trace metal concentrations in January, 2013. Predictions from SPEICIATE profiles are not available for these 6 metals. Units are µg/m^3.

Based on the profiles presented in Table 6 and predicted regional source contributions to total primary $PM_{2.5}$ mass concentrations, concentrations of each chemical component in primary $PM_{2.5}$ as well as the contributions to the chemical components due to the 6 sources contributions can be determined. As an example, Fig. 21 shows the spatial distribution of Pb. The concentration of Pb can be as high as 1 $\mu g/m^3$. The highest concentration is in Central, East and North China, which is mainly attributed to power plant (Fig.21 (b)) and residential (Fig. 21(d)). Dust emission could also be an important source in spring and fall, originated from the dust regions in the western part of China. In summertime, it indicates less regional distribution of Pb than it in other seasons. The regional plot of some other chemical components included EC, Fe and Ti can be found in Appendix (Fig. S-12, 13, 14).

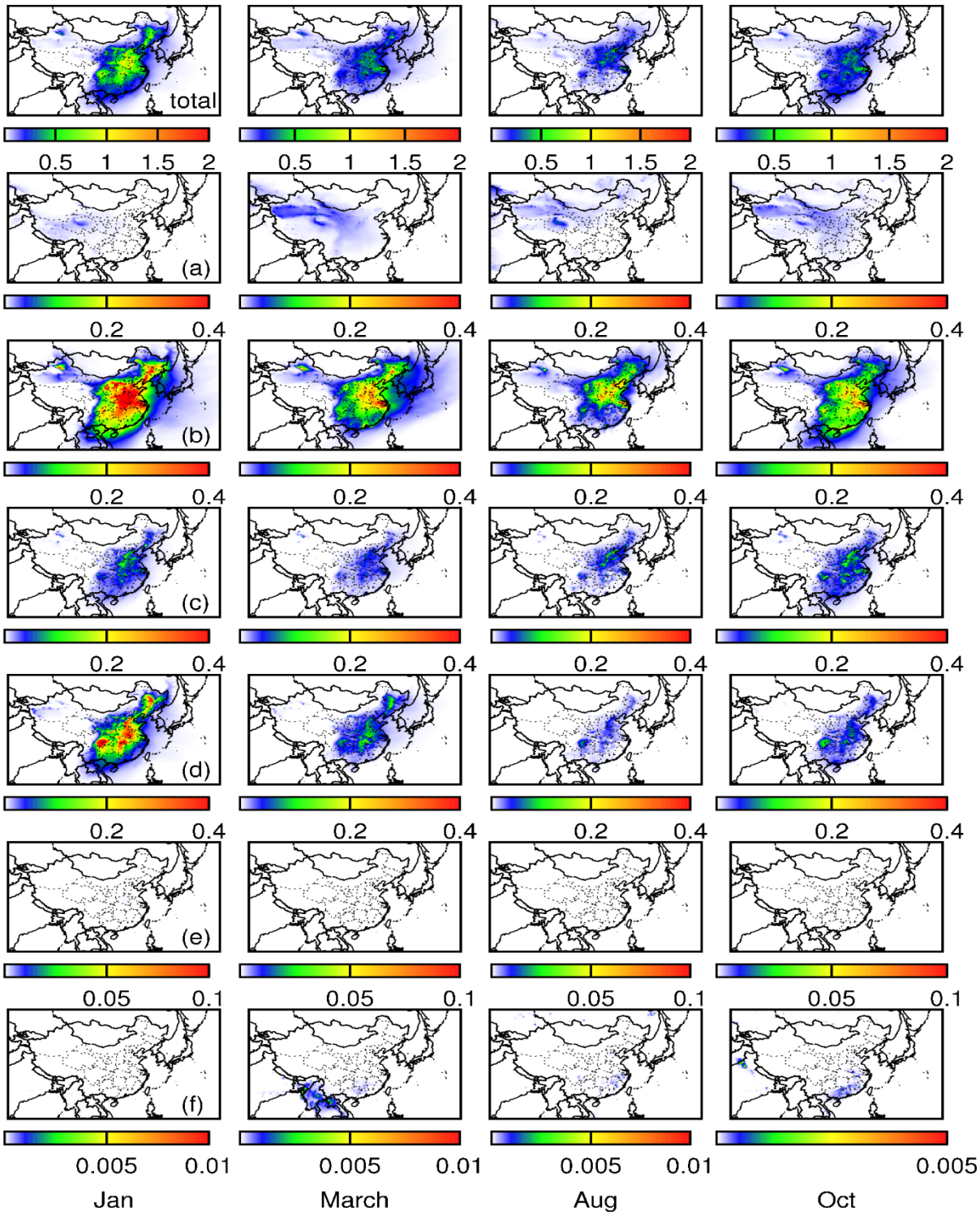

Figure 21 Regional distribution of Pb concentration in primary $PM_{2.5}$ in four seasons. Panels (a)-(f) represent contribution from (a) dust, (b) power plant, (c) industries, (d) residential, (e) transportation emissions, and (f) open burning, respectively, Units are $\mu g/m^3$. Scales are different to better illustrate the regional distribution.

Given the dependence of the calculated speciation profile, the source contributions to different species in different seasons are shown in Fig. 22. Different metals have diverse sources. Fe and Mn are mostly generated from power plant in the process of combustion. Al, Si and Ca mainly come from dust emission and power plant. Residential emission is the most important source for Na, Cr, As in winter and spring. In summer and fall time, the impact of residential emission is of less significance while power plant and dust emission make up the majority of contribution. Dust emission is the most important contributor to most elements in spring and fall as a result from frequent sand storm event in those periods.

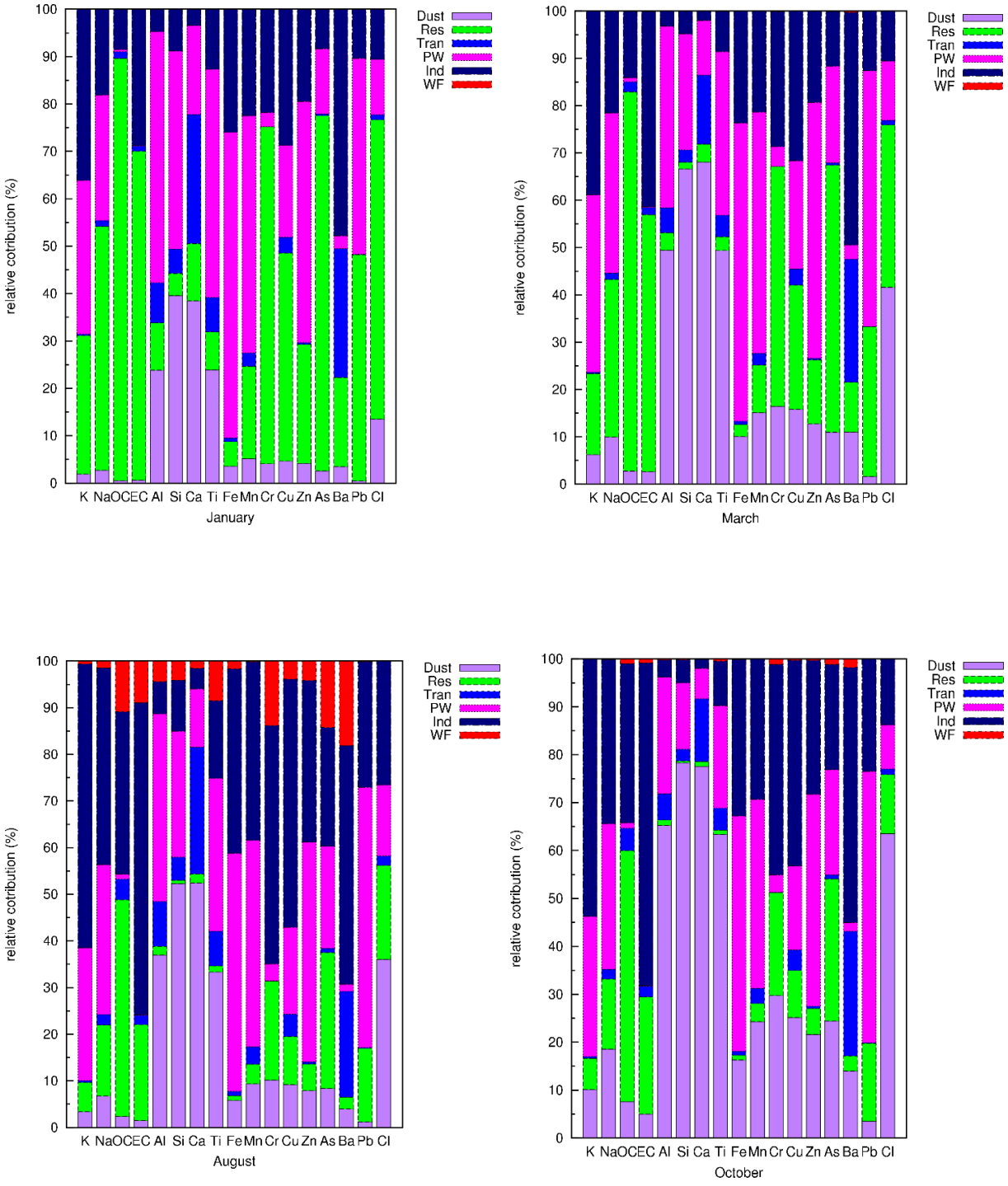

Figure 22 Relative contributions to primary $PM_{2.5}$ components from 6 sources in Beijing in four seasons

4.4 Conclusions

In this chapter, a source-oriented CMAQ model (CMAQ-p) is applied to determine the source and source region contributions to the primary $PM_{2.5}$ concentration in China. The results show that the highest primary $PM_{2.5}$ pollution occurs in Central and East China with a maximum concentration of approximately 100 $\mu g/m^3$ in winter. Residential and industries are the most important emission sources in all seasons, accounting for more than 60% contributions to total primary $PM_{2.5}$. Dust emission is another important source especially in spring and the most impacted area is in Western China. The relative contributions from individual source and region in Beijing and Shanghai are quantitatively determined. Local residential emission is the most significant contributor of Beijing in winter (45%), and in other seasons, industrial (10%-25%) and residential (8%-25%) emissions from Hebei Province have important influence on the primary PM air pollution in Beijing. For Shanghai, local emission from industrial activities is the most important contributor, accounting for more than 50% primary $PM_{2.5}$ in all seasons. An alternative set of primary $PM_{2.5}$ chemical component speciation profiles are calculated by multi-linear regression of observed chemical component concentrations and predicted source contributions to primary $PM_{2.5}$. By using these profiles, the sources for each chemical component in primary $PM_{2.5}$ are determined.

5. CONCLUSIONS

Quantitative information on source and source region contributions to particulate matter (PM) concentrations in China is currently poorly understood but is urgently needed to make cost-effective emission control strategies. In this study, source-oriented Community Multi-scale Air Quality (CMAQ) models are used to study the formation of, and source contributions to primary and secondary PM in China. The results show that inter-region transport of sulfate, nitrate and ammonium ion (SNA) occurs frequently, especially in the winter. The emissions from non-local regional can contribute 30-70% of the total SNA in different regions and seasons. It is also found that surface heterogeneous reactions of NO_2 and SO_2 and higher emissions of NH_3 are needed to better reproduce the observed high concentrations of SNA in Beijing, and potentially in other areas. Residential sources account for significant fractions (19%-68% in Beijing and 6%-30% in Shanghai) of primary $PM_{2.5}$, with higher contributions occur in winter. Industrial emissions are important throughout the year (15%-45% in Beijing and 39%-60% in Shanghai). Dust contributions can be as much as 20-30% in spring and fall seasons. Contributions to primary $PM_{2.5}$ from other sources are relatively small. In Shanghai, local emissions account for 70%-90% of primary $PM_{2.5}$. However, local emissions only contribute to 45%-55% of primary $PM_{2.5}$ in Beijing. These suggest that inter-regional emission control strategies are necessary to reduce PM pollution in China. Source and source region contributions to primary $PM_{2.5}$ components are determined using a novel multi-linear regression technique that combines the observation data and the source-oriented model predictions of primary $PM_{2.5}$ mass concentrations.

REFERENCES

Alexander, B., Park, R.J., Jacob, D.J., Gong, S., 2009. Transition metal-catalyzed oxidation of atmospheric sulfur: Global implications for the sulfur budget. Journal of Geophysical Research 114.

Appel, K.W., Pouliot, G.A., Simon, H., Sarwar, G., Pye, H.O.T., Napelenok, S.L., Akhtar, F., Roselle, S.J., 2013. Evaluation of dust and trace metal estimates from the Community Multiscale Air Quality (CMAQ) model version 5.0. Geosci Model Dev 6, 883-899.

Aw, J., Kleeman, M.J., 2003. Evaluating the first-order effect of intraannual temperature variability on urban air pollution. J Geophys Res-Atmos 108.

Boylan, J.W., Russell, A.G., 2006. PM and light extinction model performance metrics, goals, and criteria for three-dimensional air quality models. Atmospheric Environment 40, 4946-4959.

Buzcu, B., Yue, Z.W., Fraser, M.P., Nopmongcol, U., Allen, D.T., 2006. Secondary particle formation and evidence of heterogeneous chemistry during a wood smoke episode in Texas. J Geophys Res-Atmos 111.

Cao, J.-J., Shen, Z.-X., Chow, J.C., Watson, J.G., Lee, S.-C., Tie, X.-X., Ho, K.-F., Wang, G.-H., Han, Y.-M., 2012. Winter and Summer PM2.5Chemical Compositions in Fourteen Chinese Cities. J Air Waste Manage 62, 1214-1226.

Carter, W.P.L., 2010. Development of the SAPRC-07 chemical mechanism. Atmospheric Environment 44, 5324-5335.

Chan, C.K., Yao, X., 2008. Air pollution in mega cities in China. Atmospheric Environment 42, 1-42.

Chen, D.S., Cheng, S.Y., Liu, L., Chen, T., Guo, X.R., 2007. An integrated MM5-CMAQ modeling approach for assessing trans-boundary PM10 contribution to the host city of 2008 Olympic summer games - Beijing, China (vol 41, pg 1237, 2007). Atmospheric Environment 41, 7683-7683.

Choi, Y.J., Fernando, H.J.S., 2008. Implementation of a windblown dust parameterization into MODELS-3/CMAQ: Application to episodic PM events in the US/Mexico border. Atmospheric Environment 42, 6039-6046.

Dentener, F.J., Carmichael, G.R., Zhang, Y., Lelieveld, J., Crutzen, P.J., 1996. Role of mineral aerosol as a reactive surface in the global troposphere. J Geophys Res-Atmos 101, 22869-22889.

Eder, B., Yu, S.C., 2006. A performance evaluation of the 2004 release of Models-3 CMAQ. Atmospheric Environment 40, 4811-4824.

EPA, U., 2007. Guidance on the Use of Models and Other Analyses for demonstrating Attainment of Air Quality Goals for Ozone, PM2.5, and Regional Haze. http://www.epa.gov/scram001/guidance/guide/final-03-pm-rh-guidance.pdf

Fast, J.D., Gustafson, W.I., Easter, R.C., Zaveri, R.A., Barnard, J.C., Chapman, E.G., Grell, G.A., Peckham, S.E., 2006. Evolution of ozone, particulates, and aerosol direct radiative forcing in the vicinity of Houston using a fully coupled meteorology-chemistry-aerosol model. J Geophys Res-Atmos 111.

Foley, K.M., Roselle, S.J., Appel, K.W., Bhave, P.V., Pleim, J.E., Otte, T.L., Mathur, R., Sarwar, G., Young, J.O., Gilliam, R.C., Nolte, C.G., Kelly, J.T., Gilliland, A.B., Bash, J.O., 2010. Incremental testing of the Community Multiscale Air Quality (CMAQ) modeling system version 4.7. Geosci Model Dev 3, 205-226.

Gu, J., Bai, Z., Li, W., Wu, L., Liu, A., Dong, H., Xie, Y., 2011. Chemical composition of PM2.5 during winter in Tianjin, China. Particuology 9, 215-221.

IARC, 2006. Complete List of Agents Evaluated and their Classification.

Jacob, D.J., Crawford, J.H., Kleb, M.M., Connors, V.S., Bendura, R.J., Raper, J.L., Sachse, G.W., Gille, J.C., Emmons, L., Heald, C.L., 2003. Transport and Chemical Evolution over the Pacific (TRACE-P) aircraft mission: Design, execution, and first results. J Geophys Res-Atmos 108, 1-19.

Jacobson, M., 1997. Development and application of a new air pollution modeling system- II. Aerosol module structure and design. Atmospheric Environment 31, 14.

Jia, Y.T., Rahn, K.A., He, K.B., Wen, T.X., Wang, Y.S., 2008. A novel technique for quantifying the regional component of urban aerosol solely from its sawtooth cycles. J Geophys Res-Atmos 113.

Kebin He, F.Y., Yongliang Ma, Qiang Zhang, Xiaohong Yao, 2001. The characteristics of PM2.5 in Beijing, China. Atmospheric Environment 35, 4959-4970

Kelly, F.J., Fussell, J.C., 2012. Size, source and chemical composition as determinants of toxicity attributable to ambient particulate matter. Atmospheric Environment 60, 504-526.

Lammel, G., Leip, A., 2005. Formation of nitrate and sulfate in the plume of Berlin. Environ Sci Pollut R 12, 213-220.

Li, J.Y., Ying, Q., Yi, B.Q., Yang, P., 2013a. Role of stabilized Criegee Intermediates in the formation of atmospheric sulfate in eastern United States. Atmospheric Environment 79, 442-447.

Li, P., Xin, J., Wang, Y., Wang, S., Shang, K., Liu, Z., Li, G., Pan, X., Wei, L., Wang, M., 2013b. Time-series analysis of mortality effects from airborne particulate matter size fractions in Beijing. Atmospheric Environment 81, 253-262.

Li, Y.Z., Tong, H.L., Zhuo, Y.Q., Wang, S.J., Xu, X.C., 2006. Simultaneous removal of SO2 and trace SeO2 from flue gas: Effect of SO2 on selenium capture and kinetics study. Environ Sci Technol 40, 7919-7924.

Liu, H., Wang, X.M., Pang, J.M., He, K.B., 2013. Feasibility and difficulties of China's new air quality standard compliance: PRD case of PM2.5 and ozone from 2010 to 2025. Atmospheric Chemistry and Physics 13, 12013-12027.

Louie, P.K., Chow, J.C., Chen, L.W., Watson, J.G., Leung, G., Sin, D.W., 2005. PM2.5 chemical composition in Hong Kong: urban and regional variations. The Science of the total environment 338, 267-281.

Lu, K.D., Hofzumahaus, A., Holland, F., Bohn, B., Brauers, T., Fuchs, H., Hu, M., Haseler, R., Kita, K., Kondo, Y., Li, X., Lou, S.R., Oebel, A., Shao, M., Zeng, L.M., Wahner, A., Zhu, T., Zhang, Y.H., Rohrer, F., 2013. Missing OH source in a suburban environment near Beijing: observed and modelled OH and HO2 concentrations in summer 2006. Atmospheric Chemistry and Physics 13, 1057-1080.

Luo, C., Wang, Y.H., Mueller, S., Knipping, E., 2011. Diagnosis of an underestimation of summertime sulfate using the Community Multiscale Air Quality model. Atmospheric Environment 45, 5119-5130.

Martin, L.R., Hill, M.W., 1987. Optical Measurement of Aqueous Kinetics at Micromolar Concentrations. J Phys E Sci Instrum 20, 1383-1387.

Martin, R., Good, T., 1991. Catalyzied oxidation of sulfur dioxide in solution: the iron-manganese synergism. Atmospheric Environment 25A, 5.

McNaughton, C.S., Clarke, A.D., Kapustin, V., Shinozuka, Y., Howell, S.G., Anderson, B.E., Winstead, E., Dibb, J., Scheuer, E., Cohen, R.C., Wooldridge, P., Perring, A., Huey, L.G., Kim, S., Jimenez, J.L., Dunlea, E.J., DeCarlo, P.F., Wennberg, P.O., Crounse, J.D., Weinheimer, A.J., Flocke, F., 2009. Observations of heterogeneous reactions between Asian pollution and mineral dust over the Eastern North Pacific during INTEX-B. Atmospheric Chemistry and Physics 9, 8283-8308.

Misenis, C., Zhang, Y., 2010. An examination of sensitivity of WRF/Chem predictions to physical parameterizations, horizontal grid spacing, and nesting options. Atmos Res 97, 315-334.

Querol, X., Alastuey, A., Ruiz, C.R., Artiñano, B., Hansson, H.C., Harrison, R.M., Buringh, E., ten Brink, H.M., Lutz, M., Bruckmann, P., Straehl, P., Schneider, J., 2004. Speciation and origin of PM10 and PM2.5 in selected European cities. Atmospheric Environment 38, 6547-6555.

Sarwar, G., Fahey, K., Kwok, R., Gilliam, R.C., Roselle, S.J., Mathur, R., Xue, J., Yu, J.Z., Carter, W.P.L., 2013. Potential impacts of two SO2 oxidation pathways on regional sulfate concentrations: Aqueous-phase oxidation by NO2 and gas-phase oxidation by Stabilized Criegee Intermediates. Atmospheric Environment 68, 186-197.

Seinfeld, Pandis, 2006. Atmospheric Chemistry and Physics - From Air Pollution to Climate Change (2nd Edition).

Streets, D.G., Bond, T.C., Carmichael, G.R., Fernandes, S.D., Fu, Q., He, D., Klimont, Z., Nelson, S.M., Tsai, N.Y., Wang, M.Q., Woo, J.H., Yarber, K.F., 2003. An inventory of gaseous and primary aerosol emissions in Asia in the year 2000. J Geophys Res-Atmos 108.

Sun, Y., Zhuang, G., Wang, Y., Han, L., Guo, J., Dan, M., Zhang, W., Wang, Z., Hao, Z., 2004. The air-borne particulate pollution in Beijing?concentration, composition, distribution and sources. Atmospheric Environment 38, 5991-6004.

Sun, Y.L., Zhuang, G.S., Tang, A.H., Wang, Y., An, Z.S., 2006. Chemical characteristics of PM2.5 and PM10 in haze-fog episodes in Beijing. Environ Sci Technol 40, 3148-3155.

Tsimpidi, A.P., Karydis, V.A., Pandis, S.N., 2007. Response of Inorganic Fine Particulate Matter to Emission Changes of Sulfur Dioxide and Ammonia: The Eastern United States as a Case Study. J Air Waste Manage 57, 1489-1498.

Underwood, G.M., Song, C.H., Phadnis, M., Carmichael, G.R., Grassian, V.H., 2001. Heterogeneous reactions of NO2 and HNO3 on oxides and mineral dust: A combined laboratory and modeling study. J Geophys Res-Atmos 106, 18055-18066.

Usher, C.R., Michel, A.E., Grassian, V.H., 2003. Reactions on mineral dust. Chem Rev 103, 4883-4939.

Wang, L.T., Hao, J.M., He, K.B., Wang, S.X., Li, J.H., Zhang, Q., Streets, D.G., Fu, J.S., Jang, C.J., Takekawa, H., Chatani, S., 2008. A modeling study of coarse particulate matter pollution in Beijing: Regional source contributions and control implications for the 2008 summer Olympics. J Air Waste Manage 58, 1057-1069.

Wang, L.T., Wei, Z., Yang, J., Zhang, Y., Zhang, F.F., Su, J., Meng, C.C., Zhang, Q., 2014a. The 2013 severe haze over southern Hebei, China: model evaluation, source apportionment, and policy implications. Atmospheric Chemistry and Physics 14, 3151-3173.

Wang, X., Bi, X., Sheng, G., Fu, J., 2006a. Chemical composition and sources of PM10 and PM2.5 aerosols in Guangzhou, China. Environmental monitoring and assessment 119, 425-439.

Wang, Y., Zhang, Q.Q., He, K., Zhang, Q., Chai, L., 2013. Sulfate-nitrate-ammonium aerosols over China: response to 2000–2015 emission changes of sulfur dioxide, nitrogen oxides, and ammonia. Atmospheric Chemistry and Physics 13, 2635-2652.

Wang, Y., Zhang, R., Saravanan, R., 2014b. Asian pollution climatically modulates mid-latitude cyclones following hierarchical modelling and observational analysis. Nature communications 5, 3098.

Wang, Y., Zhuang, G.S., Sun, Y.L., An, Z.S., 2006b. The variation of characteristics and formation mechanisms of aerosols in dust, haze, and clear days in Beijing. Atmospheric Environment 40, 6579-6591.

Wang, Y.S., Yao, L., Wang, L.L., Liu, Z.R., Ji, D.S., Tang, G.Q., Zhang, J.K., Sun, Y., Hu, B., Xin, J.Y., 2014c. Mechanism for the formation of the January 2013 heavy haze pollution episode over central and eastern China. Sci China Earth Sci 57, 14-25.

Wu, S.W., Deng, F.R., Wei, H.Y., Huang, J., Wang, X., Hao, Y., Zheng, C.J., Qin, Y., Lv, H.B., Shima, M., Guo, X.B., 2014. Association of Cardiopulmonary Health Effects with Source-Appointed Ambient Fine Particulate in Beijing, China: A Combined Analysis from the Healthy Volunteer Natural Relocation (HVNR) Study. Environ Sci Technol 48, 3438-3448.

Wu, Z.J., Hu, M., Shao, K.S., Slanina, J., 2009. Acidic gases, NH3 and secondary inorganic ions in PM10 during summertime in Beijing, China and their relation to air mass history. Chemosphere 76, 1028-1035.

Yang, F., Tan, J., Zhao, Q., Du, Z., He, K., Ma, Y., Duan, F., Chen, G., Zhao, Q., 2011. Characteristics of PM2.5speciation in representative megacities and across China. Atmospheric Chemistry and Physics 11, 5207-5219.

Ye, B., Ji, X., Yang, H., Yao, X., Chan, C.K., Cadle, S.H., 2002. Concentration and chemical composition of PM2.5 in Shanghai for 1-year period. Atmospheric Environment 37, 499-510

Ying, Q., Cureño, I.V., Chen, G., Ali, S., Zhang, H., Malloy, M., Bravo, H.A., Sosa, R., 2014a. Impacts of Stabilized Criegee Intermediates, surface uptake processes and higher

aromatic secondary organic aerosol yields on predicted PM2.5 concentrations in the Mexico City Metropolitan Zone. Atmospheric Environment 94, 438-447.

Ying, Q., Kleeman, M., 2009. Regional contributions to airborne particulate matter in central California during a severe pollution episode. Atmospheric Environment 43, 1218-1228.

Ying, Q., Kleeman, M.J., 2006. Source contributions to the regional distribution of secondary particulate matter in California. Atmospheric Environment 40, 736-752.

Ying, Q., Wu, L., Zhang, H., 2014b. Local and inter-regional contributions to PM2.5 nitrate and sulfate in China. Atmospheric Environment 94, 582-592.

York, D., Evensen, N.M., Martinez, M.L., Delgado, J.D., 2004. Unified equations for the slope, intercept, and standard errors of the best straight line. Am J Phys 72, 367-375.

Zhang, H.L., Li, J.Y., Ying, Q., Yu, J.Z., Wu, D., Cheng, Y., He, K.B., Jiang, J.K., 2012. Source apportionment of PM2.5 nitrate and sulfate in China using a source-oriented chemical transport model. Atmospheric Environment 62, 228-242.

Zhang, H.L., Ying, Q., 2010. Source apportionment of airborne particulate matter in Southeast Texas using a source-oriented 3D air quality model. Atmospheric Environment 44, 3547-3557.

Zhang, J.K., Sun, Y., Liu, Z.R., Ji, D.S., Hu, B., Liu, Q., Wang, Y.S., 2014. Characterization of submicron aerosols during a month of serious pollution in Beijing, 2013. Atmospheric Chemistry and Physics 14, 2887-2903.

Zhang, Q., Streets, D.G., Carmichael, G.R., He, K.B., Huo, H., Kannari, A., Klimont, Z., Park, I.S., Reddy, S., Fu, J.S., Chen, D., Duan, L., Lei, Y., Wang, L.T., Yao, Z.L., 2009. Asian emissions in 2006 for the NASA INTEX-B mission. Atmospheric Chemistry and Physics 9, 5131-5153.

Zhang, y., 2004. Source Apportionment of Fine-Particle Pollution in Beijing: Urbanizaiton, Energy, and Air Pollution in China: the Challenges Ahead-Proceedings of Symposium. The National Academies Press.

Zhang, Y.X., Dubey, M.K., 2009. Comparisons of WRF/Chem simulated O-3 concentrations in Mexico City with ground-based RAMA measurements during the MILAGRO period. Atmospheric Environment 43, 4622-4631.

Zhao, P.S., Zhang, X.L., Xu, X.F., 2011. Long-term visibility trends and characteristics in the region of Beijing, Tianjin, and Hebei, China. Abstr Pap Am Chem S 242.

Zhao, X.J., Zhao, P.S., Xu, J., Meng, W., Pu, W.W., Dong, F., He, D., Shi, Q.F., 2013. Analysis of a winter regional haze event and its formation mechanism in the North China Plain. Atmospheric Chemistry and Physics 13, 5685-5696.

Zhao, Y., Zhang, J., Nielsen, C.P., 2014. The effects of energy paths and emission controls and standards on future trends in China's emissions of primary air pollutants. Atmospheric Chemistry and Physics 14, 8849-8868.

Zheng, B., Zhang, Q., Zhang, Y., He, K.B., Wang, K., Zheng, G.J., Duan, F.K., Ma, Y.L., Kimoto, T., 2014a. Heterogeneous chemistry: a mechanism missing in current models to explain secondary inorganic aerosol formation during the January 2013 haze episode in North China. Atmospheric Chemistry and Physics Discussions 14, 16731-16776.

Zheng, G.J., Duan, F.K., Ma, Y.L., Cheng, Y., Zheng, B., Zhang, Q., Huang, T., Kimoto, T., Chang, D., Su, H., Pöschl, U., Cheng, Y.F., He, K.B., 2014b. Exploring the severe winter haze in Beijing. Atmospheric Chemistry and Physics Discussions 14, 17907-17942.

Zheng, J.Y., Che, W.W., Zheng, Z.Y., Chen, L.F., Zhong, L.J., 2013. Analysis of Spatial and Temporal Variability of PM10 Concentrations Using MODIS Aerosol Optical Thickness in the Pearl River Delta Region, China. Aerosol Air Qual Res 13, 862-876.

Zhuang, X., Wang, Y., He, H., Liu, J., Wang, X., Zhu, T., Ge, M., Zhou, J., Tang, G., Ma, J., 2014. Haze insights and mitigation in China: An overview. Journal of Environmental Sciences 26, 2-12.

APPENDIX

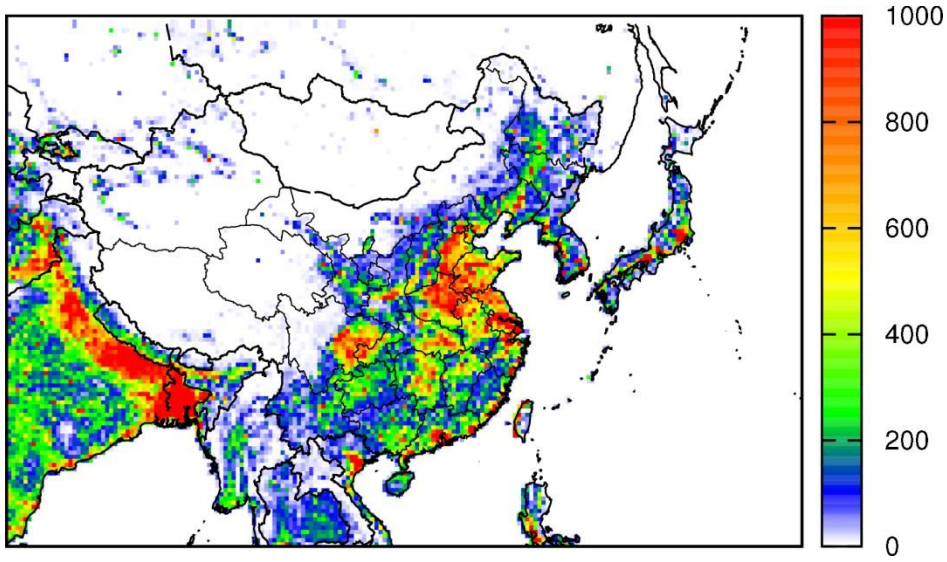

Fig S1 Gridded population density based on 2008 data. Units are people per km^2

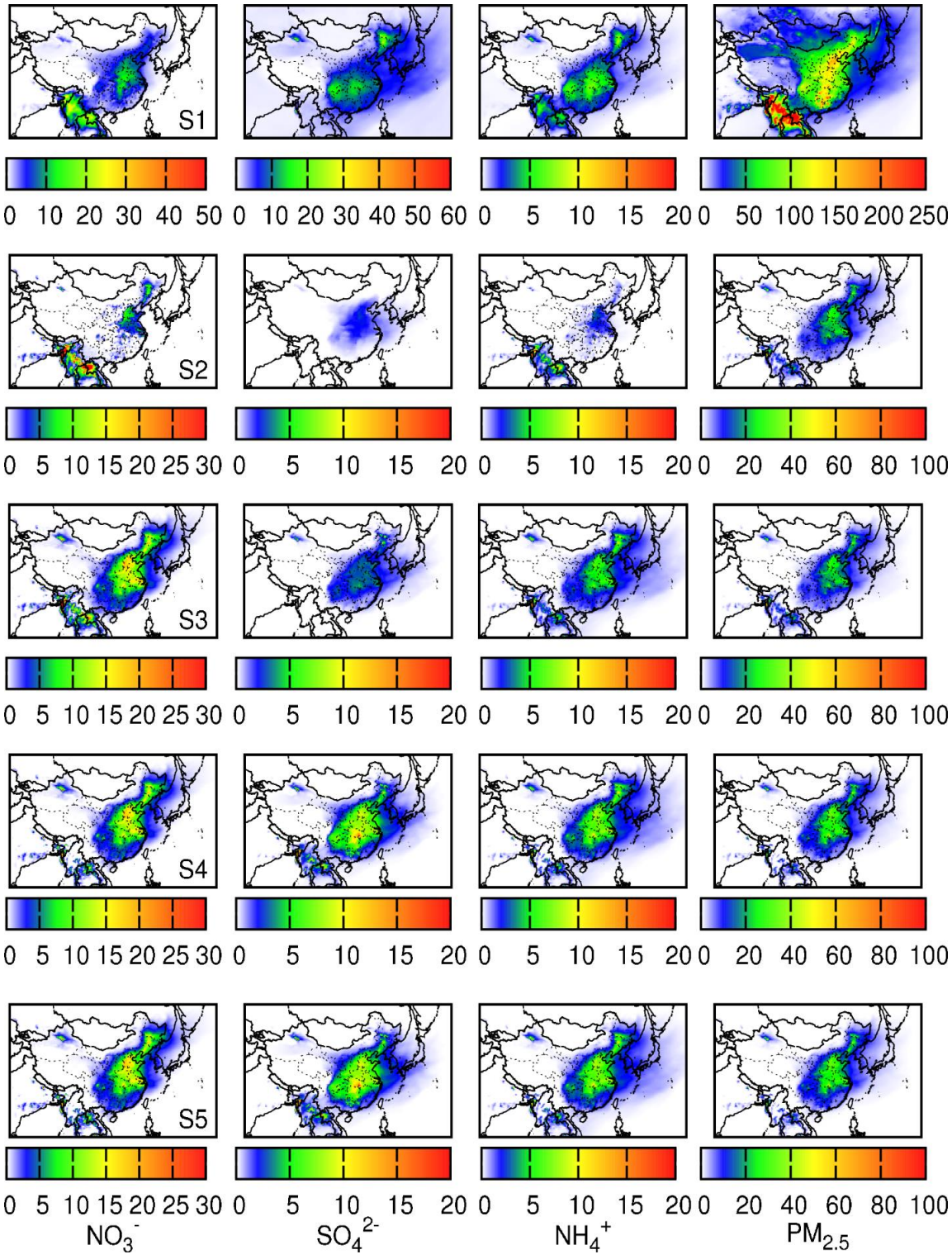

Fig S2 Similar as Fig. 10, but for March, 2013

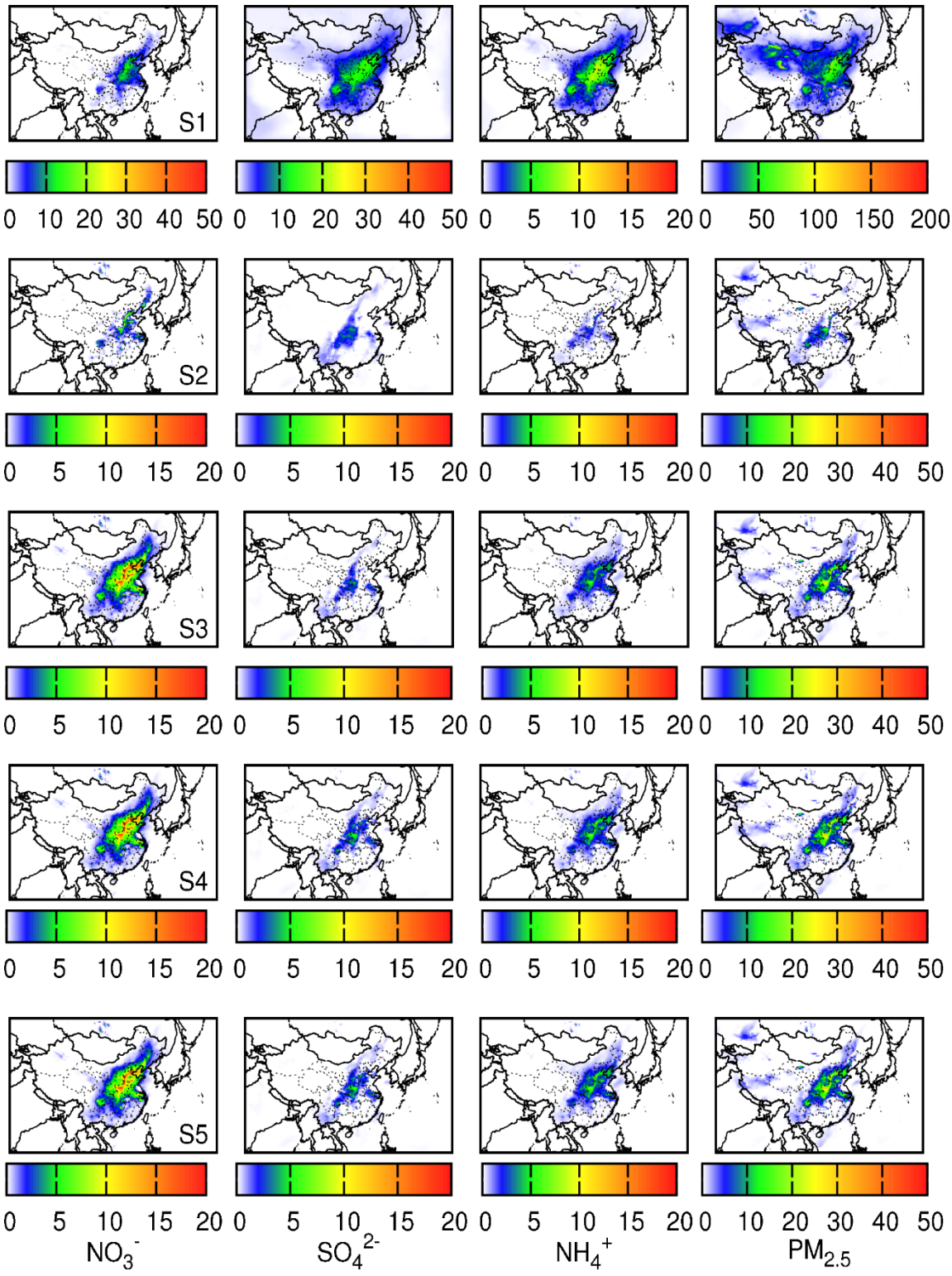

Fig. S3 Similar as Fig. 10, but for August, 2012

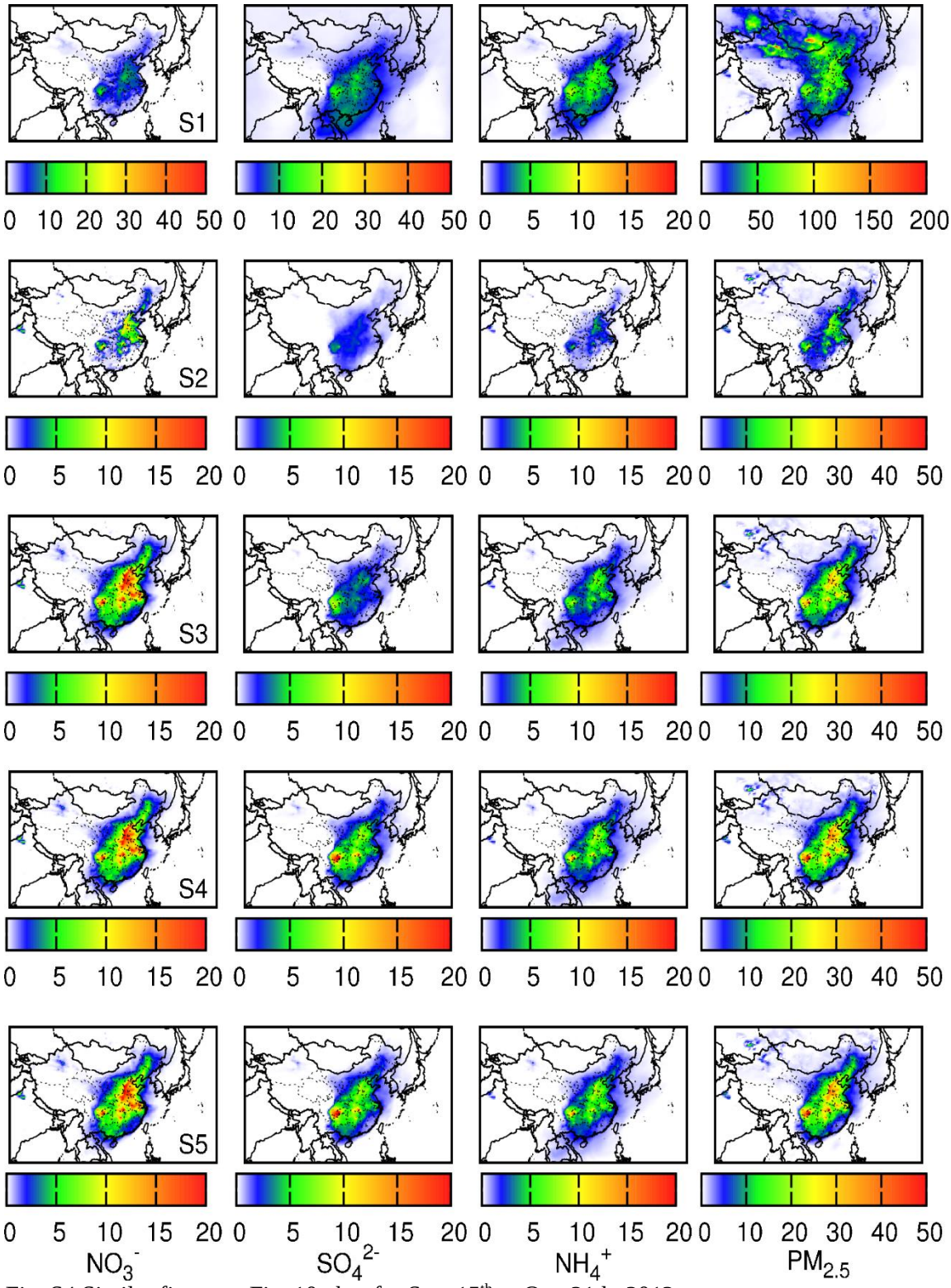

Fig. S4 Similar figure as Fig. 10 , but for Sep. 15th to Oct. 21th, 2012

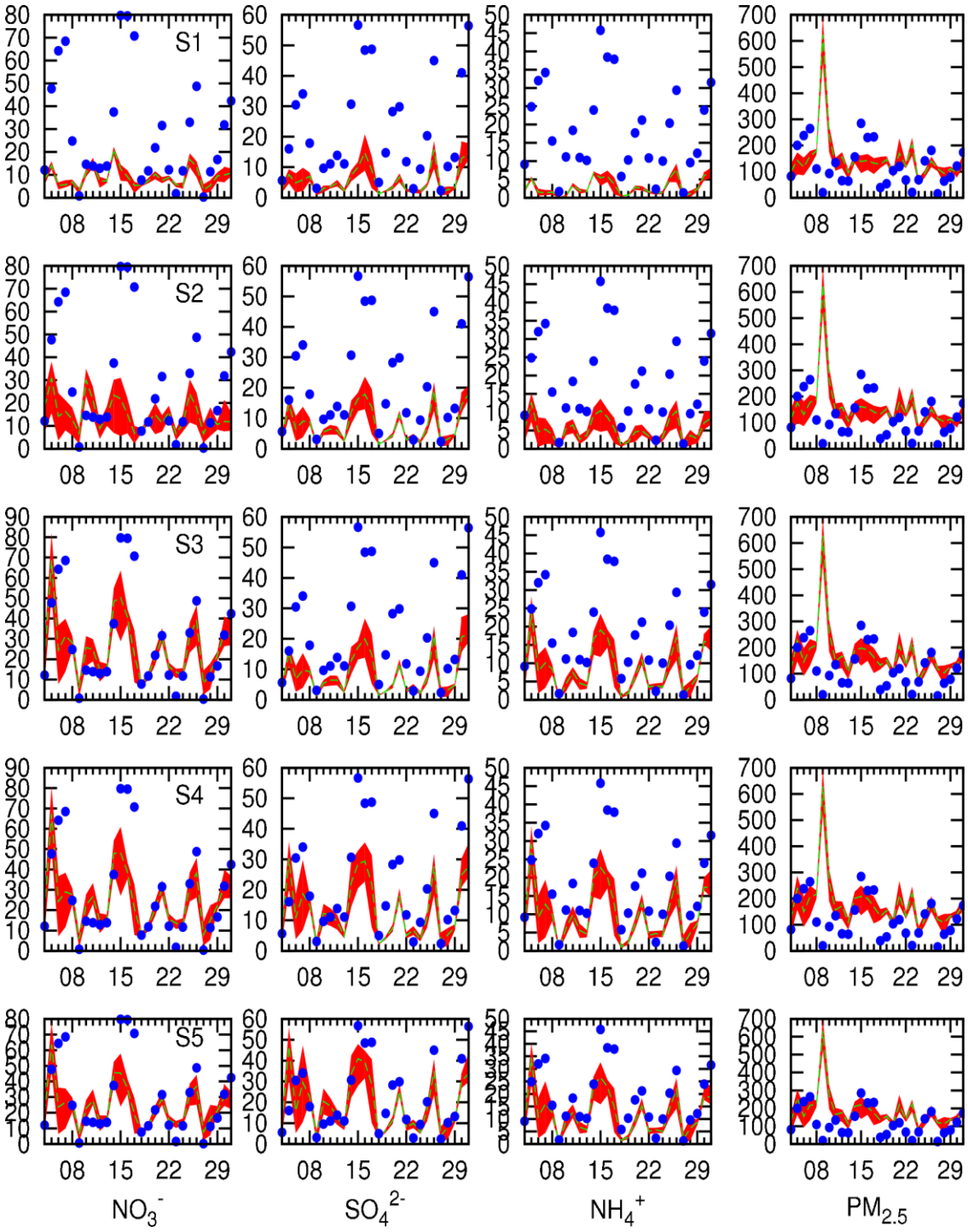

Fig. S5 Similar is Fig. 11, but for March, 2013

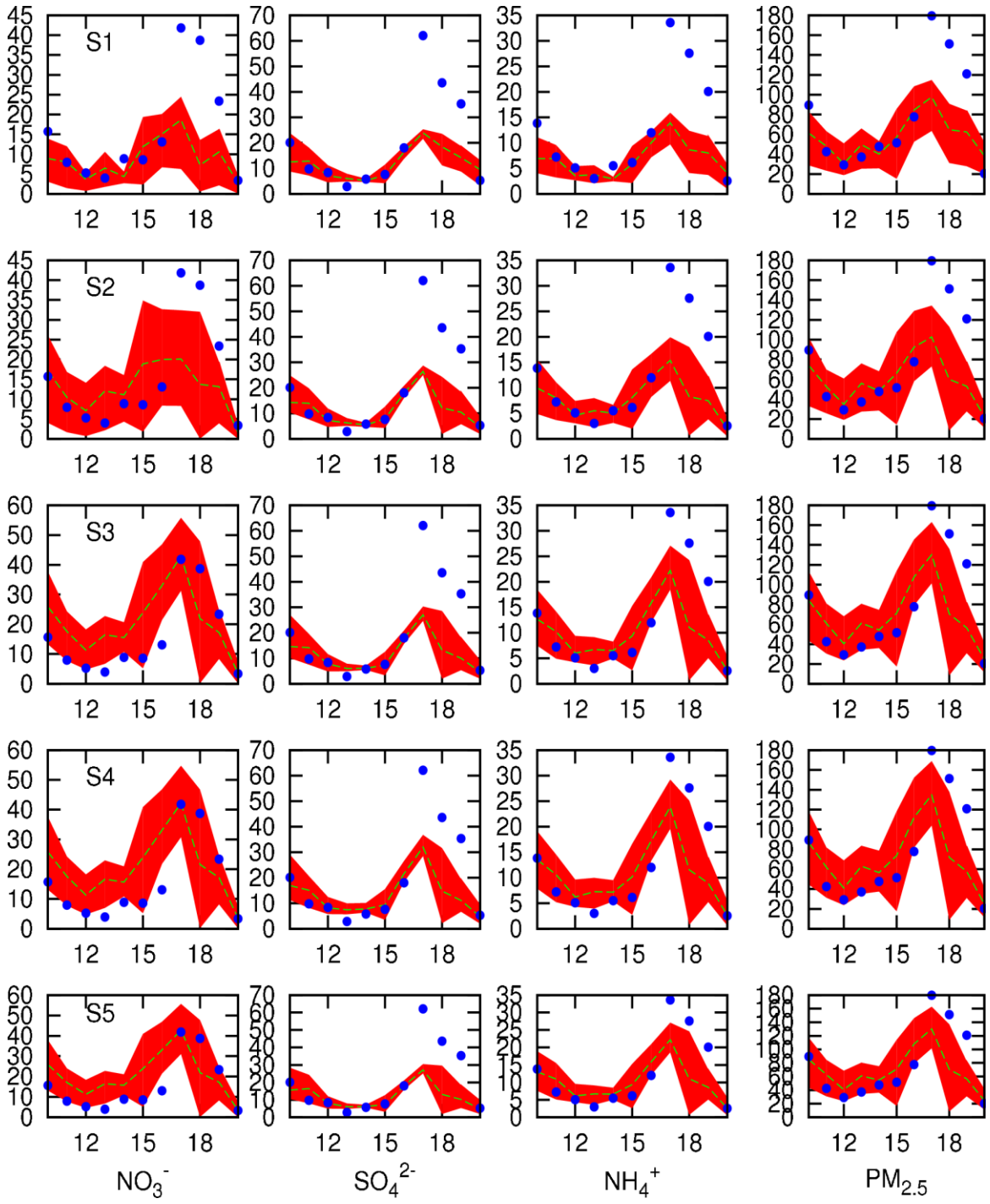

Fig. S6 Similar as Fig. 11, but for Aug, 2012

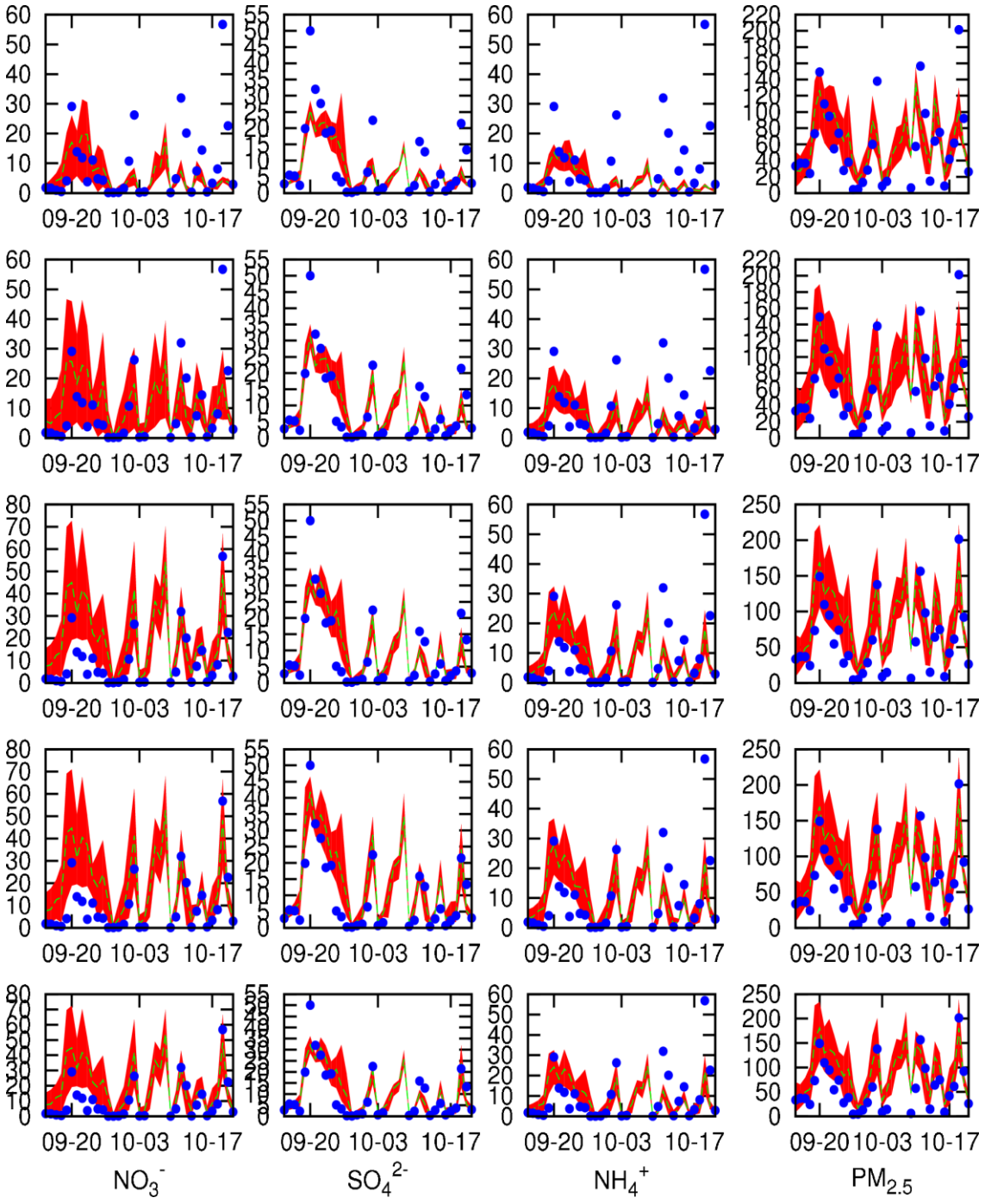

Fig. S7 Similar as Fig. 11, but for Sep 15th to Oct 21th, 2012

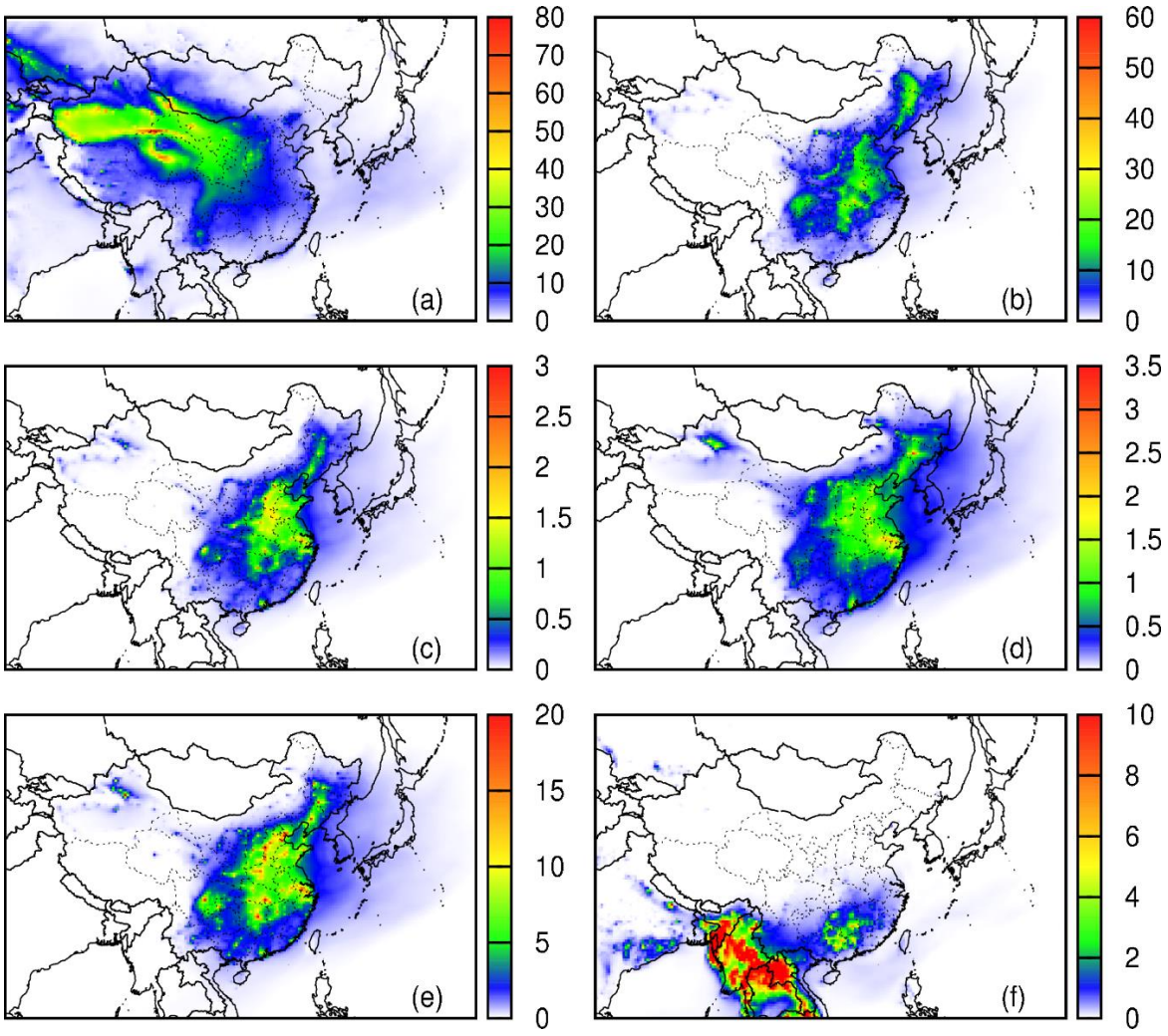

Fig S8 Similar as Fig. 14, but for March, 2013

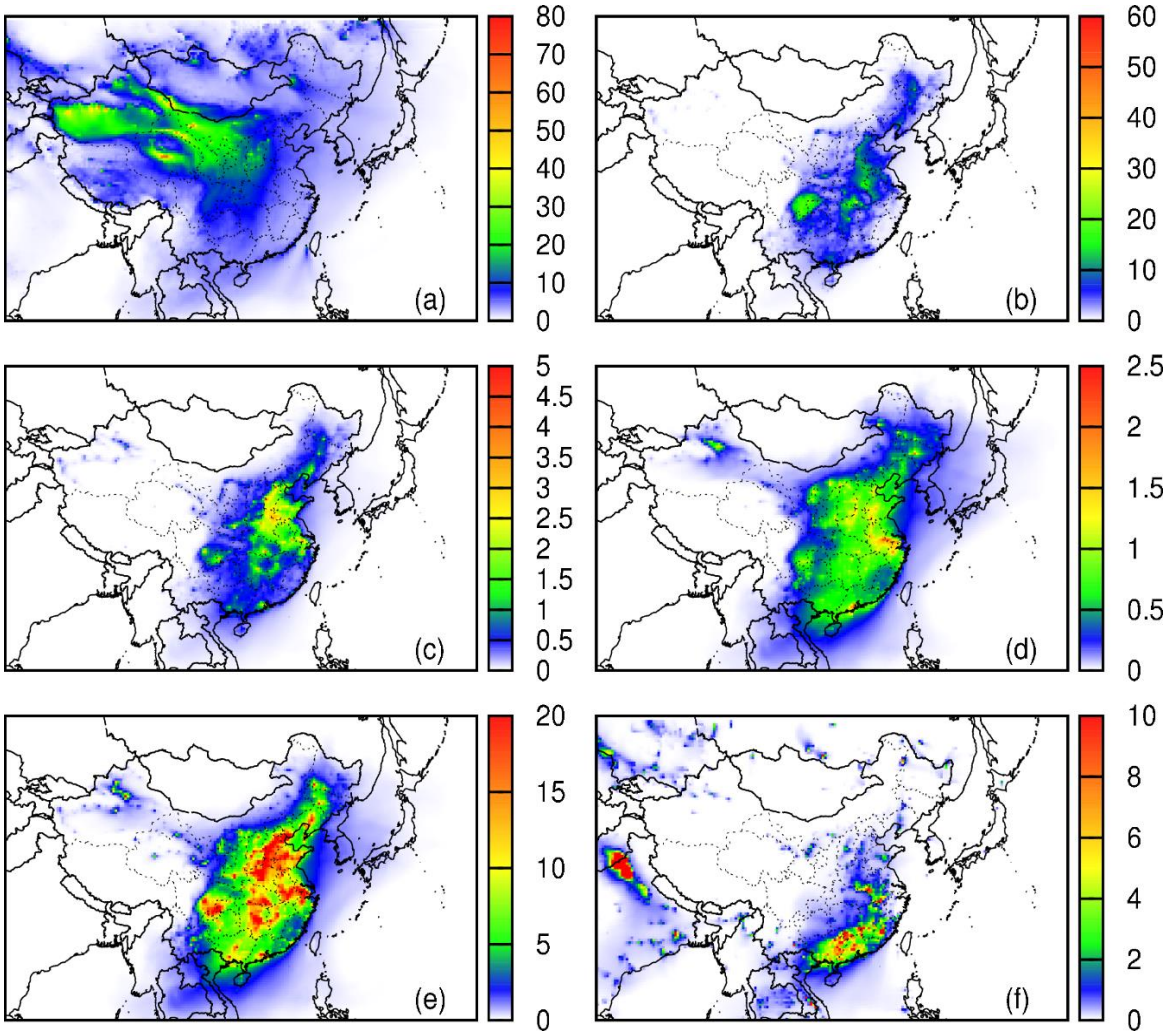

Fig S9 Similar as Fig. 14, but for Oct., 2012

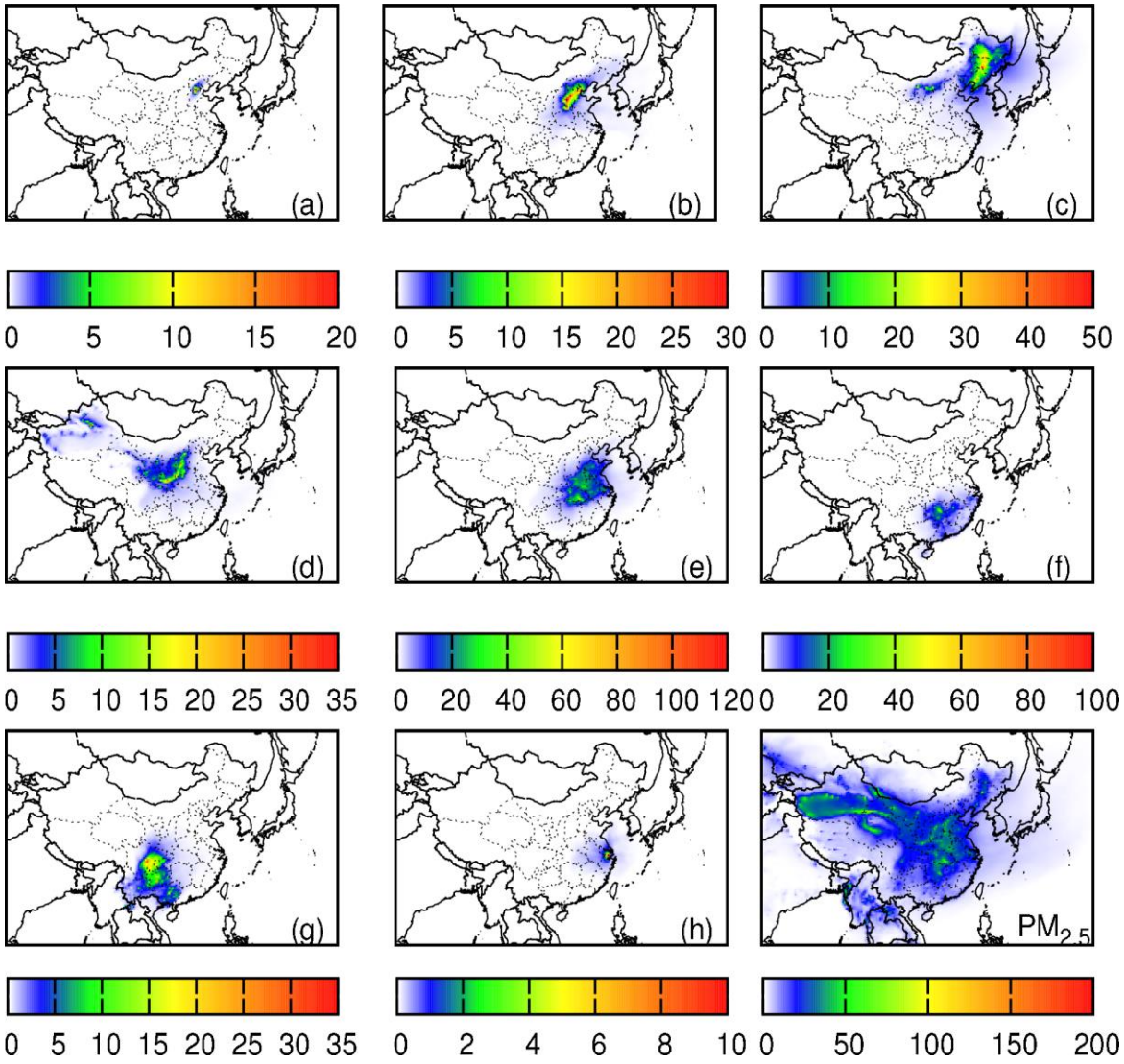

Fig S10 Similar figure as Fig. 15, but for March, 2013

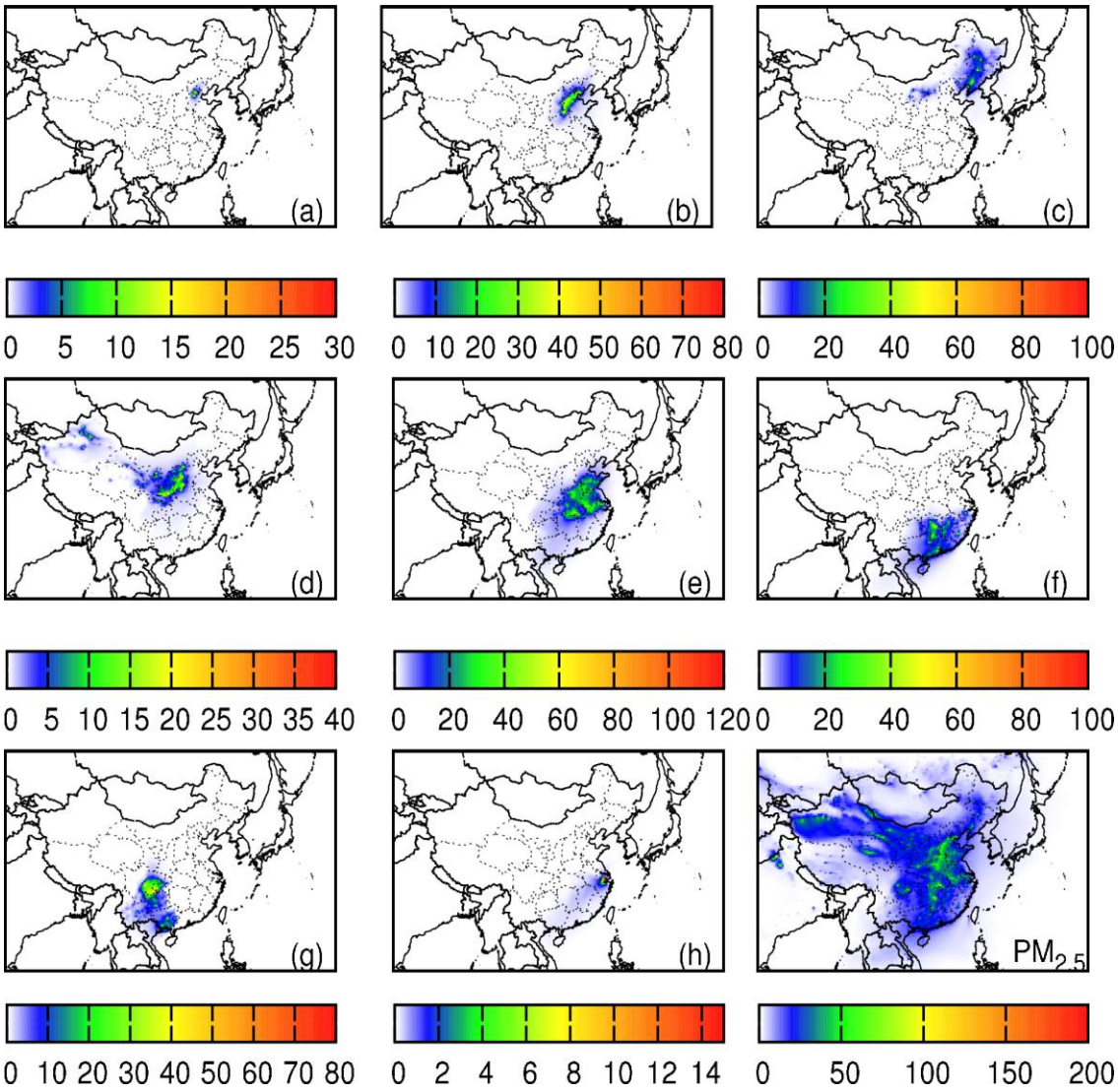

Fig. S11 Similar figure as Fig. 15, but for Oct., 2012

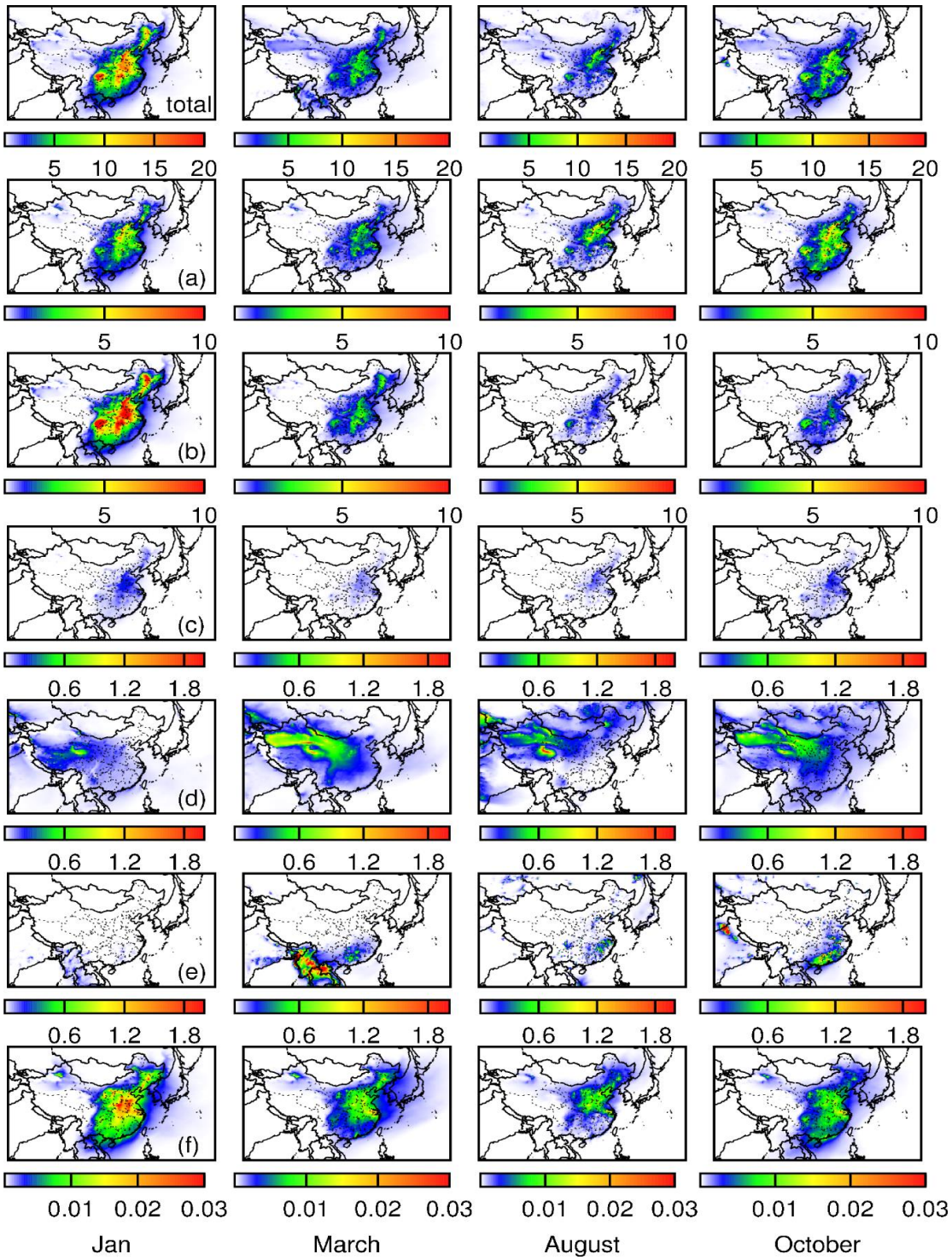

Fig. S12 Similar figure as Fig. 21, but for Elemental Carbon (EC). Source (a) to (f) represent: , industries(a), residential(b), transportation(c), dust(d), open burning(e), power plant(f) .

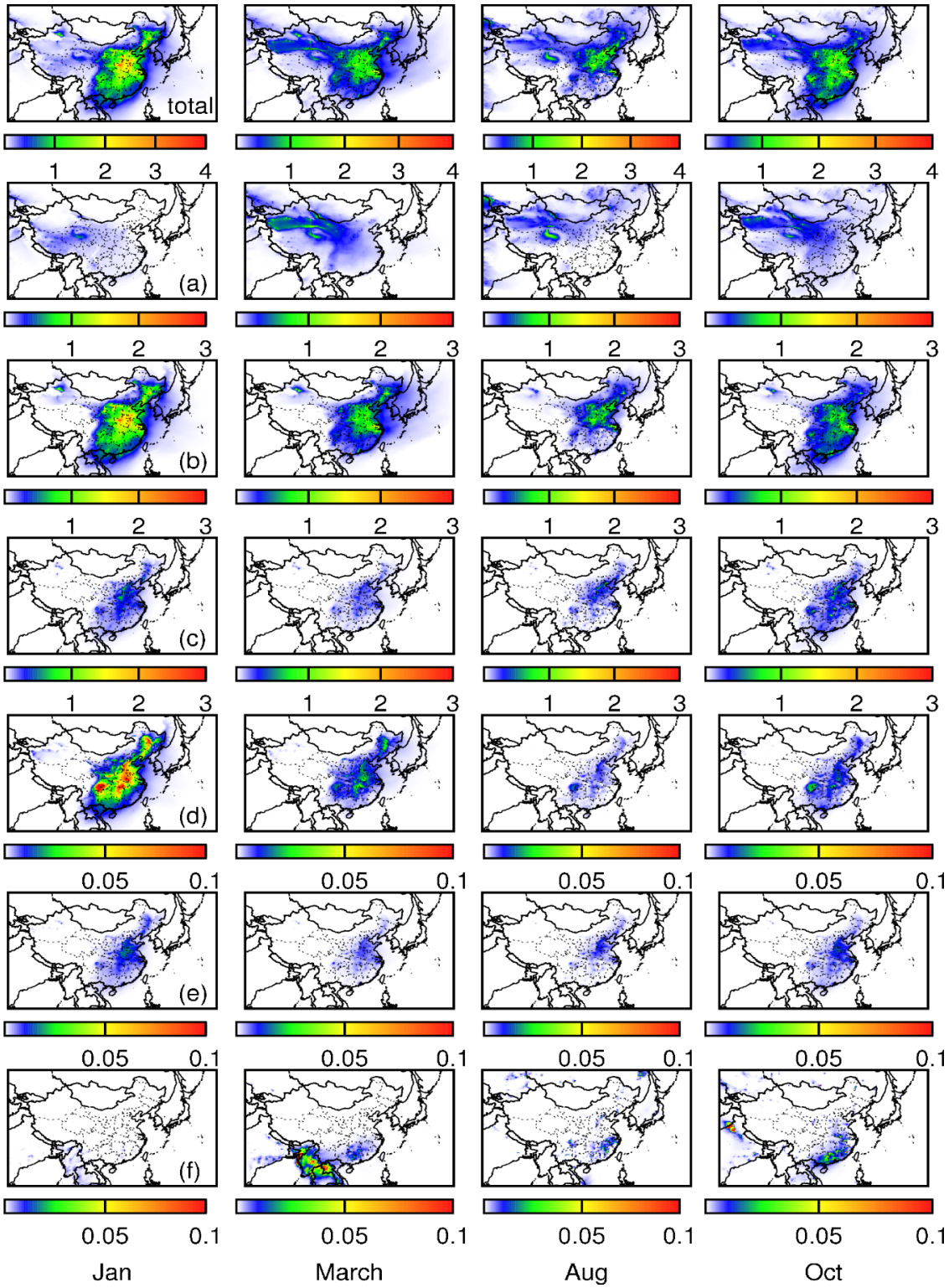

Fig. S13 Similar figure as Fig. 21, but for Fe. Sources (a) to (f) represent: dust (a), power plant (b), industry(c), residential (d), transportation (e) and open burning (f).

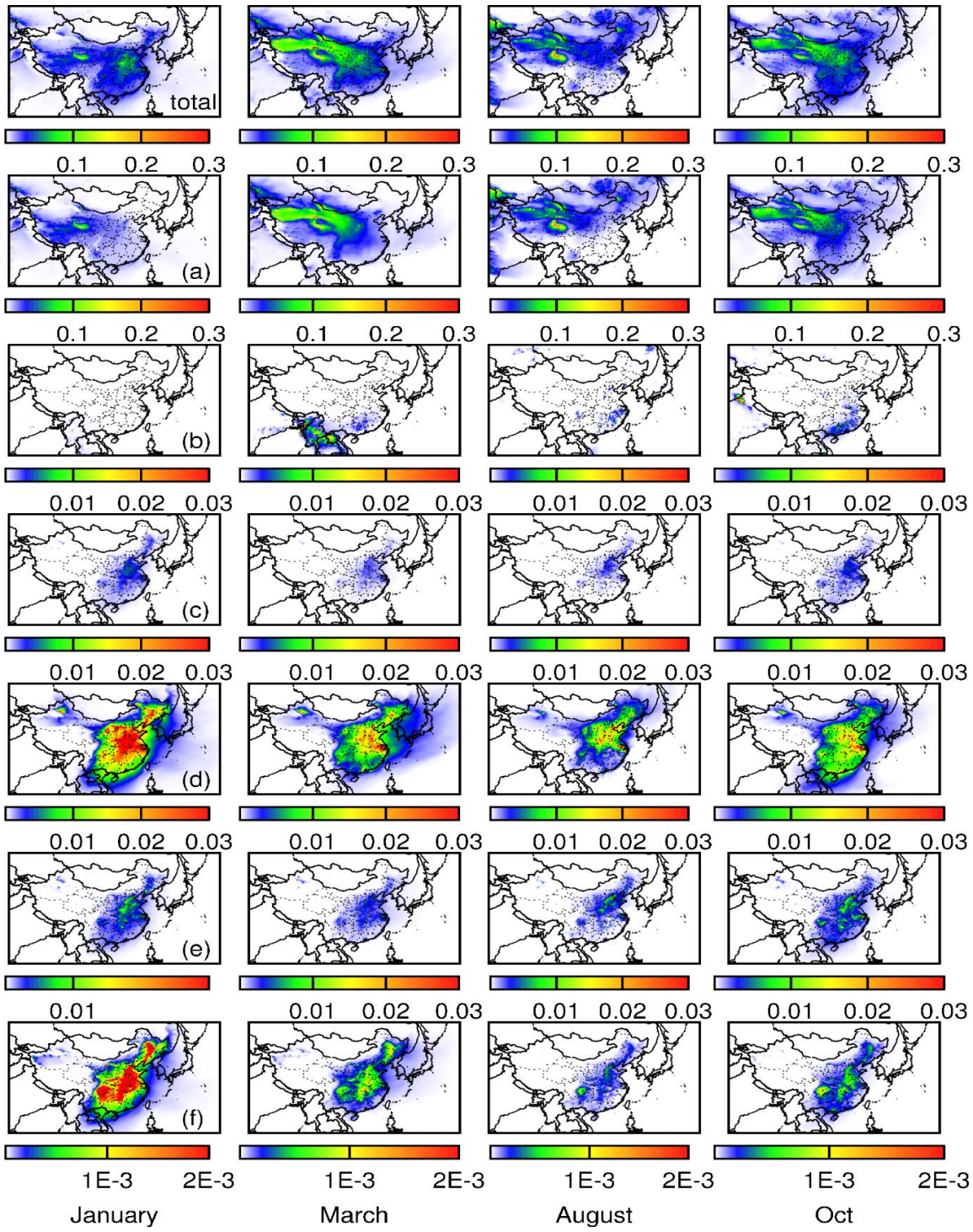

Fig. S14 Similar figure as Fig. 21, but for Ti. Source (a) to (f) represent dust (a), open burning (b), transportation (c), power plant (d), industry (e), residential (f),

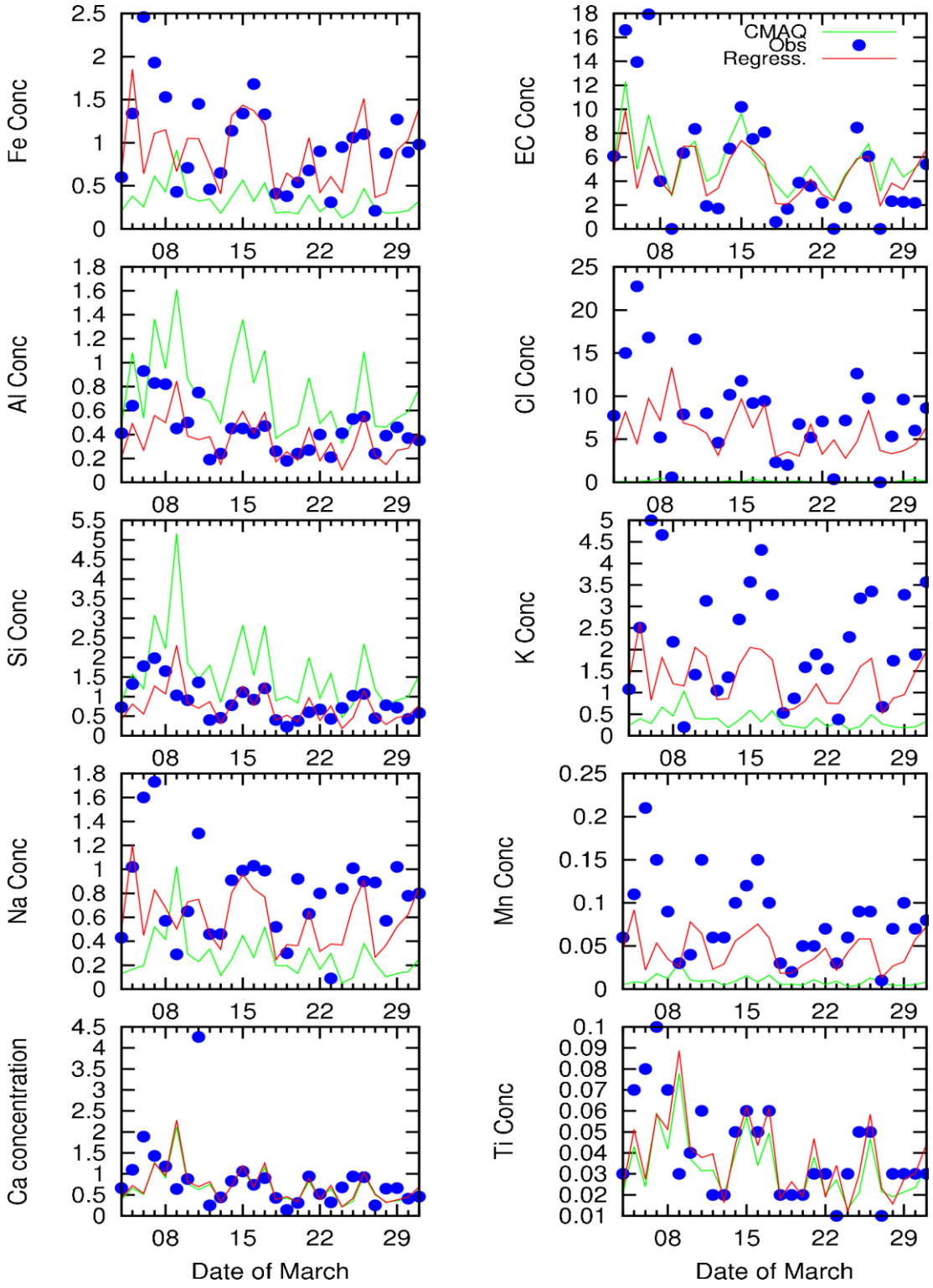

Fig. S15 Similar figure as Fig. 19, but for March, 2013.

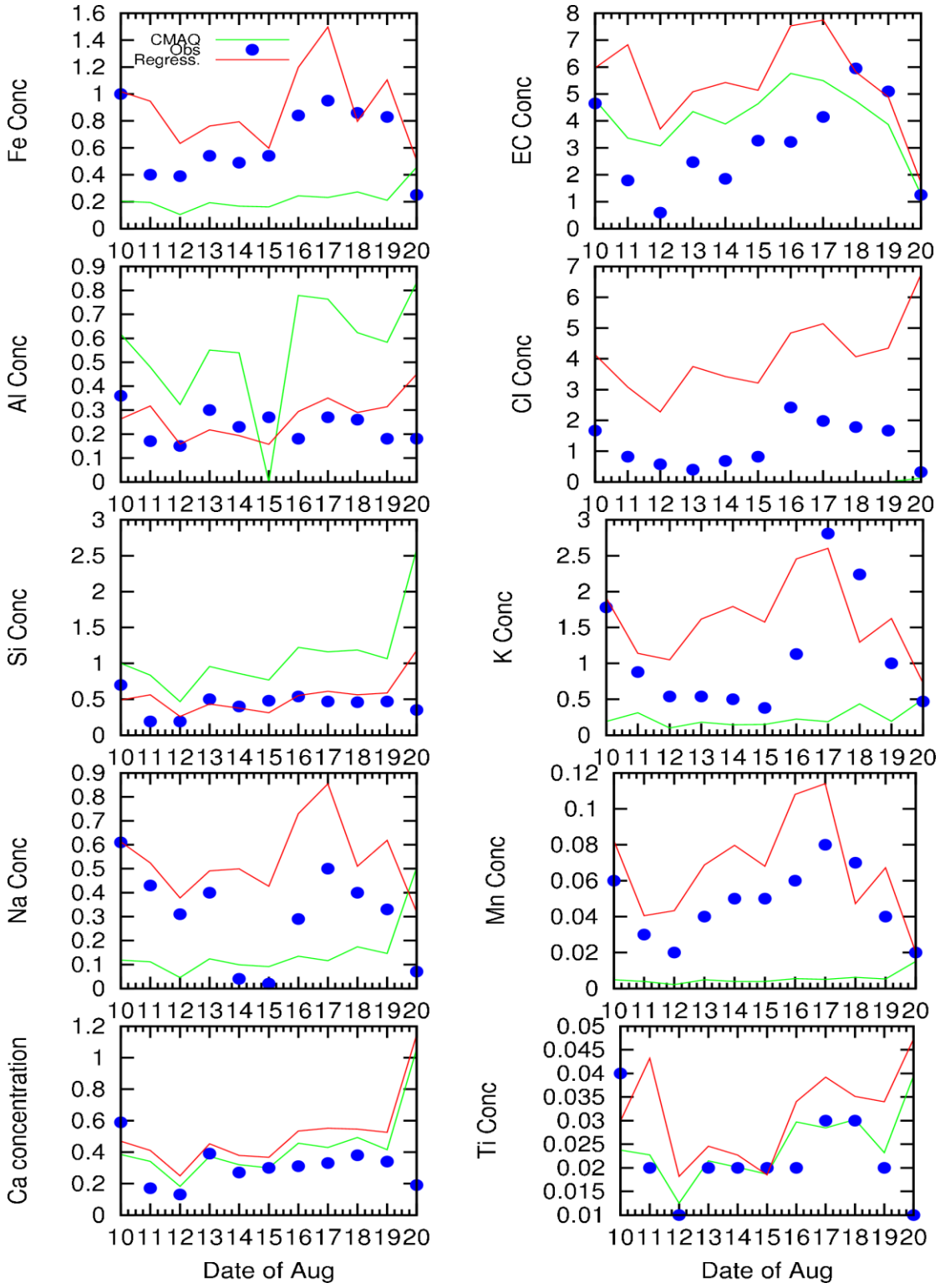

Fig. S16 Similar figure as Fig. 19, but for August, 2012.

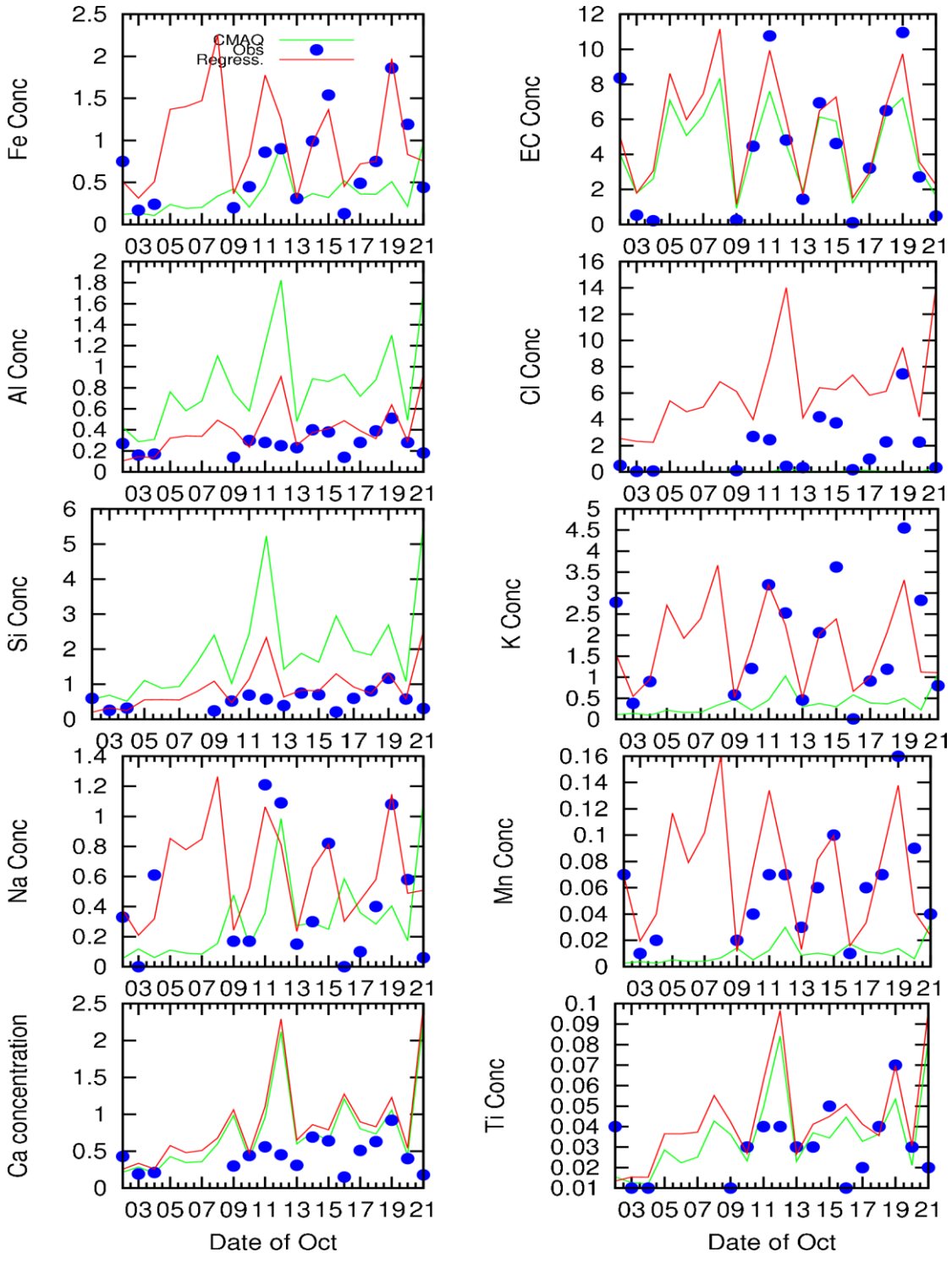

Fig. S17 Similar figure as Fig. 19, but for Oct., 2012.

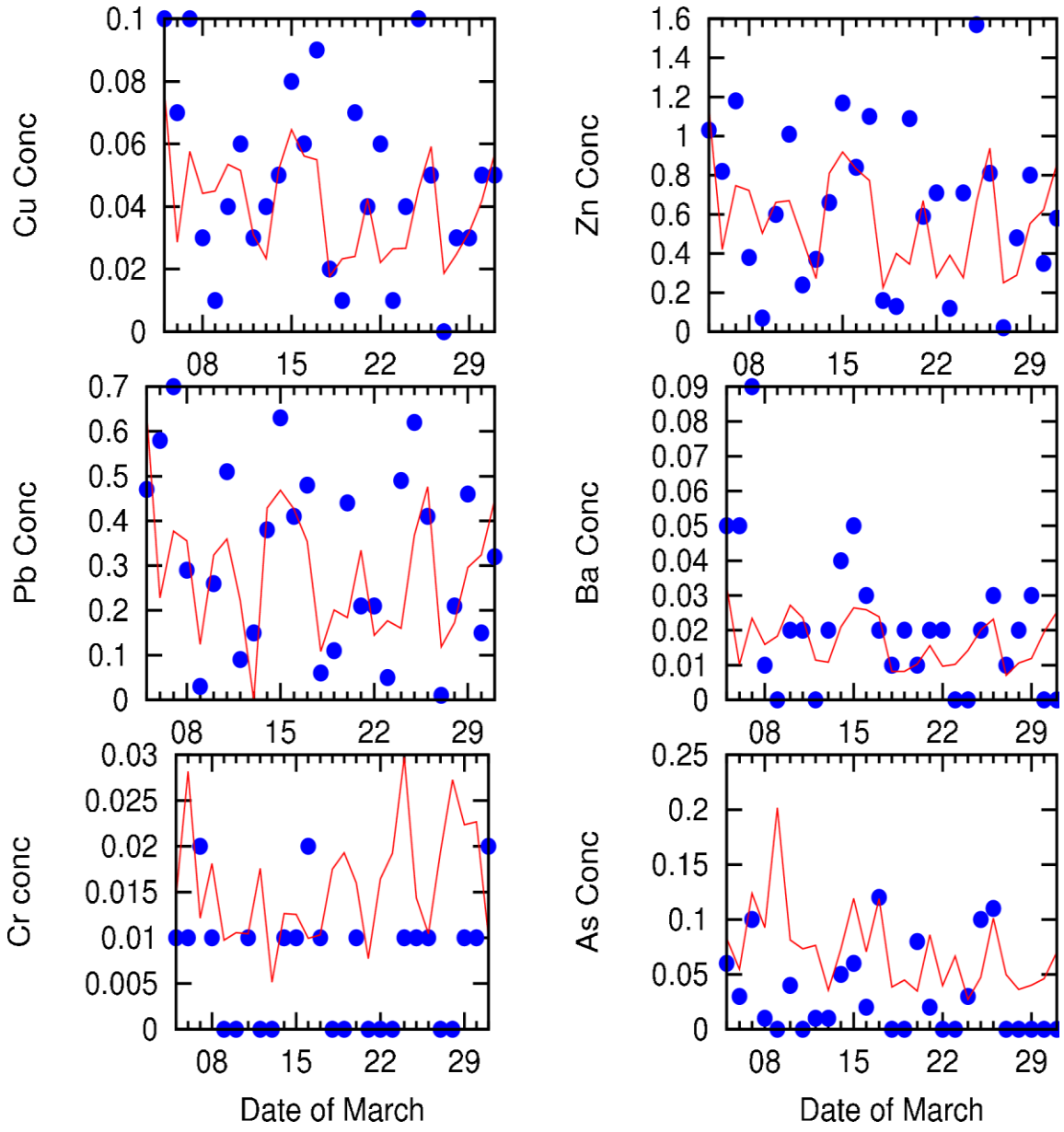

Fig. S18 Similar figure as Fig. 20, but for March, 2013

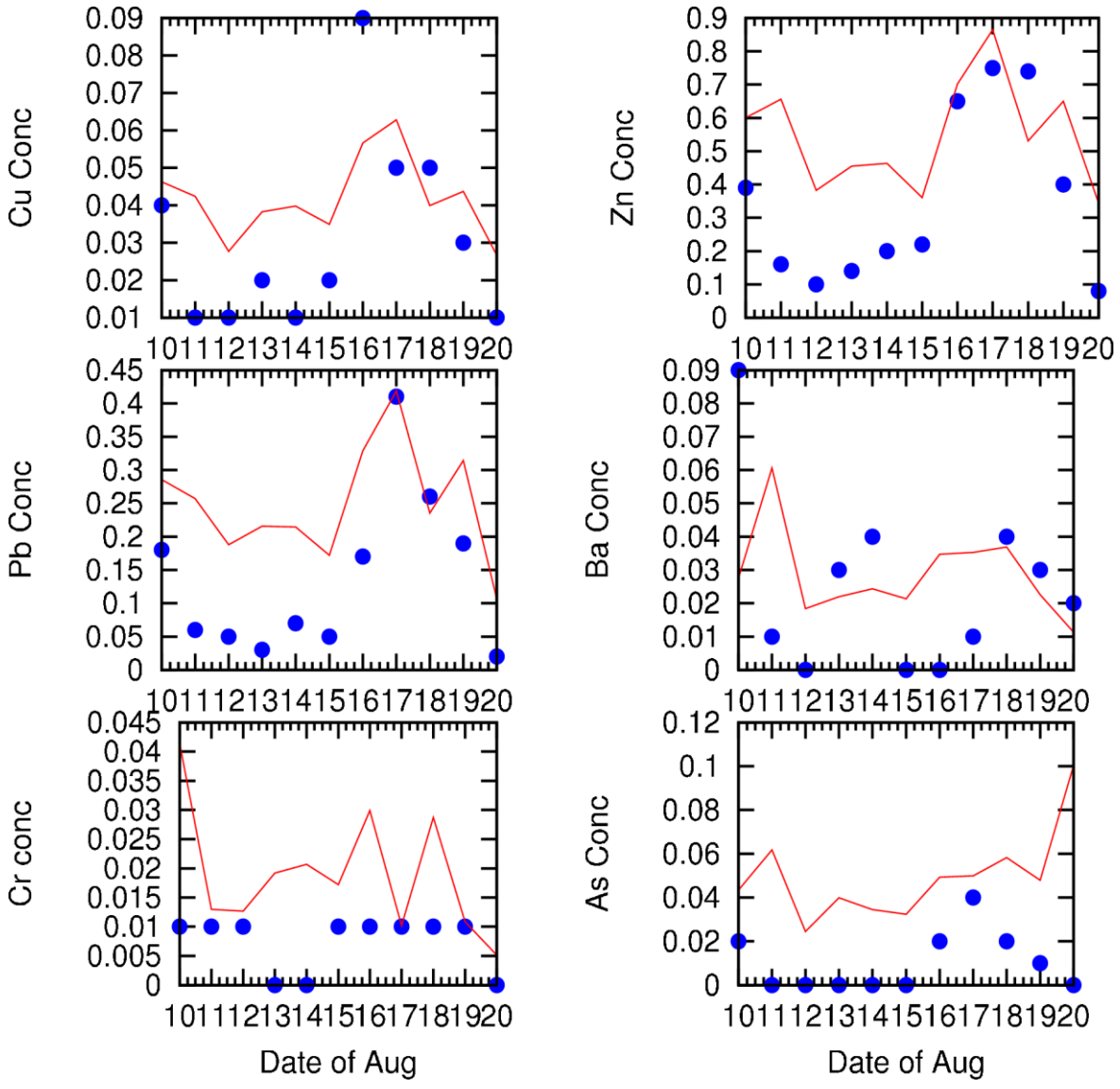

Fig. S19 Similar figure as Fig. 20, but for August, 2012

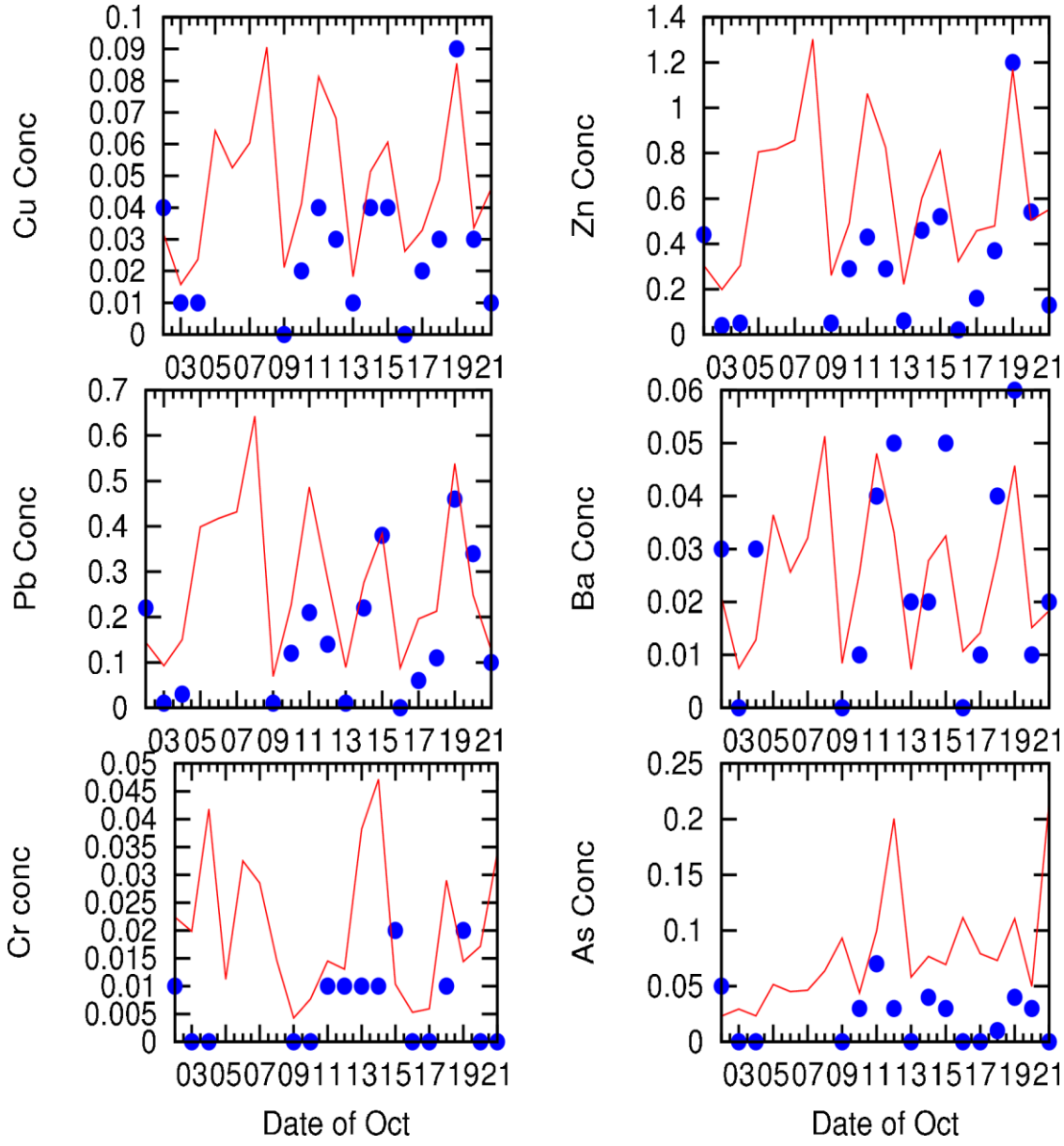

Fig. S20 Similar figure as Fig. 20, but for Oct., 2012